![ktu 1922]

BIRUTĖ PALIAKAITĖ

INVESTIGATION OF PHOTOPLETHYSMOGRAPHY FOR DETECTION OF LIFE-THREATENING ARRHYTHMIAS

DOCTORAL DISSERTATION

Kaunas
2023

KAUNAS UNIVERSITY OF TECHNOLOGY

BIRUTĖ PALIAKAITĖ

INVESTIGATION OF PHOTOPLETHYSMOGRAPHY FOR DETECTION OF LIFE-THREATENING ARRHYTHMIAS

Doctoral dissertation
Technological Sciences, Measurement Engineering (T 010)

Kaunas, 2023

KAUNO TECHNOLOGIJOS UNIVERSITETAS

BIRUTĖ PALIAKAITĖ

GYVYBEI PAVOJINGŲ ARITMIJŲ ATPAŽINIMO FOTOPLETIZMOGRAMOJE TYRIMAS

Kaunas, 2023

Contents

List of terms and abbreviations

Acc	Classification accuracy
bpm	Beats per minute
CKD	Chronic kidney disease
CNN	Convolutional neural network
CV	Cardiovascular
E	Root mean square error
ECG	Electrocardiogram
ESKD	End-stage kidney disease
HD	Hemodialysis
$\mathcal{M}_\mathrm{o}$	Original photoplethysmogram simulation model
$\mathcal{M}_\mathrm{a}$	Model adjusted to simulate life-threatening arrhythmias
PPG	Photoplethysmogram
PSD	Power spectral density
RR interval	Time interval between two contractions of the ventricles
RMS	Root mean square
ROC	Receiver operating characteristic
Se	Sensitivity
SCD	Sudden cardiac death
SNR	Signal-to-noise ratio
Sp	Specificity
SQI	Signal quality index

INTRODUCTION

Relevance of the research

Almost 700 million people, or 9.1% of the world's population, have a chronic kidney disease (CKD). In less than three decades since 1990, the prevalence of CKD has increased by 29.3% mostly due to the population growth, aging and an increasing burden of risk factors for CKD, such as diabetes and hypertension [1]. In 2017, CKD caused 1.2 million deaths, and the number is projected to rise at least to 2.2 million by 2040 [1, 2]. CKD is a progressive condition with kidney failure, or end-stage kidney disease (ESKD), as a final stage. More than 5 million people suffer from ESKD and need kidney replacement therapy. To date, in-center hemodialysis (HD) is the most common modality of kidney replacement therapy, received by 69.4% of patients with treated ESKD. The incidence of HD has been steadily increasing, especially in low- and middle-income countries, and the number of HD recipients is estimated to double by 2030 [3].

CKD and ESKD patients have a high prevalence of cardiovascular diseases. In early stages of CKD, the prevalence is 63.4%, while in advanced stages of CKD and ESKD the proportion of patients with cardiovascular diseases increases to 75.3% [4]. Cardiovascular diseases are a major cause of death in the CKD population. They account for as many as 58% of deaths in ESKD patients [5]. Out of all cardiovascular deaths, most are attributed to sudden cardiac death due to life-threatening arrhythmias, such as ventricular fibrillation or extreme bradycardia [6]. Individuals in need for primary or secondary prevention of sudden cardiac arrest are considered for cardiac device implantation. In most patients, a cardioverter-defibrillator is implanted to prevent ventricular tachycardia evolving to ventricular fibrillation. However, in patients with an impaired kidney function, pacemakers could be more suitable since extreme bradycardia, which can result in asystole, has been frequently observed in this population [7]. The risk of life-threatening arrhythmias is markedly increased during the long interdialytic interval in patients with ESKD on thrice-weekly HD. Arrhythmogenic propensity of HD patients can also be seen in an increased frequency (burden) of premature heart contractions, known as ectopic beats [8].

Apparently, the intermittent nature of HD-based blood cleaning facilitates the arrhythmia-triggering processes, such as the volume overload, accumulation of toxins, and rapid electrolyte shifts [9]. Unfortunately, the benefit of cardiac device implantation in ESKD patients is undermined by their susceptibility to postimplantation complications [10] and the lack of information about the underlying arrhythmia threatening with sudden cardiac death. Since an individual risk–benefit ratio should be carefully considered, long-term monitoring for the detection of the initial episodes of life-threatening arrhythmias could facilitate the decision making regarding the cardiac device implantation. Of course, other approaches towards mitigating the arrhythmogenic propensity

of HD patients can be considered, including pharmaceuticals and modifications of the dialysis schedule or dialysate. However, the efficiency of these approaches should by assessed in a quantitative way, e.g., by observing the changes in the ectopic burden.

Electrocardiogram recording is a primary technology considered in arrhythmia monitoring. However, the currently available electrocardiogram-based devices are either suitable for intermittent signal recording, uncomfortable to wear for a prolonged time, or expensive. The recent progress in wearable devices, especially smartwatches, equipped with optical sensors for photoplethysmogram (PPG) recording, shows the tremendous potential for arrhythmia monitoring [11]. This noninvasive technology could be particularly useful for long-term monitoring of ESKD patients on HD. However, the development of algorithms for the detection of arrhythmias, other than atrial fibrillation, by using wrist-worn devices is hindered by the susceptibility of PPG to artifacts and lack of annotated databases with episodes of life-threatening arrhythmias. Besides, the suitability of the wrist PPG for the assessment of the ectopic burden in ambulatory setting is also unclear.

Scientific-technological problem and working hypothesis

The specific situation of CKD patients, especially those with ESKD on HD, makes them a target population whose treatment could highly benefit from the long-term PPG-based monitoring for the detection of the initial episodes of life-threatening arrhythmias and the assessment of the ectopic burden. However, in order to accelerate the adoption of PPG-based technologies in this setting, a thorough investigation of the PPG signal and methods to facilitate the development of algorithms for arrhythmia detection are needed.

Scientific-technological problem: How can the obstacles hindering the development and application of PPG-based algorithms for the long-term arrhythmia monitoring be mitigated?

Working hypothesis: The application of PPG-based technologies for the detection of life-threatening arrhythmias can be advanced by performing artifact analysis, exploiting simulated data, and investigating the performance of the PPG-based algorithms in ambulatory setting.

The aim of the research

This doctoral thesis aims to develop and investigate methods for the ambulatory assessment of cardiac arrhythmias from PPG signals.

The objectives of the research

1. To explore artifacts hindering the application of ambulatory PPG signals.

2. To develop and investigate a model accounting for the influence of life-threatening arrhythmias and artifacts on PPG signals.

3. To investigate the performance of PPG-based algorithms for the detection of life-threatening arrhythmias.

4. To evaluate the suitability of PPG signals to assess the high-risk ectopic burden.

Scientific novelty

Firstly, this doctoral thesis provides insights into the quality of the wrist PPG encountered in free-living activities. For the first time, quantitative characteristics, such as artifact duration, amplitude, and the spectral content, of different-type artifacts are obtained from ambulatory PPGs. Those characteristics are invoked to develop a realistic artifact model which is applied to test the robustness of a life-threatening arrhythmia detector.

Secondly, in this thesis, the PPG model is adjusted to simulate episodes of life-threatening arrhythmias by accounting for the influence of those arrhythmias on hemodynamics. The adjusted PPG model is not only employed to test the performance of a pulse-based arrhythmia detector, but also to simulate data for the training and validation of a convolutional neural network, which detects life-threatening arrhythmias in PPG scalograms.

Finally, for the first time, a continuously acquired wrist PPG is applied to assess the daily ectopic burden under uncontrolled conditions in HD patients. Not only the potential of the technology is demonstrated, but also its weaknesses and possible aspects for the improvement are identified.

Practical significance

1. The results of the PPG investigation and the proposed simulation model can be used in the following applications:

   (a) The proposed artifact simulation model can facilitate the development and testing of wrist PPG-based arrhythmia detectors which are robust against artifacts encountered in daily activities.

   (b) The adjusted PPG model allows to employ publicly available electrocardiogram databases with annotated episodes of life-threatening arrhythmias to generate PPG signals required for the development of arrhythmia detectors. Simulated data can be used not only for testing, but also for training and validation of deep learning methods for arrhythmia detection.

   (c) In addition, the model could be employed to test and calibrate new wearable devices for healthcare applications.

(d) The simulation model is beneficial for developing detectors for prolonged monitoring of HD patients and other patient groups that are at risk of sudden cardiac death due to life-threatening arrhythmias, e.g., post-myocardial infarction patients during the first months after the event.

(e) A PPG-based approach to ectopic burden estimation has the potential to be applied in identifying HD patients eligible for an early antiarrhythmic treatment.

(f) A PPG-based approach to ectopic burden estimation can be used to gather knowledge on the efficiency of nonconventional treatment modalities (e.g., HD modification or chronotherapy) in preventing settings conducive to arrhythmia initiation.

2. The methods provided in this thesis have been developed and investigated in the framework of the project *Personalized wearable technologies for evaluating life threatening health conditions in chronic kidney disease patients — KidneyLife* funded by the European Regional Development Fund (01.2.2-LMT-K-718-01-0030) under grant agreement with the Research Council of Lithuania, 2018–2022.

3. The proposed model for simulating PPGs with episodes of life-threatening arrhythmias and motion-induced artifacts has been made publicly available on the *PhysioNet* repository.

Approval of the results

The doctoral thesis relies on two papers published and one manuscript under review in international scientific journals with the impact factor referred in the *Clarivate Analytics Web of Science* database, while, in total, the results have been published in seven scientific papers. The essential results have been presented in four international conferences.

In 2019, 2020, and 2022, promotional scholarships for academic research, granted by the Research Council of Lithuania, were received. In 2019, 2020, and 2021, the awards of the most active PhD student in the field of Measurement Engineering, granted by Kaunas University of Technology, were received.

The statements presented for defense

1. A substantial proportion of the wrist PPG in ambulatory recordings is corrupted by artifacts. The percentage of artifacts markedly increases during day-time, which coincides with the active period of the day.

2. The adjusted PPG model closely resembles changes in the pulse amplitude and morphology during the episodes of life-threatening arrhythmias. The artifact

component of the model produces motion-induced artifacts similar to the ones encountered in real-life wrist-based PPGs.

3. The performance of the pulse-based life-threatening arrhythmia detector is affected differently by different artifact types. When detecting extreme bradycardia and ventricular tachycardia, the convolutional neural network, trained and validated on simulated data, is more sensitive than the pulse-based detector. However, the latter detector is more specific for extreme bradycardia.

4. The wrist PPG can be applied to the ectopic burden assessment and identification of the high-risk ectopic burden in HD population.

Structure of the doctoral thesis

The doctoral thesis is organized as follows. Section 1 is dedicated to the analysis of the relevant scientific literature with respect to the significance of continuous monitoring for the detection of the initial life-threatening arrhythmia episodes in patients with the impaired kidney function, and the available electrocardiogram-based and emerging PPG-based technologies to accomplish that monitoring. Section 2 presents the analysis of ambulatory artifacts in the wrist PPG, PPG modeling accounting for the influence of life-threatening arrhythmias and artifacts, approaches to the detection of life-threatening arrhythmias and the assessment of the ectopic burden. Section 3 describes the databases and the relevant performance measures used in the thesis. Section 4 presents the results for the artifact analysis, evaluation of the adequacy of the PPG model, investigation of PPG-based life-threatening arrhythmia detectors, and the assessment of the ectopic burden in HD patients. The doctoral thesis is finished with general conclusions provided in Section 5.

Parts of the thesis have been quoted verbatim from the previously published articles and the manuscript under review: [12, 13, 14, 15].

The thesis consists of 118 pages, 30 figures, 10 tables, and 141 references.

Work done in collaboration

A dual-branch convolutional neural network for the detection of life-threatening arrhythmias investigated in this thesis was developed by Andrius Sološenko.

1. OVERVIEW OF THE APPROACHES TOWARDS ARRHYTHMIA DETECTION IN PATIENTS WITH KIDNEY DISEASE

1.1. Background on chronic kidney disease and cardiovascular comorbidities

1.1.1. Impaired kidney function and progression to kidney failure

Chronic kidney disease (CKD) is defined as markers of kidney damage or a decreased kidney function, present for more than three months, with implications for health. Markers of kidney damage include structural or functional abnormalities, such as high levels of protein albumin in the urine, known as albuminuria, urine sediment abnormalities, electrolyte and other abnormalities due to renal tubular disorders, histology-detected pathological abnormalities, imaging-detected structural abnormalities, and the history of kidney transplantation. The best overall indicator of the kidney function is the glomerular filtration rate, which is approximately 125 ml/min/1.73 m^2 in young healthy adults. A glomerular filtration rate of < 60 ml/min/1.73 m^2 indicates a decreased kidney function, whereas < 15 ml/min/1.73 m^2 is considered kidney failure, also known as the end-stage kidney disease (ESKD). A reduced glomerular filtration rate is associated with a higher risk of drug toxicity, metabolic and endocrine complications, such as anemia, acidosis, malnutrition, etc., cardiovascular (CV) diseases and death [16].

CKD is caused by pathological processes within the kidneys attributed to either primary kidney diseases or systemic diseases affecting the kidneys. In some cases, CKD is determined by genetics or congenital abnormalities [16]. The predominant causes of CKD vary by region. In high and upper-middle income countries, diabetes and hypertension are the most common underlying diseases. However, in low and lower-middle income countries, CKD is mostly caused by infectious diseases, damage to the glomeruli, known as glomerulonephritis, and prolonged exposure to nephrotoxins. Older age, obesity, recurrent dehydration, episodes of acute kidney injury, and prolonged obstruction of the urinary tract are the additional risk factors for the CKD onset. Considering an aging population and the trends in the socio-economic status of low and lower-middle income countries, the prevalence of CKD is expected to rise in the coming decades with diabetes, hypertension, and obesity becoming the main cause for CKD [17].

CKD is a progressive disease with the reversion or improvement in the kidney function possible only in some cases [16]. An ineffective kidney function allows for accumulation of uremic toxins in the body. These toxins are believed to contribute to the development of various complications as well as the CKD progression itself. Since most people with CKD are asymptomatic until later in the course, the disease is diagnosed either by chance through screening tests or only when the symptoms occur with advanced CKD [18]. Most of the risk factors for developing CKD, given in the paragraph above, also influence the CKD progression, and thus they are targeted

by lifestyle and dietary modifications, and pharmacological approaches [19]. A lifelong course of the treatment is usually aimed at slowing the worsening of the kidney function leading to ESKD. At this stage, kidneys are no longer able to sustain life, and the kidney replacement therapy or conservative care are needed. Despite kidney transplantation being considered the optimal therapy, most patients with ESKD initiate in-center hemodialysis (HD) [6, 20], because pre-emptive transplantation is usually not available as an initial treatment modality [19]. Before initiating the HD treatment, a surgical procedure is performed to create vascular access in the form of an arteriovenous fistula, an arteriovenous graft, or a central venous catheter. The access allows blood to flow to the dialysis machine for cleaning as it passes through the dialyzer. Usually, an HD session lasts from three to five hours and is performed three days a week in the dialysis center.

Risk for developing ESKD can be assessed by considering the CKD classification, provided in Table 1.1, and an individual patient's clinical status. With the advancing CKD, the risk for other adverse outcomes, such as an acute kidney injury, CV diseases, hospitalization and death, also increases. In fact, patients with CKD are more likely to die than progress to ESKD [21]. The risk of death increases with the worsening kidney function and is largely caused by CV diseases [22]. Hence, addressing CV comorbidities in patients with a reduced or failed kidney function is of special importance.

Table 1.1. Classification of CKD according to the level of albuminuria, given as albumin excretion rate (AER), and the level of kidney function, given as glomerular filtration rate (GFR), to describe the risk of patients with CKD progressing to adverse outcomes, such as ESKD, CV diseases, hospitalization, acute kidney injury, or death. LR, low risk; MIR, moderately increased risk; HR, high risk; VHR, very high risk. Adapted from [16, 17]

				Persistent albuminuria categories (AER mg/24 hours)		
				A1 Normal to mildly increased <30	**A2** Moderately increased 30–300	**A3** Severely increased >300
GFR categories (ml/min/1.73 m²)	**G1**	Normal or high	⩾90	LR	MIR	HR
	G2	Mildly decreased	60–89	LR	MIR	HR
	G3a	Mildly to moderately decreased	45–59	MIR	HR	VHR
	G3b	Moderately to severely decreased	30–44	HR	VHR	VHR
	G4	Severely decreased	15–29	VHR	VHR	VHR
	G5	Kidney failure	<15	VHR	VHR	VHR

1.1.2.   Cardiovascular comorbidities and sudden cardiac death

The risk for CV mortality increases with a decreasing glomerular filtration rate or raised albuminuria [5]. In fact, the proportion of deaths from CV diseases increases with each

CKD stage and reaches 58% in ESKD [5, 22]. The biggest to date epidemiological study including over 1 million people has shown that the adjusted hazard ratio for adverse CV events, defined as hospitalization for coronary artery disease, heart failure, stroke and peripheral artery disease, increases according to each declining interval of the glomerular filtration rate [23]. Since CKD is frequently caused by hypertension and diabetes, the increased CV risk was attributed to these underlying diseases for a long time [5]. However, the aforementioned study and meta-analyses have shown that CKD is a CV risk factor independently of hypertension and diabetes [23, 24, 25].

The umbrella of pathophysiological disorders involving the heart and kidneys is termed the cardiorenal syndrome, with type 4, or chronic renocardial syndrome, specifically defining CV complications in patients with CKD [26]. The high incidence of CV diseases in early CKD stages is mostly attributed to the traditional risk factors, such as hypertension, diabetes, obesity, dyslipidemia, and smoking. However, in patients with advanced CKD, nontraditional CKD-related risk factors magnify the risk of CV diseases by accelerating the aging processes in vasculature and myocardium [19, 27]. A few of these kidney-specific risk factors are chronic inflammation, calcification, uremic toxins, and increased oxidative stress [27, 28]. They cause CV abnormalities such as vascular stiffness, valvular heart disease, left-ventricular hypertrophy, and ischemic heart disease. CV comorbidities are further stimulated by overactivity of the renin-angiotensin and sympathetic nervous systems in CKD patients. The relevance of kidney-specific risk factors increases as CKD progresses, and thus CV mortality is markedly increased in patients with the advanced stages of CKD or treated with HD [5]. The pathophysiological interactions in type 4 cardiorenal syndrome are graphically presented in Fig. 1.1.

Approximately 50% of all CV deaths in the general population is attributed to sudden cardiac death (SCD). It is defined as "sudden natural death presumed to be of cardiac cause that occurs within 1 h of onset of symptoms in witnessed cases, and within 24 h of last being seen alive when it is unwitnessed" [30]. A similar or even higher proportion of SCD is observed in CKD patients, and the rate increases as the kidney function further declines [31]. In ESKD patients undergoing HD, SCD due to cardiac arrest and life-threatening arrhythmias accounts for 82% of CV deaths, or 45% of all deaths with known causes [6]. The risk of SCD is markedly increased during the period immediately after HD initiation [32], which coincides with a poor first-year survival in patients with ESKD starting the HD therapy [6]. A high incidence of SCD in CKD patients is determined by the high prevalence of cardiac and vascular abnormalities leading to CV diseases, such as ischemic heart disease or cardiomyopathy. These diseases predispose CKD patients to conduction abnormalities, arrhythmias, and then SCD. The effect is probably exacerbated by electrolyte shifts and metabolism abnormalities, sympathetic overactivation, and inflammation [33, 34]. A possible pathophysiological mechanism of an increased risk of SCD in CKD patients is provided
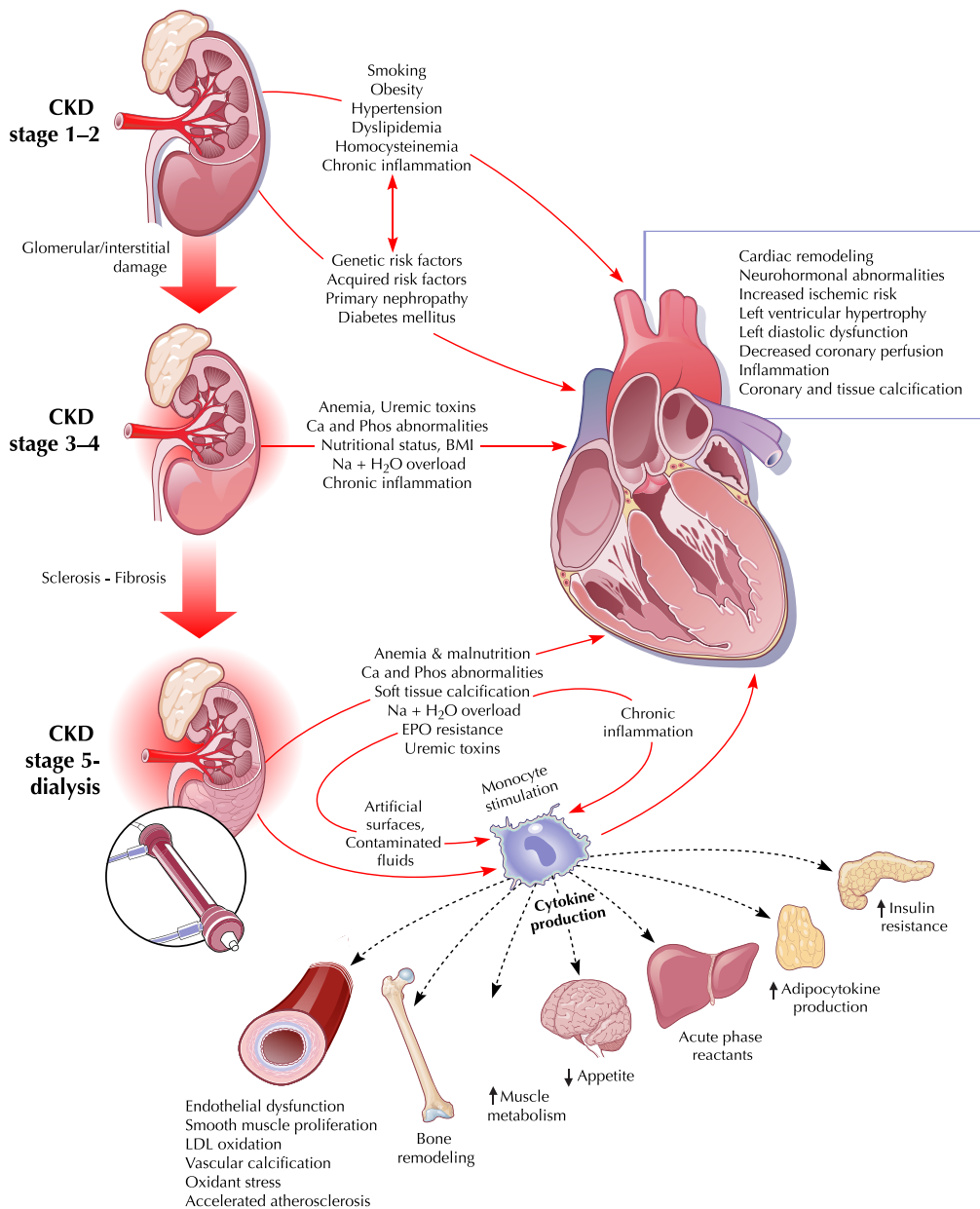
Figure 1.1. Pathophysiological interactions between heart and kidneys in chronic renocardial syndrome. BMI, body mass index; EPO, erythropoietin; LDL, low-density lipoprotein. Illustration by Rob Flewell reprinted from [29], with permission from Elsevier

in Fig. 1.2.

In general, SCD is often preceded by ventricular tachycardia evolving to ventricular fibrillation [35]. However, most studies point to the fact that extreme bradycardia

Chronic kidney disease

Pathophysiologic triggers
Uremic cardiomyopathy
Ischemic heart disease
Inflammation
Sympathetic activation

Dialytic triggers
Electrolyte shifts
High-rate ultrafiltration
Hypotension

Risk of sudden cardiac death

Structural alterations
Myocardial hypertrophy
Myocardial fibrosis
Endothelial dysfunction
Vascular calcification

Electrical remodeling
Repolarization alteration
QTc prolongation
Myocardial stunning
Ventricular arrhythmias

Figure 1.2. Risk factors and hypothesized mechanism of SCD in CKD. Adapted from [34], with permission from Elsevier

followed by asystole, rather than tachycardia, is the preeminent pattern of serious arrhythmias and SCD in ESKD patients [7, 36, 37, 38, 39, 40, 41, 42]. Paradoxically, a life-saving HD treatment is associated with an initial acceleration of CV mortality and may as well be a trigger for life-threatening arrhythmias and SCD [19, 34]. Recent studies show that hours towards the end of a long interdialytic interval together with the ensuing conventional thrice-weekly HD session carry the highest risk of arrhythmias [7]. While in the hours preceding HD, bradyarrhythmias are more common, other arrhythmias, such as tachycardia and ectopic beats, manifest more often during or in a couple of hours after HD, pointing towards possibly different mechanisms increasing arrhythmogenicity. The end of the interdialytic interval, especially a long one, is a period of an increased risk for volume overload, accumulation of toxins and high potassium levels. On the other hand, the rapid shift of fluids and electrolyte concentrations during HD might increase cardiac stress and also trigger arrhythmias [9]. A long interdialytic interval also often leads to an increased volume and rate of ultrafiltration rendering patients susceptible to intradialytic hypotension, which is associated with a higher rate of intradialytic arrhythmias [43].

Parts of the paragraph above have been quoted verbatim from the previously published article and the manuscript under review: [14, 15].

1.1.3. Mitigating the burden of life-threatening arrhythmias

The prevention of SCD due to life-threatening arrhythmias in CKD consists of pharmacological and device therapies, and, in patient with ESKD undergoing HD, may also include dialysis modifications [34]. Beta-blockers and renin-angiotensin system blockers are recommended to reduce mortality due to heart failure and SCD [30],

and have been demonstrated to improve the survivability of CKD and HD patients in retrospective studies [33, 34]. Calcium channel blockers have also been shown to improve the chances of survival of HD patients after cardiac arrest [44]. However, there is a lack of large, double-blinded randomized controlled trials in patients with CKD or ESKD; therefore, the indications for the use of these drugs should be derived from the trials in patients without CKD [33]. Since common medications for the SCD prevention have heart rate- and blood pressure-lowering properties, their effect in CKD patients should be cautiously monitored to avoid episodes of bradyarrhythmias or hypotension due to compromised homeostasis in kidney dysfunction or failure.

An implantable cardioverter-defibrillator is the first choice of cardiac device therapy for primary and secondary prevention of SCD. A wearable cardioverter-defibrillator may also be considered in those at risk of SCD but temporarily not candidates for an implantation procedure due to, e.g., antibiotic treatment [30]. However, the gains of an implantable cardioverter-defibrillator for the primary prevention in CKD patients are not clear. In the early stages of CKD, the device implantation has been reported to reduce the risk of SCD, but, in more advanced CKD stages, the benefits are eliminated [45]. The only randomized controlled trial so far performed in dialysis patients found that prophylactic implantation of a cardioverter-defibrillator was not associated with a reduced rate of SCD or all-cause mortality [46]. This might be explained by extreme bradycardia and asystole, which are unshockable rhythms, being the cause of SCD or severe electrolyte imbalances leading to ineffective shock therapy [42].

Since bradyarrhythmias have been shown to be the predominant mechanism of SCD in HD patients, the cardiac resynchronization therapy with a pacemaker could be more suitable to prevent SCD in this population [7]. Unfortunately, the information regarding the outcomes of pacemaker implantation in HD patients is scarce [9]. Furthermore, the possible benefits of cardiac device implantation are mitigated by the high rate of post-implantation complications in ESKD undergoing dialysis [10, 46]. Though CKD patients at risk of SCD due to life-threatening arrhythmias could potentially benefit from the implantation of a cardiac pacemaker or a cardioverter-defibrillator [47], the high cost and device-related complications should be considered. Long-term monitoring for the detection of the initial episodes of life-threatening arrhythmias could facilitate individual assessment of the risk–benefit ratio to guide the decision making regarding cardiac device implantation.

There is some evidence that, while often benign, frequent ectopic beats can initiate or indicate the presence of serious and even life-threatening arrhythmias. For example, frequent ventricular ectopic beats increase the risk of SCD [48], whereas atrial ectopic beats are linked with the development of atrial fibrillation, a higher risk of death and stroke [49]. Patients with ESKD are susceptible to an increased ectopic activity due to electrolyte imbalance and the arrhythmogenic propensity of HD sessions [8]. Frequent ectopic beats in patients on HD were found to be associated with a higher risk

for nonsustained ventricular tachycardia and paroxysmal atrial fibrillation [50]. Data regarding the prognostic significance of frequent ectopic beats in ESKD patients treated with HD are limited [51]. Long-term monitoring for the assessment of the ectopic burden is needed to enable studies intended for a comprehensive investigation of an increased ectopic activity, its prognostic value, and relationships with life-threatening arrhythmias. Considering a markedly increased risk of SCD during a couple of months following HD initiation, patients with ESKD could be monitored to identify those requiring antiarrhythmic treatment [32].

The risk of arrhythmias can potentially be reduced by applying a less aggressive potassium removal or by modifying the conventional HD schedule, e.g. by including more daily and nightly sessions [9]. The more frequent daily or nightly HD reduces ultrafiltration volumes and episodes of intradialytic hypotension, whereas the less aggressive potassium removal suppresses the burden of intradialytic ventricular ectopic beats threefold [9]. However, technologies for continuous monitoring of ectopic beats and other arrhythmias, allowing to assess the antiarrhythmic effects of HD modifications on individual basis and identify patients who could benefit from nonconventional HD the most, are still lacking. Combined arrhythmia and electrolyte monitoring [52] could also potentially facilitate the assessment of adherence to a dietary plan, drug selection and dosing in order to ensure potassium homeostasis and low arrhythmogenicity between HD sessions.

The discussed scientific literature shows that, in order to initiate a proper treatment and careful supervision of patients with CKD, **monitoring for the detection of the initial episodes of life-threatening arrhythmias and the assessment of the ectopic burden is needed**. Such monitoring would be particularly valuable for the ESKD patients on HD who may experience life-threatening arrhythmias during the long interdialytic period when they are at home [7,42]. Potentially, the prolonged monitoring could facilitate the arrhythmia research and reduce CV mortality in this population.

Parts of Section 1.1.3 have been quoted verbatim from the previously published article and the manuscript under review: [13, 15].

1.2. Technologies for arrhythmia detection

Monitoring for the detection of arrhythmias primarily relies on the technologies that enable acquisition of biosignals with information on cardiac activity. In this section, conventional and emerging technologies suitable for arrhythmia detection are discussed.

1.2.1. Electrocardiogram-based technologies

Heart rhythm abnormalities are usually detected and diagnosed in electrocardiogram (ECG) tracings. Below, ECG-based technologies are reviewed from the perspective of their suitability for the early detection of the initial episodes of life-threatening

arrhythmias and the assessment of the ectopic burden (see also Table 1.2). Devices used for the arrhythmia treatment or SCD prevention, such as pacemakers or cardioverter-defibrillators, are not reviewed since they are prescribed upon the risk evaluation or detection and diagnosis of arrhythmias in the first place.

Table 1.2. Advantages, disadvantages and monitoring properties of the technologies for arrhythmia detection. The table is compiled considering the suitability of the technologies for the detection of initial episodes of life-threatening arrhythmias and the assessment of ectopic burden

	Advantages	Disadvantages	Monitoring
Noninvasive ECG-based			
12-lead ECG	Gold standard	Recorded at the hospital	Several seconds
Holter	Clinically acceptable	Adhesive electrodes; connecting wires	Continuous; up to a week
Patch	Clinically acceptable; wireless; easy-to-use	Single use; adhesive electrode	Continuous; up to a month
Chest strap	No adhesive	May be uncomfortable; susceptible to artifacts	Continuous; prolonged
Handheld	Wireless; easy-to-use	User-activated	Intermittent; prolonged
Smartwatch	Integrated into a consumer device	User-activated; susceptible to artifacts	Intermittent; prolonged
Invasive ECG-based			
Loop recorder	Hardly noticeable	Expensive; implantable	Continuous; up to 5 years
PPG-based			
Smartphone camera	Integrated into a consumer device	User-activated; no guidelines for analysis	Intermittent; prolonged
Band (for arm, forehead, etc.)	Versatile placement; easy-to-use	Susceptible to artifacts; no guidelines for analysis	Continuous; prolonged
Wearable (smartwatch, ring, etc.)	Integrated into a consumer device	Susceptible to artifacts; no guidelines for analysis	Continuous; prolonged

Noninvasive devices

Twelve-lead ECG tracings recorded at the hospital are commonly used for the confirmation of persistent or permanent arrhythmias, such as atrial fibrillation or chronic sinus node dysfunction. However, due to the short-term nature, this approach is not suitable for the detection of the brief initial episodes of arrhythmias or the assessment of their occurrence in relation to daily activities or possible stressors, such as an HD session. Monitoring over a period of 1–7 days with the Holter monitor is appropriate for the detection of daily and relatively frequent arrhythmias. The devices come in different sizes and modifications, and can offer single- to 12-lead ECGs. However, the monitor is uncomfortable to wear for extended periods of time because of frequent

skin irritation, difficulty of use, and disturbance to the patient's daily activities [53]. Thus, early termination of Holter monitoring is not uncommon, and the approach is not suitable for extended monitoring over a longer period of months and years.

Contrary to the Holter monitors, ECG patches are well-tolerated, easy-to-use and praised for the high patient compliance [54] thanks to "their low-profile, water-resistant, wireless, and self-adhesive form-factors" [11]. ECG patches have been validated and widely used in clinical trials, and at least a few different companies have their patches CE-marked and cleared by the United States Food and Drug Administration [11, 55]. Due to the extended monitoring period, ECG patches are as effective or even exceed the effectiveness of the traditional Holter monitors in arrhythmia detection. However, these single-use devices have a relatively short battery life and durability of the adhesive, which restricts monitoring duration to a month at most [11]. Such a period is not enough to capture arrhythmia occurrence patterns and identify arrhythmia-triggering factors [7], e.g., when assessing the ectopic burden.

Another ECG-based device for continuous monitoring is a chest strap. The structure of the device allows for single-lead ECG recording without adhesive electrodes. The device uses a rechargeable or replaceable battery and is attached to the body with a chest belt. So far, chest straps have been mostly used for the heart rate monitoring during sports, but they may also have clinical utility [11]. However, some users find the devices bulky and uncomfortable while wearing [55].

The final type of noninvasive devices for the ECG recording consists of smartwatches and handheld devices [11, 55]. They mostly provide a single-lead ECG, but some modifications allow for a six-lead signal [56]. Smartwatch or handheld ECG is obtained as needed, thus the devices could be considered as user-activated recorders. Such an intermittent approach is suitable for obtaining an ECG during an infrequent symptomatic arrhythmia [57]. However, the technology cannot be used to assess changes in the arrhythmia occurrence, e.g., the ectopic burden.

Invasive devices

Unlike pacemakers and cardioverter-defibrillators which are implanted for arrhythmia treatment, implantable loop recorders are used for prolonged arrhythmia monitoring in patients with a risk of life-threatening arrhythmias and related adverse outcomes, such as stroke [30]. Implantable loop recorders are implanted subcutaneously in the chest area and are hardly noticeable due to a small form-factor. The device enables continuous arrhythmia monitoring for months, up to five years [58]. It registers a single-lead ECG, which is saved for a later examination only if an arrhythmia event is automatically detected. Continuous, long-term monitoring of life-threatening arrhythmias, especially extreme bradycardia, in HD patients was recently established as an important procedure, accomplished by using an implantable loop recorder [36]. However, implantable devices are expensive and carry the risk of postimplantation

complications due to the susceptibility of HD patients to infections [38]. Besides, no studies employing implantable loop recorders for the investigation of arrhythmia prevalence have ever assessed the ectopic burden [7]. Therefore, studies intended for a comprehensive investigation of an increased ectopic activity could benefit from the ability to assess the ectopic burden in a more convenient and accessible way.

Parts of the paragraph above have been quoted verbatim from the previously published article and the manuscript under review: [14, 15].

1.2.2. Potential of wearable photoplethysmogram-based technologies

Photoplethysmography (PPG) is an optical technique enabling acquisition of a peripheral pulse waveform. Changes in the light intensity, which reflects changes in the tissue blood volume within the skin surface, are detected by using a light source and a photodetector [11]. In the clinical practice, fingertip PPG is employed to measure oxygen saturation, commonly referred to as SpO_2, and the pulse rate. However, most consumer devices are also suitable for PPG acquisition. Intermittent PPG can be acquired with a smartphone camera and a LED flashlight by placing a finger over the camera or recording a facial video. The versatility of the PPG sensor also allows for its integration into various bands and wearable devices, such as smartwatches, rings and ear buds, enabling continuous acquisition of the PPG signal in daily life at a low cost [11]. PPG-based technologies are juxtaposed with ECG-based technologies in Table 1.2.

Bands worn on the wrist, forearm, upper arm or forehead are widely used by athletes to monitor the heart rate during physical activity. However, the accuracy of such PPG monitors is highly variable during exercise [59]. Similarly, wrist-worn devices are outperformed by the ECG-based chest strap in cardiac rehabilitation [60]. The quality of the PPG signal and the accuracy of the heart rate measurement are highly influenced by the contact of the PPG sensor with the skin, which could be easily altered during physical activity. Hence, PPG-based analysis of the heart rate and the subsequent arrhythmia detection are more accurate in individuals in the restful state than in ambulatory patients [11].

While bands are prioritized by athletes, smartwatches are widespread in general population and worn in daily living. They can serve as an accessory and communication tool, and they also enable continuous heart rate monitoring. Therefore, smartwatches with embedded optical sensors are being considered as convenient means to initial cardiac arrhythmia detection, which may precede and instigate a comprehensive medical examination and timely clinical intervention [61, 62]. Recently, the detection of atrial fibrillation in PPG has demonstrated encouraging results and received wide-scale research attention [63, 64, 65, 66, 67, 68]. The largest to date siteless study using a commercially available smartwatch with the accompanying smartphone application—

The Apple Heart Study—has demonstrated that a PPG-based device can detect atrial fibrillation in individuals without a history of this arrhythmia [65]. However, as per 2020 European Society of Cardiology Guidelines for the diagnosis and management of atrial fibrillation, PPG alone cannot be used for arrhythmia diagnosis. Therefore, a confirmation by ECG with a clinician's oversight is needed [69]. In such cases, smartwatches with integrated electrodes allowing for ECG acquisition may come in handy. The ongoing HEARTLINE trial investigates whether detecting atrial fibrillation by using a smartwatch-based combination of PPG and ECG improves clinical outcomes [55]. Albeit ECG will obviously remain a gold standard for arrhythmia detection, PPG-based devices show potential to become beneficial for the prolonged monitoring of target populations and the selection of individuals for comprehensive medical examination [61, 62].

The use of PPG-based devices for the detection of other arrhythmias lags far behind its use for atrial fibrillation. Likely, the tremendous potential of smartwatches capable of detecting atrial fibrillation will spawn the development of other type arrhythmia detectors. PPG-based detection of the initial life-threatening arrhythmia episodes could improve health management of HD patients at a high risk of SCD. However, differently from atrial fibrillation, which could be detected relying solely on the heart rhythm information, the detection of extreme bradycardia and ventricular tachycardia is more challenging. That is, ventricular tachycardia must be distinguished from nonfatal tachycardias (e.g., atrial tachycardia, AV node tachycardia), whereas, extreme bradycardia must not be confused with the segment of a lost signal. Thus far, only a single attempt to detect life-threatening arrhythmias in a wrist-based PPG has been published [70].

Similarly, just a single study has dealt with the detection of ectopic beats in a smartwatch-based PPG, primarily to suppress false alarms of atrial fibrillation [71]. A few more studies assessed the suitability of a finger-based PPG obtained either by using a pulse oximeter [72, 73, 74] or a smartphone camera [75]. Nevertheless, no studies have investigated the possibility to detect ectopic beats under uncontrolled conditions in HD patients whose blood flow in the wrist may be affected by a nonfunctional arteriovenous fistula or vascular calcification. The wrist PPG-based approach to the ectopic burden monitoring supplemented by the detection of other relevant arrhythmias, such as atrial fibrillation [64], bradycardia and tachycardia, could help to identify patients who would benefit most from nonconventional HD or early antiarrhythmic treatment.

Of note, PPG-based approaches for the assessment and monitoring of other CV comorbidities common in CKD and ESKD patients, such as hypertension and vascular stiffness, are also being developed [76, 77, 78].

Parts of Section 1.2.2 have been quoted verbatim from the previously published articles and the manuscript under review: [12, 13, 15].

1.2.3. Factors hindering the adoption of photoplethysmogram-based technologies

Even though the wrist-worn PPG-based devices offer important advantages of convenience, a low cost and no risk of infection, there are factors hindering their application for arrhythmia detection, especially concerning life-threatening arrhythmias. In the paragraphs below, these factors shall be presented.

Susceptibility to artifacts

Susceptibility to artifacts hinders the application of a wrist PPG in activities of daily living since artifacts often result in missed arrhythmia episodes and false alarms. Efforts have been made to reduce motion artifacts by using accelerometer and gyroscope signals [79, 80, 81, 82, 83, 84, 85], whereas finer hand motions, which do not reflect in biomechanical data, can be dealt by using different PPG wavelengths and a piezoelectric transducer [86, 87, 88]. Signal processing techniques have also been invoked for PPG quality estimation [89] and motion artifact reduction [90]. Yet, none of these approaches to artifact suppression have been applied for cardiac arrhythmia detection.

A common way to deal with artifact-corrupted PPGs, and thus improve the reliability of arrhythmia detectors, is to exclude segments of unacceptable signal quality [64, 91, 92] as well as accelerometer-identified motion [65, 66, 67, 91, 92, 93, 94]. Although segment removal conceals the true detection performance, it is not a major problem in case of atrial fibrillation which often lasts for hours without being dangerous [95]. In contrast, even short episodes of extreme bradycardia and ventricular tachycardia can be life-threatening and require an immediate intervention.

PPG artifacts have already been studied in the context of finger oximetry and neck PPG [96, 97]. Nevertheless, the characteristics of these artifacts are not the same in case of the wrist PPG since distinct body locations have different tissue optical properties for different wavelengths and are prone to specific interference [98]. It is useful to investigate artifact characteristics of a green-light PPG which is often used in commercial smartwatches to acquire the pulse rate. Green is preferred to red and infrared since this wavelength does not penetrate deep into the tissue thus causing fewer artifacts from a nonpulsatile slow-changing component [99]. The quality of a long-term green-light PPG, acquired by using a smartwatch, has been investigated earlier [100]. Yet, no characteristics specific to artifact types, such as device displacement, forearm motion, hand motion, and poor contact, were reported.

Lack of publicly available databases

The performance of atrial fibrillation detectors has so far only been established on short-term PPG data [68]. That is because the analysis of the detector performance in long-term signals requires a time-consuming and costly annotation of arrhythmias.

Another impeding factor is that annotations must rely on a simultaneously acquired ECG due to the absence of guidelines for PPG-based arrhythmia diagnosis. Apparently, these restrictions have a large impact on the lack of available databases containing PPGs with annotated arrhythmia episodes. The lack of publicly available databases restrains the development of PPG-based arrhythmia detectors. For that matter, the identification of target patients for the collection of signal databases is markedly facilitated when dealing with an often long-lasting arrhythmia, such as atrial fibrillation, thus making detector development and validation less complicated. However, the problem is expressed more in case of life-threatening arrhythmia detectors.

The problem of publicly available databases can be mitigated by developing and testing the arrhythmia detectors on simulated PPG signals that allow to convert annotated ECG databases to PPG equivalents and to control for various properties, such as the signal-to-noise ratio (SNR) [101]. A phenomenological PPG simulator, originally developed for simulating the sinus rhythm, ectopic beats and atrial fibrillation [101], can be adjusted to model extreme bradycardia and ventricular tachycardia. The main advantage of such a model is that publicly available ECG databases (MIT-BIH Arrhythmia, MIT-BIH Malignant Ventricular Arrhythmia, MGH/MF Waveform, Creighton University Ventricular Tachyarrhythmia) [102], containing annotated episodes of life-threatening arrhythmias, could be employed to generate PPG signal databases.

Another important aspect of modeled PPGs is the artifact component. Detectors are usually tested in a controlled environment, thus offering incomplete insight into the feasibility to detect arrhythmias in free-living activities [103]. Accordingly, such algorithms cannot claim robustness without considering artifact influence on the performance. Unfortunately, only a stationary artifact component can be simulated by the currently available model without considering various artifact types which may have different influence on the detection performance [101]. To build a realistic PPG artifact model, quantitative characteristics, such as the artifact duration, amplitude, and spectral content, have to be accounted for [104, 105]. Different-type artifacts should be quantitatively assessed from ambulatory PPGs, and their characteristics should be invoked to develop an artifact model. A PPG simulation model with a realistic artifact component is of importance for developing and testing detectors for ambulatory arrhythmia monitoring.

Location influence and other factors

When developing an algorithm for a specific task, it is important to consider the location of the PPG acquisition. Initially, most PPG-based arrhythmia detectors have been developed by using finger PPGs from pulse oximeters widely used in hospitals. However, the developed algorithms should always be tested on signals from the specific location intended for future applications. This is because not only an anatomy-determined waveform morphology [106], but also artifact characteristics (see

the above) affect the final appearance of the acquired PPG signal. Other individual factors that may influence the results obtained from the PPG analysis are the skin tone, the presence of obesity, the age and gender [106]. The effectiveness of PPG-based monitoring can also be determined by the body mass index, since the thickness of the skin increases with obesity.

Parts of Section 1.2.3 have been quoted verbatim from the previously published articles: [12, 13].

1.3. Conclusions of the chapter

1. The risk for developing a CKD is increased by widespread heath disorders, such as diabetes, hypertension, and obesity. CKD is a progressive disease, and the risk for adverse outcomes, including CV comorbidities and death, increases with advancing disease stages.

2. Death from CV diseases, especially SCD, dominates the causes of death in CKD patients. The risk of SCD is especially increased in ESKD patients undergoing HD, which, despite being a life-saving treatment, can also act as a trigger for life-threatening arrhythmias and SCD.

3. SCD due to life-threatening arrhythmias could possibly be prevented by using medications, implantable devices, and even dialysis modifications. However, in order to initiate treatment, the initial episodes of life-threatening arrhythmias should be detected. To assess the effectiveness of pharmacological treatment and HD modification, arrhythmogenicity in terms of the ectopic burden should be tracked continuously.

4. Noninvasive ECG-based devices are intended for either intermittent or limited-in-time arrhythmia monitoring. Some of them are more convenient than others depending on the means of sensor connectivity to the body. Implantable loop recorders allow for considerably prolonged monitoring but are costly, require surgical intervention, and are unsuitable for assessing the ectopic burden.

5. A widespread use of personal wearable devices, especially smartwatches, capable of acquiring PPG, opens the possibility to monitor patients at a high risk of life-threatening arrhythmias and assess the ectopic burden. However, PPG has so far been widely applied only for atrial fibrillation detection in screening.

6. The adoption of PPG-based devices in arrhythmia detection and monitoring is mostly hindered by the susceptibility to artifacts and the lack of annotated PPG databases. Thus, the development and testing of the algorithms for the ambulatory detection of life-threatening arrhythmias could be facilitated by using simulated annotated-by-design PPG signals with realistic artifacts.

2. METHODS FOR EXPLORING THE PHOTOPLETHYSMOGRAM FOR DETECTING LIFE-THREATENING ARRHYTHMIAS

2.1. Analysis of artifacts in the wrist photoplethysmogram

Artifact analysis is implemented in four steps: identification, extraction, classification, and characterization, see Fig. 2.1. Artifact-corrupted PPG segments are identified by relying on the signal quality index (SQI) proposed in [64]. Then, the artifacts are extracted by canceling the modeled pulsatile PPG component, and classified into four types characterized by a transition probability, an artifact duration, a spectral slope, and a normalized root mean square (RMS) amplitude.
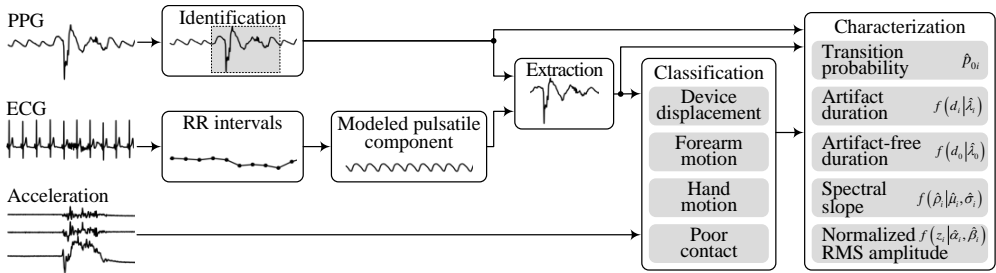
Figure 2.1. Block diagram of artifact analysis consisting of artifact identification, extraction, classification, and characterization

Section 2.1 has been quoted verbatim from the previously published article: [13].

Identification

Artifacts in PPG are identified by using an SQI on the pulse-to-pulse basis [64]. Before applying the SQI, the PPG is filtered with a low-pass infinite impulse response filter with a cut-off frequency of 6 Hz. The baseline wander is removed by using a fifth-order least mean squares adaptive filter. The occurrence times of PPG pulses are determined by using a peak detector similar to the one described in [107].

The signal quality of the kth pulse $x_k(n)$, $k = 1, \dots$, is assessed by correlating it to a template pulse $g_k(n)$ at different time shifts θ_k, using the sample correlation coefficient. Before correlating, $x_k(n)$ and $g_k(n)$ are standardized, and $g_k(n)$ is resampled to the width of $x_k(n)$. The signal quality is considered acceptable when the maximum correlation coefficient $\hat{c}_{\max,k}$ exceeds the threshold η_c, i.e., the binary SQI s_k is defined by

$$s_k = \begin{cases} 1, & \text{if } \hat{c}_{\max,k} \geqslant \eta_c, \\ 0, & \text{otherwise.} \end{cases} \qquad (2.1)$$

The initial template pulse $g_1(n)$ is a predefined PPG pulse $h(n)$ with a dicrotic notch [108]. The subsequent templates $g_{k+1}(n)$ are determined by the preceding

pulse $x_k(n)$ if $\hat{c}_{\text{max},k}$ exceeds the threshold ξ_c and $\hat{\theta}_k$ is contained in the time interval $[\theta_{\min}, \theta_{\max}]$; if not, $g_{k+1}(n)$ is reinitialized by $h(n)$, i.e.,

$$g_{k+1}(n) = \begin{cases} x_k(n), & \text{if } \hat{c}_{\text{max},k} \geqslant \xi_c \text{ and } \hat{\theta}_k \in [\theta_{\min}, \theta_{\max}], \\ h(n), & \text{otherwise,} \end{cases} \qquad (2.2)$$

where ξ_c is set to 0.95 and $[\theta_{\min}, \theta_{\max}]$ are set to $[-0.05, 0.05]$ s. The threshold η_c is set to 0.7 based on the findings of the previous study, in which the PPG pulses with the maximum correlation coefficient $\hat{c}_{\text{max},k}$ below 0.7 were considered to be of unacceptable quality [64].

By inspecting PPGs acquired in free-living activities, high-amplitude artifacts similar to PPG pulses and exceeding the threshold $\eta_c = 0.7$ have been observed. Taking this into account, pulses with a peak-to-peak amplitude higher than 95th percentile of all pulses in the entire recording, and also satisfying $\hat{c}_{\text{max},k} < 0.9$, are considered of unacceptable quality. Adjacent unacceptable-quality pulses, as well as those separated by a single acceptable-quality pulse, are assumed to constitute a single continuous artifact-corrupted PPG segment.

Extraction

An unprocessed PPG is a subject to artifact extraction only with a slow-changing component below 0.5 Hz eliminated. Then, it is assumed that the remaining PPG consists of heart contraction-related pulsations and artifacts. An artifact-free pulsatile component is generated by using a PPG simulation model described in Section 2.2.1 on page 31 and [12, 101], which uses RR intervals of the synchronously acquired ECG as an input. The lth artifact $\nu_l(n)$, $l = 1, ...,$ is extracted by canceling the modeled component from the PPG using a least-mean squares adaptive filter. It should be noted that artifacts cannot be extracted when ECG of sufficient quality for obtaining RR intervals is unavailable.

Classification

The extracted artifacts are classified into four types: device displacement, forearm motion, hand motion, and poor contact (Fig. 2.2). The classification of the lth artifact $\nu_l(n)$ is based on three features obtained from a synchronously acquired accelerometer signal and the artifact itself.

Acceleration. The mean absolute acceleration u_l, quantified from the accelerometer signal, is used to identify device displacement and forearm motion, and is defined by

$$u_l = \frac{1}{N_l} \sum_{n=1}^{N_l} \left(|a_{\text{x}}(n)| + |a_{\text{y}}(n)| + |a_{\text{z}}(n)| \right), \qquad (2.3)$$
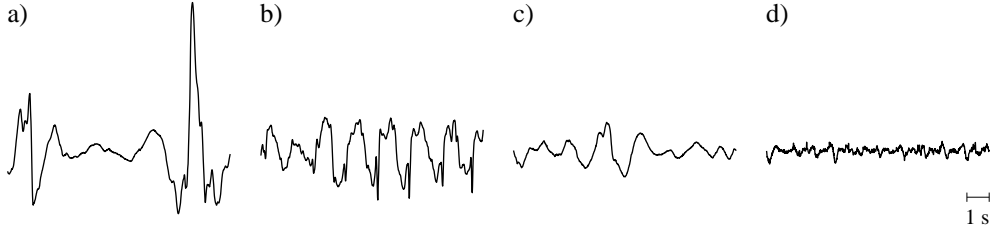
Figure 2.2. Examples of common artifacts encountered in the wrist PPG: a) device displacement, b) forearm motion, c) hand motion, and d) poor contact. The modeled pulsatile PPG component is canceled

where N_l determines the number of samples in the lth artifact, whereas a_x, a_y, a_z represent an accelerometer signal, high-pass filtered with a cut-off frequency at 0.5 Hz, in g units from x, y, and z directions.

Amplitude. The adjusted amplitude v_l represents the largest amplitude difference within the artifact, and is defined by

$$v_l = \frac{\max\limits_{1<n<N_l} \nu_l(n) - \min\limits_{1<n<N_l} \nu_l(n)}{\mathrm{iqr}_\nu},$$
(2.4)

where iqr_ν is the interquartile range of amplitude values in all extracted artifacts over the entire recording.

Spectral properties. The spectral flatness w_l expresses the resemblance of artifact spectral properties to those of white noise, and is calculated as a ratio between geometric and arithmetic means of the power spectral density (PSD) of the extracted artifact

$$w_l = \frac{\exp\left(\frac{1}{M}\sum\limits_{m=0}^{M-1} \ln \hat{P}_l(m)\right)}{\frac{1}{M}\sum\limits_{m=0}^{M-1} \hat{P}_l(m)},$$
(2.5)

where $\hat{P}_l(m)$ is a nonparametric PSD estimate at each frequency bin m, and M is the number of frequency bins.

Artifacts are classified by comparing u_l, v_l, and w_l with the predefined thresholds η_u, η_v, and η_w. The type of the artifact $\nu_l(n)$ is determined according to the following rules:

$$\begin{array}{ll} \text{device displacement,} & \text{if } u_l > \eta_\mathrm{u} \text{ and } v_l > \eta_\mathrm{v}, \\ \text{forearm motion,} & \text{if } u_l > \eta_\mathrm{u} \text{ and } v_l \leqslant \eta_\mathrm{v}, \\ \text{hand motion,} & \text{if } u_l \leqslant \eta_\mathrm{u} \text{ and } w_l \leqslant \eta_\mathrm{w}, \\ \text{poor contact,} & \text{if } u_l \leqslant \eta_\mathrm{u} \text{ and } w_l > \eta_\mathrm{w}. \end{array}$$
(2.6)

Given that even very brief artifacts, lasting just a few seconds, are also likely, the minimal artifact duration d_min has to be determined to increase feature robustness. The

values of thresholds η_u, η_v, and η_w, and the minimal artifact duration d_min are set in Section 4.1.1 on page 51.

Characterization

Each artifact type is characterized by the transition probability and distributions of the artifact duration, the spectral slope, and the normalized RMS amplitude.

Transition probability. The transition probability p_{0i} from an artifact-free interval to an artifact is estimated as

$$\hat{p}_{0i} = \frac{R_i}{\sum\limits_{i=1}^{4} R_i}, \tag{2.7}$$

where R_i is the number of artifacts classified as type i. The index i equal to 1 indicates device displacement, 2 – forearm motion, 3 – hand motion, and 4 – poor contact.

Artifact duration. The duration d_i of the extracted artifacts can be described by an exponential distribution

$$f(d_i|\lambda_i) = \begin{cases} \lambda_i e^{-\lambda_i d_i}, & \text{if } d_i \geqslant 0, \\ 0, & \text{if } d_i < 0, \end{cases} \tag{2.8}$$

where λ_i is the rate parameter equal to the reciprocal of the mean. An estimate of the rate parameter $\hat{\lambda}_i$ is obtained by using maximum likelihood estimation. The duration of artifact-free intervals is described in the same way with an estimate of the rate parameter denoted by $\hat{\lambda}_0$.

Spectral characteristics. The spectral slope ρ_i, which depends on the artifact spectral characteristics, is estimated from the average PSD calculated as

$$\bar{P}_i(m) = \frac{10 \sum\limits_{r_i=1}^{R_i} N_{r_i} \log_{10} \hat{P}_{r_i}(m)}{\sum\limits_{r_i=1}^{R_i} N_{r_i}}, \tag{2.9}$$

where $\hat{P}_{r_i}(m)$ is a nonparametric PSD estimate of the rth standardized artifact of type i, whereas N_{r_i} is the number of samples in the artifact. Then, the spectral slope $\hat{\rho}_i$ is estimated in each recording by fitting a line to $\bar{P}_i(m)$ within a frequency range from 0.5 to 50 Hz. The spectral slope $\hat{\rho}_i$ can be described by a Gaussian distribution with mean $\hat{\mu}_i$ and standard deviation $\hat{\sigma}_i$.

Amplitude. The normalized RMS amplitude z_i of the type i artifact is estimated in 1-s segments as the RMS of the extracted artifact normalized by the RMS of the pulsatile component at the output of the adaptive filter described in the paragraph about artifact extraction on page 28. The normalized RMS amplitude z_i can be described by gamma distribution with estimated shape $\hat{\alpha}_i$ and rate $\hat{\beta}_i$ parameters.

The prevalence of different-type artifacts and their characteristics are presented and discussed in Sections 4.1.2 and 4.1.3 on pages 51 and 53.

2.2. Photoplethysmogram modeling

2.2.1. Hemodynamics-based modeling of life-threatening arrhythmia episodes

Simulation of PPGs with life-threatening arrhythmias uses the adjusted phenomenological PPG model, originally proposed in [101]. An original model $\mathcal{M}_o$ and that adjusted to simulate life-threatening arrhythmias $\mathcal{M}_a$ share the same approach to modeling a single PPG pulse [101]. The modeled PPG pulse $\phi(t; \vec{\theta})$ is a linear combination of three weighted, time-shifted and time-scaled functions: one log-normal and two Gaussian. Estimation of the model parameter vector $\vec{\theta}$, which minimizes the difference between the PPG pulse template (see Section 3.3 on page 43) and the modeled PPG pulse $\phi(t; \vec{\theta})$, is given in [101]. The block diagram of the model is shown in Fig. 2.3.
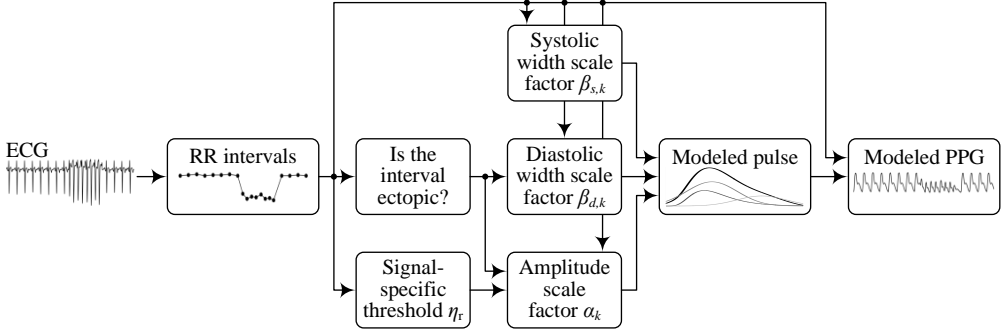
Figure 2.3. Block diagram for modeling the individual PPG pulse and the connected PPG signal with life-threatening arrhythmias

Simulated individual PPG pulses are modified and then connected into a PPG signal according to the RR interval series. The width of the systolic and diastolic parts of the PPG pulse is defined by two time scale factors $\beta_{s,k}$ and $\beta_{d,k}$, respectively,

$$\beta_{s,k} = \frac{1}{r_k}, \tag{2.10}$$

$$\beta_{d,k} = \begin{cases} \dfrac{1}{r_{k+1}}, & \text{if } r_k \text{ is an ectopic beat,} \\ \dfrac{1}{r_k}, & \text{otherwise,} \end{cases} \tag{2.11}$$

where r_k is the RR interval preceding the kth PPG pulse.

Since premature ectopic beats are especially common among HD patients and may cause significant hemodynamic alterations, the decision on whether the RR interval

is ectopic or not is made according to [109]. The RR interval r_k is considered ectopic if at least one of the following rules is satisfied:

$$1.15 r_k < r_{k-1} \text{ and } 1.15 r_k < r_{k+1}, \tag{2.12}$$

or

$$|r_{k-1} - r_k| < 0.3 \text{ and } r_{k-1} < 0.8 \text{ and } r_k < 0.8 \text{ and } 1.2 \cdot \frac{r_{k-1} + r_k}{2} < r_{k+1}, \tag{2.13}$$

or

$$|r_k - r_{k+1}| < 0.3 \text{ and } r_k < 0.8 \text{ and } r_{k+1} < 0.8 \text{ and } r_{k-1} > 1.2 \cdot \frac{r_k + r_{k+1}}{2}. \tag{2.14}$$

The original model $\mathcal{M}_\mathrm{o}$ assumes that the amplitude of the PPG pulse is linearly proportional to the ventricular filling time, which is arguable [110]. Hence, the following rationale to relate the amplitude of the PPG pulse to the left ventricular stroke volume is invoked. Ventricular filling spans almost the entire ventricular diastole and can be divided into three phases: early rapid filling, diastasis, and atrial systole. Only the first and the third phases, which are independent of the duration of the RR interval, contribute to the stroke volume [110]. On the contrary, diastasis depends on the RR interval, but does not increase the stroke volume [110]. As a result, the stroke volume is usually constant when the RR interval is longer than 0.75 s [110, 111]. A detailed examination of PPG signals of a low heart rate (average $r_k > 1$ s) revealed that such signals still show a variation in the PPG amplitude. Accordingly, a signal-specific threshold η_r is introduced which defines the duration of the RR interval corresponding to the maximum stroke volume,

$$\eta_\mathrm{r} = \max \left(\frac{\frac{1}{K} \sum_{k=1}^{K} r_k}{1 - \frac{1}{6K} \sum_{k=1}^{K} r_k}, 0.75 \right), \tag{2.15}$$

where K is the total number of RR intervals in the signal. The duration of diastasis becomes negative when $r_k < \eta_\mathrm{r}$, thereby leading to an overlap of the phases of early rapid filling and atrial systole, which results in a decreased stroke volume [110].

The change in the stroke volume as well as in the PPG pulse amplitude is defined as [111]:

$$\Delta\alpha_k = - \int_{1/\eta_\mathrm{r}}^{1/r_k} \left(0.136 r^2 - 10.044 r + 21.18 \right) dr. \tag{2.16}$$

A premature ectopic beat results in a reduced stroke volume [112, 113]; therefore, the model assumes that the amplitude of the ectopic pulse changes exponentially [114].

32

A post-ectopic beat has a slightly increased pulse amplitude [112, 113], which is accounted for by allowing the increase of the amplitude even when $r_k \geqslant \eta_\mathrm{r}$. Finally, the amplitude of the normalized PPG pulse is given by

$$\alpha_k = \begin{cases} \left(\dfrac{r_k}{\eta_\mathrm{r}}\right)^{1.32}, & \text{if } r_k \text{ is ectopic,} \\ 1 + \dfrac{\Delta\alpha_k}{C \cdot \eta_\mathrm{r}}, & \text{if } r_k < \eta_\mathrm{r} \text{ or } r_{k-1} \text{ is ectopic,} \\ 1, & \text{otherwise,} \end{cases} \tag{2.17}$$

where C is the integration constant set to 25 according to [111].

PPG pulse, denoted as $s_{a,k}(t)$, is modified by scaling the amplitude of $\phi(t; \vec{\theta})$ with α_k, and the width with either $\beta_{s,k}$ or $\beta_{d,k}$ as defined in [101]:

$$s_{a,k}(t) = \begin{cases} \alpha_k \cdot \phi\big(\beta_{s,k}(t - t_p); \vec{\theta}\big), & -\infty < t < t_p \\ \alpha_k \cdot \phi\big(\beta_{d,k}(t - t_p); \vec{\theta}\big), & t_p \leqslant t < \infty, \end{cases} \tag{2.18}$$

where t_p is the time instant of the largest positive peak in $\phi(t; \vec{\theta})$. The kth PPG pulse $s_{a,k}(t)$ is sampled by

$$s_k(n) = s_{a,k}(t = nT), \ n = 0, 1, ... \tag{2.19}$$

where T is a sampling period. A modeled signal $x(n)$ is obtained by placing PPG pulses at the heart beat occurrence times δ_k, obtained from the RR interval series,

$$x(n) = \sum_{k=1}^{K} s_k(n - \delta_k). \tag{2.20}$$

Section 2.2.1 has been quoted verbatim from the previously published article: [12]. The results on the adequacy of the adjusted model are presented in Section 4.2 on page 55.

2.2.2. Modeling of wrist artifacts

The transitions between artifact-free intervals and artifacts are modeled by a five-state continuous-time Markov chain, where state 0 represents an artifact-free interval, and the states from 1 to 4 correspond to ith-type artifacts with i equal to 1 indicating device displacement, 2 – forearm motion, 3 – hand motion, and 4 – poor contact. The transition from the artifact-free interval to all four artifact types is possible; however, only the transition to the artifact-free interval is allowed from the artifact. The generator matrix

of the described Markov process is defined by

$$Q = \begin{bmatrix} -\lambda_0 & \lambda_0 p_{01} & \lambda_0 p_{02} & \lambda_0 p_{03} & \lambda_0 p_{04} \\ \lambda_1 & -\lambda_1 & 0 & 0 & 0 \\ \lambda_2 & 0 & -\lambda_2 & 0 & 0 \\ \lambda_3 & 0 & 0 & -\lambda_3 & 0 \\ \lambda_4 & 0 & 0 & 0 & -\lambda_4 \end{bmatrix}. \tag{2.21}$$

The type i artifact is generated by filtering white noise with a 250th order finite impulse response filter designed so that its arbitrary shape frequency response is determined by the spectral slope taken from the Gaussian distribution with the parameters $\hat{\mu}_i$ and $\hat{\sigma}_i$. The amplitude of the generated artifact is scaled by the normalized RMS amplitude taken from the gamma distribution with the parameters $\hat{\alpha}_i$ and $\hat{\beta}_i$. Finally, the connected signal of artifacts and artifact-free intervals is added to the modeled pulsatile component to produce a PPG with life-threatening arrhythmias and artifacts as shown in Fig. 2.4.
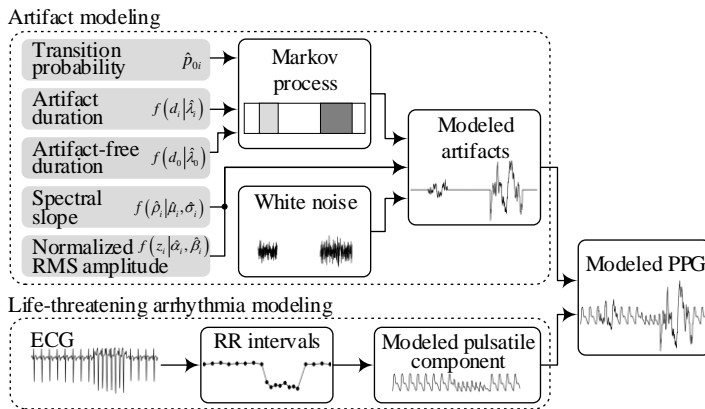
Figure 2.4. Block diagram for modeling the PPG signal with life-threatening arrhythmias and artifacts

Section 2.2.2 has been quoted verbatim from the previously published article: [13]. The artifact model is applied to investigate the influence of artifacts on the life-threatening arrhythmia detection performance. The results of this investigation are presented in Section 4.3.2 on page 63.

2.3. Detection of life-threatening arrhythmias

This section describes two different algorithms for the detection of life-threatening arrhythmias, namely, extreme bradycardia and ventricular tachycardia, which are investigated in this thesis. The first one relies on a dual-branch convolutional neural network (CNN). The second one is a pulse-based detector that indicates the arrhythmia if the

pulse rate exceeds or drops below a certain threshold. Thus far, only the latter approach has been introduced in the scientific literature [70]. Hence, this work investigates the use of a deep learning algorithm applied to the detection of life-threatening arrhythmias for the first time and the already-known pulse-based detector. In the following text, ventricular tachycardia is sometimes referred to as simply *tachycardia*, and extreme bradycardia is sometimes referred to as simply *bradycardia*.

Parts of Section 2.3.1 have been quoted verbatim from the previously published article: [14]. The performance of the detectors described in the following text is investigated in Section 4.3.1 on page 58.

2.3.1. Convolutional neural network-based detector

A deep learning method for detecting life-threatening arrhythmias is composed of signal preprocessing and segmentation, signal quality assessment, and the computation of the scalogram serving as an input to the CNN-based detector. The block diagram in Fig. 2.5 summarizes the detector structure as well as the datasets for training, validation and testing of the CNN-based detector, which are described in detail in Sections 3.3 and 3.4.
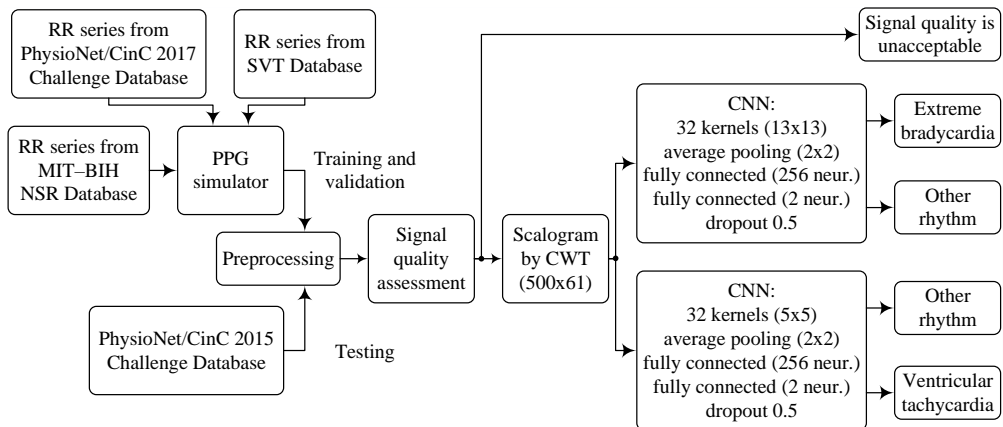
Figure 2.5. Block diagram of the deep learning method for the detection of extreme bradycardia and ventricular tachycardia, including information on the datasets used for training, validation, and testing. CWT, continuous wavelet transform

Signal preprocessing and segmentation

The PPG signals, sampled at a rate of 100 Hz, are preprocessed by using a band-pass filter with cut-off frequencies at 0.5 and 40 Hz. To further reduce the influence of baseline wander, an adaptive, normalized least mean squares filter is employed, with the reference input set to 1 [64]. Subsequent analysis is performed in nonoverlapping 5-s segments.

Signal quality assessment

To reduce the number of false alarms due to motion artifacts, the signal quality is assessed by performing spectral analysis of the PPG signal. The location of the largest spectral peak within each 5-s segment is determined. If the peak is outside the 0.6–3 Hz range, equivalent to 3–15 beats, which is a reasonable number of beats to occur within a 5-s segment, the segment is assessed to be of unacceptable quality and excluded from further analysis. Figure 2.6 shows examples of PPG segments excluded after signal quality assessment.
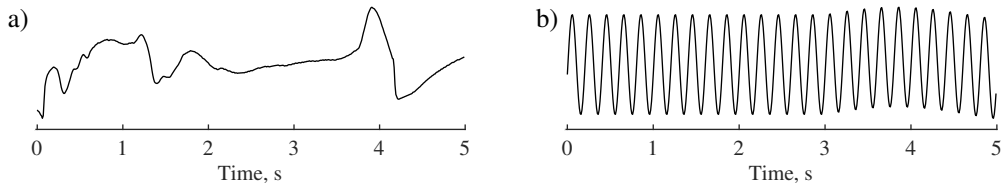
Figure 2.6. Examples of unacceptable-quality PPG segments excluded after signal quality assessment, with the largest spectral peak at a) 0.4 Hz and b) 5 Hz, i.e., both frequencies outside the 0.6–3 Hz range

CNN-based detection

The continuous wavelet transform, offering good resolution in both time and frequency, is computed in each 5-s segment assessed to be of good quality. When using the generalized Morse wavelets, the resulting scalograms are treated as images with a size of 500×61 pixels, i.e., 500 samples and 61 scales. The minimum and maximum scales are determined by the distribution of the energy across the different scales. Figure 2.7 presents two examples of simulated and real PPG signals whose scalograms exhibit similar characteristics.

The detection of bradycardia and tachycardia relies on two CNNs, where each arrhythmia is handled by its own particular model. Each model consists of two 2D convolutional layers with 32 kernels, where each kernel is followed by average pooling layers (size of 2×2 and a stride of 2) and two fully connected layers (input layer with 256 neurons and output layer with 2 neurons for segment classification). The kernel size of the two CNN models differs since bradycardia is composed of lower frequencies than tachycardia and therefore calls for a larger kernel size, here set to 13×13 (extreme bradycardia) and 5×5 (ventricular tachycardia). The stride of the convolutional kernels is set to 1. All layers, except the output layer, are activated by using rectified linear unit (ReLU) functions followed by a dropout rate of 0.5 to minimize overfitting; the output layer is softmax activated.

Before training the CNNs, the dataset of simulated signals is balanced by under-sampling the majority class, i.e., by randomly removing non-bradycardia (non-
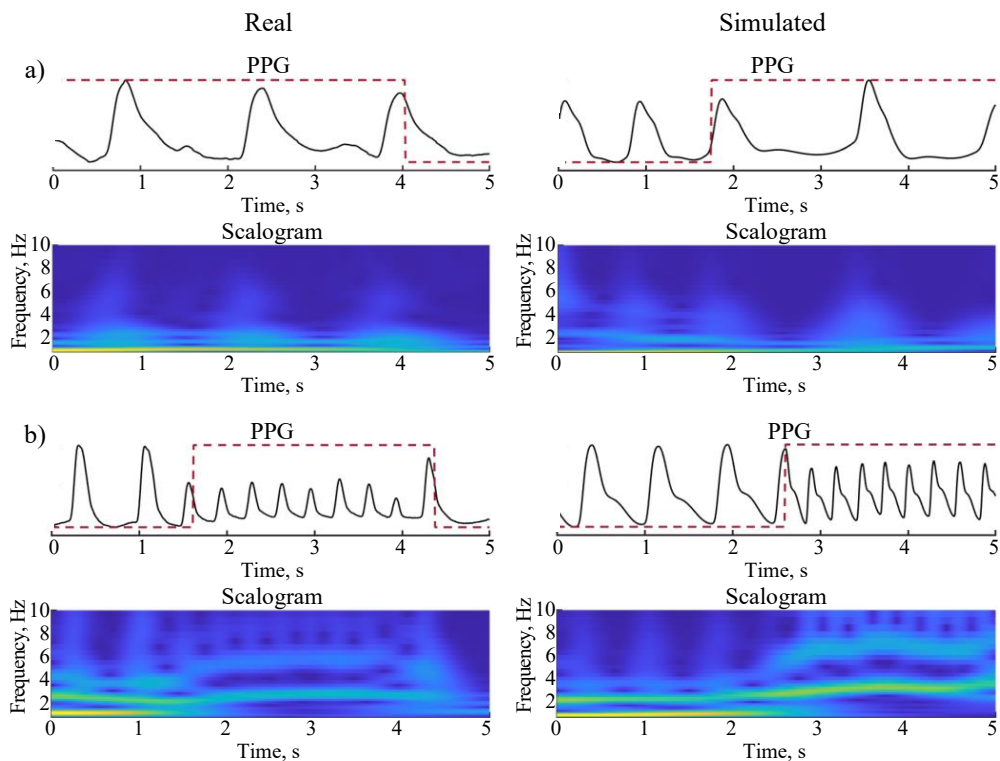
Figure 2.7. Examples of PPG signal segments and related scalograms of real and simulated signals in a) extreme bradycardia and b) ventricular tachycardia. Since most of the power of a PPG signal is confined to lower frequencies, the vertical scale of the displayed scalograms is upper limited to 10 Hz. The annotation is marked with a red dashed line. The real signals are extracted from b124s and v837l of the PhysioNet/CinC 2015 Challenge Database, whereas the simulated signals are generated by using A07531 of the PhysioNet/CinC 2017 Challenge Database and RRt3 of the Spontaneous Ventricular Tachyarrhythmia Database

tachycardia) segments to match the number of bradycardia (tachycardia) segments. Then the dataset is split so that 70% is used for training and 30% for validation. The CNNs are trained using the Adam optimizer described in [115] with a learning rate of 0.01. Training is stopped when the classification accuracy on the validation set has stopped improving.

Whenever the output of the bradycardia-trained CNN exceeds a certain threshold, the segment is classified as extreme bradycardia, otherwise it is perceived as other rhythm; the same applies to the output of the tachycardia-trained CNN except that another threshold is used. Both thresholds are chosen so that sensitivity (*Se*) is favored over specificity (*Sp*).

2.3.2. Pulse-based detector

A pulse-based life-threatening arrhythmia detector is similar to the one described in [70]. The PPG signal is band-pass filtered with cut-off frequencies at 0.5 and 6 Hz (instead of 40 Hz) to suppress the high-frequency noise. The pulse rate, which is an equivalent of the heart rate, is obtained from the pulse-to-pulse intervals, where the occurrence times of the pulses are again determined by using a threshold-based detector similar to the one described in [107]. The signal quality of each pulse is assessed by applying the SQI [64] (see the paragraph on artifact identification on page 27). The quality is assessed as acceptable when the maximum correlation coefficient exceeds the threshold $\eta_c = 0.6$. A lower threshold is selected to preserve sensitivity of the pulse-based detector. An episode of extreme bradycardia is detected if the pulse rate drops below 40 beats per minute (bpm) for at least 3 acceptable-quality pulses, and an episode of ventricular tachycardia is detected if the pulse rate exceeds 120 bpm for at least 3 acceptable-quality pulses. The block diagram of the detector is given in Fig. 2.8. The output of the pulse-based detector is divided into 5-s segments to facilitate a comparison of performance with the CNN-based detector.
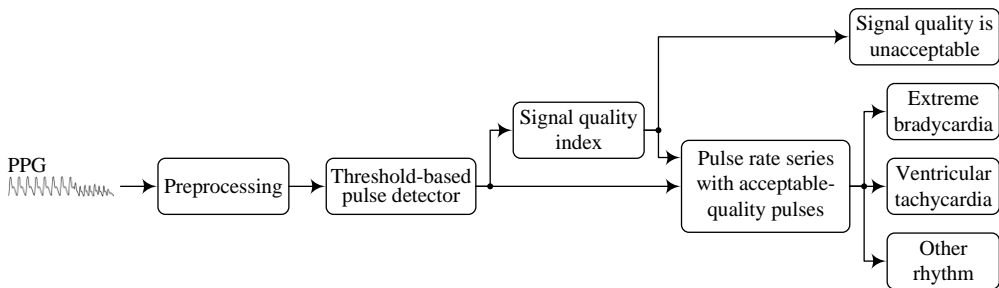
Figure 2.8. Block diagram of the pulse-based life-threatening arrhythmia detector

The same pulse-based detector is used to demonstrate an application of the artifact model to testing a life-threatening arrhythmia detector in Section 4.3.2 on page 63. However, in this case, a minimum episode length of five acceptable-quality pulses is assumed.

2.4. Assessment of the ectopic burden

This section briefly describes PPG-based and reference ECG-based approaches for the detection of ectopic beats, and the subsequent assessment of the ectopic burden.

Section 2.4 has been quoted verbatim from the manuscript under review: [15]. The results on the suitability of PPG signals to estimate the ectopic burden and detect the high-risk ectopic burden are presented in Section 4.4 on page 66.

PPG-based ectopic beat detector

The wrist PPG is preprocessed, and the PPG pulses are determined as already described in the paragraph on artifact identification on page 27. Again, the quality of each pulse is assessed by applying the SQI [64]. However, since ectopic beats are detected in individual pulses, a higher correlation threshold of 0.8 is used to suppress false alarms. Similarly, high-amplitude artifacts resembling PPG pulses are assigned to unacceptable quality by identifying pulses with a correlation coefficient below 0.9 and a peak-to-peak amplitude higher than the 95th percentile of all pulses in the entire recording.

Ectopic beats of both ventricular and atrial origin (see Fig. 2.9) are detected in acceptable-quality PPG segments by using a high-performing ectopic beat detector described in detail in [73]. Briefly, the detector is based on a feed-forward artificial neural network that uses preceding, current, and subsequent pulse-to-pulse intervals to detect ectopic PPG pulses.
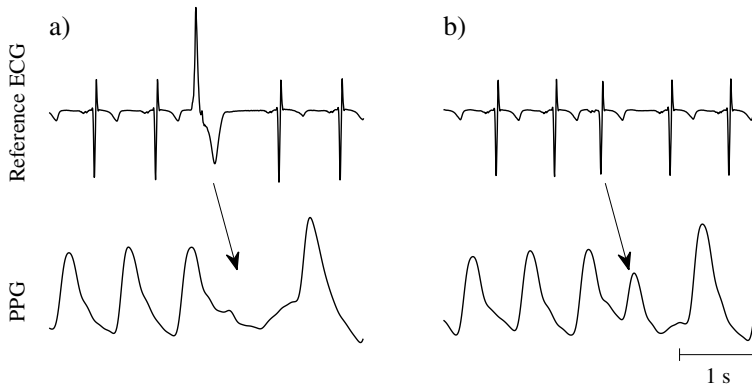
Figure 2.9. Ectopic beats of a) ventricular and b) atrial origin in the reference ECG and PPG

Reference ECG-based ectopic beat detector

Reference ectopic beats are detected in ECG lead II. ECG is band-pass filtered to the 0.5–40 Hz frequency range [116]. Peak detector *jqrs*, available from the PhysioNet Cardiovascular Signal Toolbox [102, 116], is used to identify QRS complexes [117, 118]. ECG quality is determined by using an SQI *bsqi* with the default settings from the same toolbox [119, 120]. The SQI provides the percentage of beats that match when detected by two distinct QRS detectors. For this task, a wave delineator is used as the other QRS detector [121]. The aforementioned SQI occasionally overlooks high-amplitude spikes and flat-line ECG due to disconnected electrodes. Taking this into account, 1-s ECG segments with peak-to-peak amplitudes below 0.1 mV or above three medians of peak-to-peak amplitudes of segments with unitary SQI are considered of unacceptable quality.

Relying on QRS indices from *jqrs*, candidate ectopic beats in acceptable-quality ECG segments are detected by using the R-DECO software [122, 123]. From the candidate ectopic beats, only the ones corresponding with the beat-to-beat intervals <90% of the preceding normal beat-to-beat intervals serve as reference ectopic beats [124].

Definition of ectopic burden

The average daily ectopic burden for each 24-h recording is calculated by dividing the total number of ectopic beats by the duration of acceptable-quality signal within an entire recording and is expressed as beats/h. Similarly, the ectopic burden within a 1-h segment is calculated by dividing the number of ectopic beats detected in the segment by the proportion of acceptable-quality signal comprising that segment.

2.5. Conclusions of the chapter

1. An approach to the analysis of artifacts in the wrist PPG is described. The analysis consists of artifact identification, extraction, classification, and characterization. Four artifact types common in the wrist PPG are distinguished, namely, device displacement, forearm motion, hand motion, and poor contact. Artifact type-specific characteristics can be used to improve the realism of the PPG simulation model.

2. An existing PPG model is adjusted to simulate episodes with life-threatening arrhythmias by relating the amplitude of the PPG pulse to the left ventricular stroke volume. The model is further improved by including a realistic artifact component, in which various artifact properties, such as the artifact type, transition probability, duration, amplitude, and spectral content, can be controlled.

3. Two algorithms for the detection of life-threatening arrhythmias, namely, extreme bradycardia and ventricular tachycardia, are described. A CNN-based detector, trained on simulated PPG signals, uses the scalograms of the continuous wavelet transform computed in 5-s segments as an input. A pulse-based detector operates in the time domain and identifies arrhythmias according to the pulse rate obtained from the pulse-to-pulse intervals.

4. Detection of the ectopic beats in the wrist PPG signal is described. A reference ECG-based ectopic beat detector relying on the bench-marked open-source software is also presented. The ectopic beats detected by both approaches are used to assess the ectopic burden.

3. DATABASES

Four different databases and a dataset of simulated signals have been used in this work. A standardized artifact database and an ambulatory database from patients in cardiac rehabilitation were used to characterize artifacts typical of wrist PPG in daily living. A database with episodes of life-threatening arrhythmias was used to evaluate the adequacy of the model and investigate the performance of life-threatening arrhythmia detectors. Another ambulatory database from HD patients was used to investigate the feasibility to assess the ectopic burden from the wrist PPG. The dataset of simulated signals was used to train the CNN-based life-threatening arrhythmia detector. Data and all relevant performance measures are described below.

3.1. Standardized artifact database

The standardized artifact database, created by performing artifact-inducing activities, was employed to determine the thresholds for artifact classification into four distinct types (Section 4.1.1 on page 51). The database consists of signals from ten healthy participants (five females), with age 27.1 ± 2.3 years and body-mass index 22.3 ± 2.5 kg/m^2, gathered at Biomedical Engineering Institute (Kaunas, Lithuania) on a voluntary basis. The database was collected by using a wrist-worn device, shown in Fig. 3.1, capable of synchronously acquiring PPG (green light-emitting diode) and three-axis accelerometer signals, sampled at 100 Hz, and a two-lead ECG, sampled at 500 Hz [125]. The database was collected according to the following protocol in which the participants had to [87]:

1) remain still for 1 min with the properly attached wrist-worn device;
2) perform four different periodic hand motions (index finger tapping, fist opening and closing, radial and ulnar deviation, wrist extension and flexion) for 50 s with 10-s rest period in between;
3) perform three different periodic forearm motions (horizontal hand waving, vertical hand shaking, running arm swing) for 50 s with 10 s of rest in between and 50 s of intensive haphazard forearm motion with 10 s of rest;
4) move the device intentionally with the other hand for 1 min to imitate device displacement;
5) remain still for 1 min with the loosely attached device to imitate poor contact.

The periodic motions were performed at a frequency of 0.5 Hz by using a metronome.

Evaluating the performance of artifact classification
Twenty five 2-s artifacts of each type were extracted for each participant resulting in a balanced dataset containing 1000 artifacts in total. To investigate the influence of
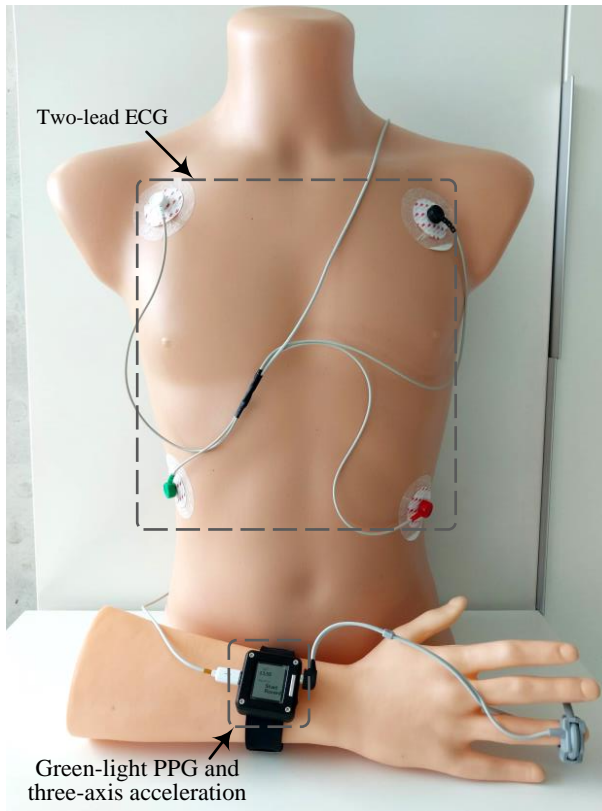
Figure 3.1. A wrist-worn device used for acquisition of PPG, ECG and accelerometer signals. A finger PPG sensor, seen in the picture, was not used in this work

the minimal artifact duration $d_{\min}$ on the classification performance, two additional datasets of 4-s and 6-s artifacts were also constructed. The classification performance is assessed by accuracy *Acc* defined as the number of correctly identified artifacts divided by the total number of artifacts [126].

Section 3.1 has been quoted verbatim from the previously published article: [13].

3.2. Ambulatory database for artifact characterization

The ambulatory database, collected by using the same device described in Section 3.1, was used to analyze artifact characteristics (Sections 4.1.2 and 4.1.3 on pages 51 and 53). Thirty-two patients (six females), 70.5 ± 9.4 years old, with body-mass index 28.0 ± 5.2 kg/m^2, were enrolled at Kulautuva Rehabilitation Hospital of Kaunas Clinics (Kaunas, Lithuania), with the approval by Kaunas Region Biomedical Research Ethics Committee (No. BE-2-20). The total monitoring time was 686.1 h (21.4 ± 3.4 h per patient). The database was gathered during cardiac rehabilitation after myocardial infarction, thus the patients were physically active for several hours during

the monitoring period, including participation in guided workout sessions.

Section 3.2 has been quoted verbatim from the previously published article: [13].

3.3.   Database with episodes of life-threatening arrhythmias

The PhysioNet/CinC 2015 Challenge database [102, 127] is one of the very few publicly available PPG databases containing episodes of life-threatening arrhythmias, in this case, extreme bradycardia and ventricular tachycardia. Thus, the database was employed in this work for multiple tasks, namely, to evaluate the adequacy of the model for simulating life-threatening arrhythmias in PPG (Section 4.2 on page 55), to test the performance of life-threatening arrhythmia detectors on real PPG signals (Section 4.3.1 on page 58), and, finally, to investigate the influence of artifacts, encountered in wrist PPG, on life-threatening arrhythmia detection (Section 4.3.2 on page 63). Only those recordings with the underlying sinus rhythm and the episodes of extreme bradycardia and ventricular tachycardia, with at least one ECG lead eligible for R-peak detection, were considered in this work.

ECG and PPG signals were sampled at 250 Hz with 12-bit precision. While each 5-min recording was originally reviewed by expert annotators who indicated whether the recording contains extreme bradycardia or ventricular tachycardia, the episode onset and end were not annotated. Therefore, the boundaries of arrhythmia episodes were manually annotated by using the simultaneously recorded ECG signals by relying on the information on the heart rate and beat morphology, while assuming a minimum episode length of three or five beats, depending on the subset. An episode was annotated as extreme bradycardia if the heart rate dropped below 40 bpm, and as ventricular tachycardia if the heart rate exceeded 120 bpm. Episodes were considered as individual if separated by at least three beats with no arrhythmia. Table 3.1 lists individual recordings assigned to separate subsets, each dedicated to one of the tasks. The description of each subset is provided below, and the main characteristics of the subsets are summarized in Table 3.2.

Evaluating the adequacy of the model

The original and adjusted models for simulating life-threatening arrhythmias were evaluated on the subset of 40 recordings, listed in Table 3.1, containing PPG signals of sufficient quality free from artifacts. The last minute of each recording was used to evaluate the models since this part of the signal contains the episode of life-threatening arrhythmia that caused the alarm.

ECGs were used for extracting RR interval series, which served as an input to the simulation model. PPGs were filtered with a band-pass zero-phase finite impulse response filter with cut-off frequencies at 0.5 and 15 Hz. A single PPG pulse template of distinctive morphology, free from noise and artifacts, was extracted from every PPG

Table 3.1. Selected recordings from the PhysioNet/CinC Challenge 2015 database containing episodes of extreme bradycardia and ventricular tachycardia

Extreme bradycardia					Ventricular tachycardia									
	Model adequacy	Detection test set I	Detection test set II	Artifact influence		Model adequacy	Detection test set I	Detection test set II	Artifact influence		Model adequacy	Detection test set I	Detection test set II	Artifact influence
b183l	+				v131l		+	+	+	v648s	+	+	+	+
b220s				+	v132s	+	+		+	v696s	+	+	+	+
b227l	+	+	+	+	v158s	+				v701l		+	+	+
b228s	+	+	+	+	v159l	+				v714s		+		+
b229l	+	+	+	+	v206s	+	+	+	+	v726s		+		+
b265l	+	+	+	+	v253l	+	+	+	+	v729l		+	+	+
b299l	+	+	+	+	v254s	+	+		+	v733l	+	+		+
b455l	+	+	+	+	v255l		+	+	+	v748s	+	+	+	+
b456s		+	+	+	v275l		+	+	+	v758s	+	+	+	+
b515l	+	+	+	+	v290s		+	+	+	v769l	+	+	+	+
b516s	+	+	+	+	v309l		+	+	+	v772s		+	+	+
b517l	+	+	+	+	v318s	+				v773l		+		+
b560s	+				v368s	+	+	+	+	v788s	+	+		+
b561l	+				v369l		+	+	+	v797l		+	+	+
b562s	+				v404s		+		+	v803l		+	+	+
b656s	+	+	+	+	v471l	+	+	+	+	v806s	+	+		+
b764s	+	+	+	+	v573l	+				v815l		+	+	+
b794s	+	+	+	+	v574s	+	+	+	+	v818s	+	+	+	+
b838s	+	+	+	+	v628s	+	+	+	+	v828s		+	+	+
b839l		+	+	+	v630s	+	+	+	+	v831l		+	+	+
					v632s		+		+	v837l		+	+	+
					v635l	+	+	+	+					

signal and used for estimating the model parameter vector $\vec{\theta}$.

The adequacy of the models $\mathcal{M}_o$ and $\mathcal{M}_a$ is evaluated by computing the RMS error between the real and modeled PPG signals,

$$E = \sqrt{\frac{1}{N}\sum_{n=1}^{N}\left(u(n)-x(n)\right)^2}, \qquad (3.1)$$

where n is a sample number, N is a total number of samples in the modeled signal $x(n)$, and $u(n)$ is the real signal. Cross-correlation was used to align real and modeled signals. Prior to computing E, both signals were normalized to the unit amplitude of the first PPG pulse.

**Testing the performance of life-threatening arrhythmia detectors**

The CNN-based and pulse-based life-threatening arrhythmia detectors were evaluated on the subset of 54 recordings, referred to as test set I, listed in Table 3.1. For

Table 3.2. Main characteristics of the subsets of the PhysioNet/CinC Challenge 2015 database used in this work

Subset	Characteristic	Extreme bradycardia	Ventricular tachycardia
Model adequacy	Recordings, #	17	23
	Total duration, min	17	23
	Total episode duration, s	305	66
	Median (range) episode length, beats	6 (5–21)	6 (5–11)
Detection test set I	Recordings, #	15	39
	Total duration, min	79	204
	5-s segments, #	948	2448
	5-s segments with arrhythmia, #	52	64
	Median (range) episode length, beats	4 (3–21)	6 (3–58)
Detection test set II	Recordings, #	15	29
	Total duration, min	79	153
	5-s segments, #	948	1836
	5-s segments with arrhythmia, #	52	45
	Median (range) episode length, beats	4 (3–21)	7 (3–58)
Artifact influence (simulated PPGs)	Recordings, #	16	39
	Total duration, min	960	2340
	Episodes, #	227	492
	Median (range) episode length, beats	5 (5–21)	7 (5–25)

this subset, a shorter minimum episode length of three beats was assumed to preserve as many arrhythmia episodes as possible. Figure 3.2 shows two excerpts from the recordings with extreme bradycardia and ventricular tachycardia episodes.
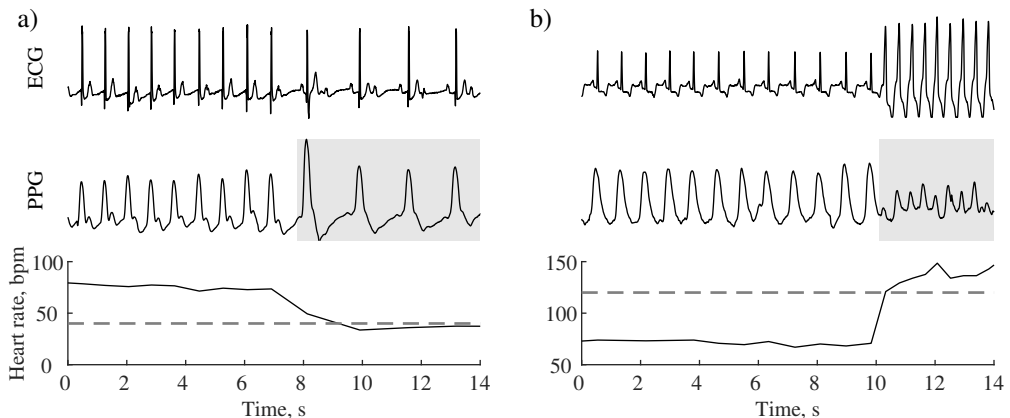
Figure 3.2. Synchronous ECG and PPG signals from the PhysioNet/CinC Challenge 2015 Database together with heart rate during a) extreme bradycardia (< 40 bpm) and b) ventricular tachycardia (> 120 bpm). The ECG-based annotation is marked with a shaded area

Due to decreased hemodynamics during tachycardia, much reduced or no periodic

pulsations were observed in 10 of the 39 recordings with ventricular tachycardia, illustrated in Fig. 3.3. Therefore, a part of test set I was defined excluding these 10 recordings, referred to as test set II.
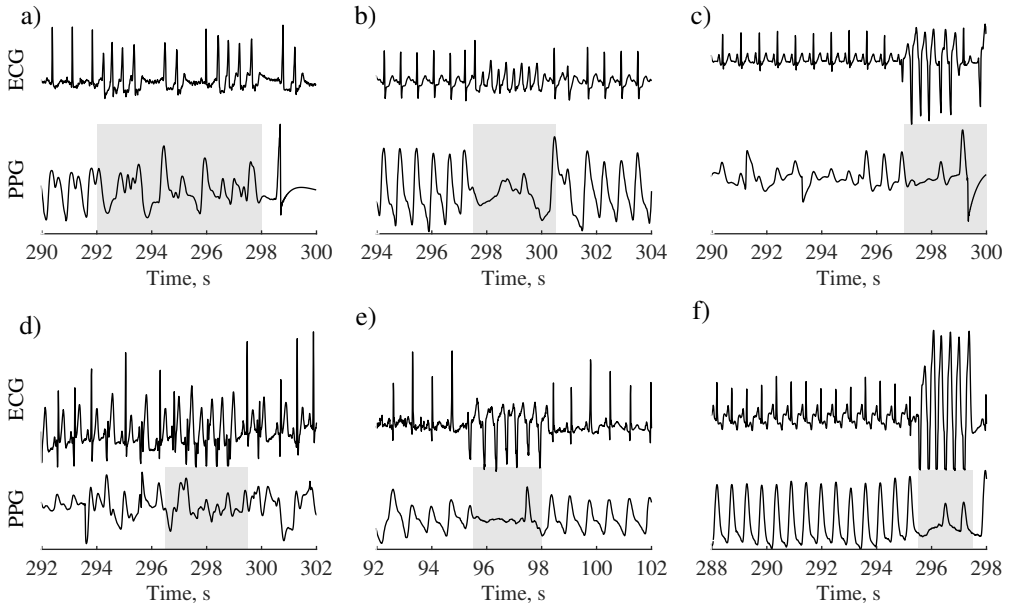
Figure 3.3. a) to f) ECG and PPG signals from the PhysioNet/CinC Challenge 2015 Database with heavily reduced or no periodic pulsations during ventricular tachycardia. The ECG-based annotation is marked with a shaded area

Based on the annotation, each 5-s segment used for detector evaluation is labeled as either extreme bradycardia, ventricular tachycardia, or other rhythm. Bradycardia is assigned if the episode lasts for at least 50% of the 5-s segment. Since tachycardia is characterized by higher frequencies, tachycardia is assigned if the episode lasts for at least 25% of the 5-s segment. The lower percentage reflects the obvious fact that more beats are contained in an episode of tachycardia than in an episode of bradycardia when both episodes have the same length in seconds.

Detection performance is evaluated in terms of sensitivity Se and specificity Sp by segmentwise comparison of the detector output to the labeling of the annotation described above. Se is defined by the number of correctly detected bradycardia (tachycardia) segments divided by the total number of bradycardia (tachycardia) segments, whereas Sp is defined by the number of correctly detected non-bradycardia (non-tachycardia) segments divided the total number of non-bradycardia (non-tachycardia) segments. These two measures are computed from the entire recordings, not just from the segments assessed to be of acceptable quality. The agreement between the CNN-based and pulse-based detectors is evaluated in terms of Cohen's kappa coefficient [128].

Investigating the influence of wrist artifacts

The developed PPG artifact model is applied to illustrate the influence of artifacts on the detection of life-threatening arrhythmias when using the pulse-based detector. ECGs from the subset of 55 recordings, listed in Table 3.1, served as a basis to simulate equivalent PPGs with extreme bradycardia and ventricular tachycardia episodes.

Taking into account that the duration of the PhysioNet/CinC Challenge 2015 recordings is only 5 min, which is too short to properly imitate arrhythmia detection in long-term recordings, the RR intervals were replicated and concatenated to form a 1-h-long RR interval series. By using the series as an input to the model described in Section 2.2.1 on page 31, a 1-h pulsatile PPG component was generated and contaminated with artifacts of the desired properties. A Dawber's pulse Type 3 was chosen for simulating PPGs since it is a predominant pulse type among older individuals [108]. The main characteristics of the generated subset for investigating the influence of artifacts on life-threatening arrhythmia detection are summarized in Table 3.2.

The detection performance is investigated in terms of *Se*, defined as the number of correctly detected bradycardia (tachycardia) episodes divided by the total number of bradycardia (tachycardia) episodes, as well as the number of false alarms per hour, and the positive predictive value, defined as the number of correctly detected bradycardia (tachycardia) episodes divided by the total number of detected bradycardia (tachycardia) episodes.

Parts of Section 3.2 have been quoted verbatim from the previously published articles: [12, 13, 14].

3.4. Dataset of simulated signals with life-threatening arrhythmias

Due to the lack of public PPG databases with annotated episodes of life-threatening arrhythmias, an unconventional approach was adopted in which simulated PPG signals were used for the training and validation of a CNN, described in Section 2.3.1 on page 35, for extreme bradycardia and ventricular tachycardia detection, whereas real, manually annotated PPG signals, described in Section 3.3, were used for testing.

Different RR interval series with one episode of extreme bradycardia were created by concatenating three subseries of RR intervals, i.e., normal sinus rhythm, bradycardia, and normal sinus rhythm. The two subseries with the normal sinus rhythm were randomly selected from the MIT–BIH Normal Sinus Rhythm Database [102] so that 50–100 RR intervals appeared before the episode and 1–100 RR intervals after the episode (the actual number of intervals before and after were selected randomly); in all subseries of the sinus rhythm, the heart rate was above 60 bpm. In total, 147 RR interval subseries with extreme bradycardia were selected from the PhysioNet/CinC Challenge 2017 database [129]. Each series was approved by visual inspection to ensure that no aberrant RR intervals were included.

On the other hand, RR interval series with one episode, and, in a few cases,

a handful of episodes, of ventricular tachycardia are contained in the Spontaneous Ventricular Tachyarrhythmia Database [102]. Since this database is not annotated, the episode onset and end were determined manually, by assuming a minimum episode length of three beats. In all recordings, tachycardia was surrounded by the sinus rhythm, and, therefore, concatenation was superfluous. From the 135 recordings, a total of 94 RR interval series were selected with episodes having a heart rate of at least 120 bpm.

By using the created RR interval series as an input to the model described in Section 2.2.1 on page 31, a dataset of simulated PPGs containing episodes of extreme bradycardia and ventricular tachycardia was created. Stationary simulated noise, described in [101], was also added. Table 3.3 summarizes the main characteristics of the dataset of simulated signals.

Table 3.3. Main characteristics of the simulated dataset used for training and validation of the CNN-based life-threatening arrhythmia detector

Characteristic	Extreme bradycardia	Ventricular tachycardia
RR interval series, #	147	94
Total duration, min	600	1200
5-s segments, #	7200	14400
5-s segments with arrhythmia, #	1092	437
Median (range) episode length, beats	23 (8–51)	14 (4–528)

Section 3.4 has been quoted verbatim from the previously published article: [14].

3.5. Ambulatory database from hemodialysis patients

The ambulatory database from HD patients was used to investigate the feasibility to assess the ectopic burden from the wrist PPG (Section 4.4 on page 66). A total of 50 adult ESKD patients receiving maintenance HD in the department of Nephrology, Hospital of Lithuanian University of Health Sciences Kaunas Clinics (Kaunas, Lithuania) were enrolled, with the approval by Kaunas Region Biomedical Research Ethics Committee (No. BE-2-43). The patients were treated with thrice-weekly HD for more than three months before the enrollment. In all patients, an initial medical history evaluation and routine laboratory tests were performed. The exclusion criteria were any condition with poor prognosis, such as myocardial infarction or ischemic stroke during the previous month, or congestive heart failure class IV.

The database was collected by using the same device described in Section 3.1. ECG served as a reference for ectopic beat detection. Data acquisition started on the dialysis day, spanned through the night, and was terminated the next day after 24 h from the beginning. The device was placed on the arm without an arteriovenous fistula. In case a central venous catheter was used as HD access, the device was placed on the nondominant arm. The exact starting and end times of the HD session, and the cause

of the current hospitalization were documented by the attending nephrologists in the data-collecting sheets. Patients were only asked to document the exact bedtime and wake-up time.

Due to medical reasons, four patients had their HD performed at the end of data acquisition, and one patient missed the dialysis due to emergency surgery. Of the initial 50 patients, data from 2 were excluded due to permanent atrial fibrillation and from 1 due to lost reference ECG. The demographic and clinical characteristics of the remaining 47 patients are given in Table 3.4.

Table 3.4. Demographic and clinical characteristics of 47 HD patients. SD, standard deviation; BMI, body mass index; CVC, central venous catheter; AVF, arteriovenous fistula

Characteristic		Characteristic	
Age, mean (SD) years	61.1 (15.8)	Hospitalized due to, # (%)	40 (85.1)
Sex, # (%)		Kidney failure	6 (12.8)
Male	28 (59.6)	Potential kidney recipient	2 (4.3)
Female	19 (40.4)	AVF formation	1 (2.1)
BMI, mean (SD) kg/m^2	24.7 (4.3)	AVF dysfunction	4 (8.5)
HD duration, mean (SD) h	3.4 (0.5)	AVF thrombosis	5 (10.6)
Vascular access, # (%)		CVC dysfunction	3 (6.4)
CVC	21 (44.7)	Sepsis	3 (6.4)
AVF	26 (55.3)	Other infection	10 (21.3)
Ambulatory, # (%)	7 (14.9)	Other causes	6 (12.8)

Evaluating the detection performance of high-risk ectopic burden

Based on the findings in [130] and meta-analysis [48], a cut-off of 30 ectopic beats/h is selected to define a high-risk ectopic burden. PPG-based detection of 1-h segments with a high-risk ectopic burden is assessed in terms of sensitivity *Se* and specificity *Sp* against the reference ectopic burden by using the segments with acceptable-quality ECG for at least 45 min.

Section 3.5 has been quoted verbatim from the manuscript under review: [15].

3.6. Conclusions of the chapter

1. Standardized and ambulatory databases were used for the artifact analysis. The standardized database allows for the objective classification of artifacts into four distinct types, whereas the ambulatory database provides characteristics of the artifacts in the wrist PPG acquired in free-living activities.

2. A single clinical database with PPG and ECG signals containing episodes of life-threatening arrhythmias was used in three nonoverlapping parts of the work. Such exploitation of the database is dictated by the lack of publicity available PPG databases with annotated arrhythmia episodes.

3. RR interval series with the normal sinus rhythm, extreme bradycardia, and ventricular tachycardia from three separate databases were used to create a dataset of simulated PPGs containing episodes of life-threatening arrhythmias. The dataset was employed to train and validate a deep learning algorithm for life-threatening arrhythmia detection.

4. A database obtained from HD patients under uncontrolled conditions was used to investigate the feasibility of assessing the ectopic burden from wrist PPG signals. Since the blood flow in the HD patient's wrist may be affected by a nonfunctional arteriovenous fistula or vascular calcification, the database provides insights into the real-life performance of the PPG-based approach.

4. RESULTS

4.1. Artifact characteristics in the ambulatory database

4.1.1. Parameter settings for artifact classification

Figure 4.1 shows artifact classification accuracy as a function of threshold values using the standardized artifact database, described in Section 3.1 on page 41. When the minimal artifact duration d_{min} is set to either 4 s or 6 s, similar classification accuracy is obtained, however, it is slightly better for 6 s. As a trade-off, 4-s minimal artifact duration is chosen to ensure that short artifacts are not overlooked. For $d_{\mathrm{min}} = 4$ s, the highest classification accuracy is obtained for the threshold values $\eta_{\mathrm{u}} = 0.08$ g, $\eta_{\mathrm{v}} = 11$ and $\eta_{\mathrm{w}} = 0.015$. This threshold set yields the average classification accuracy of 98%.
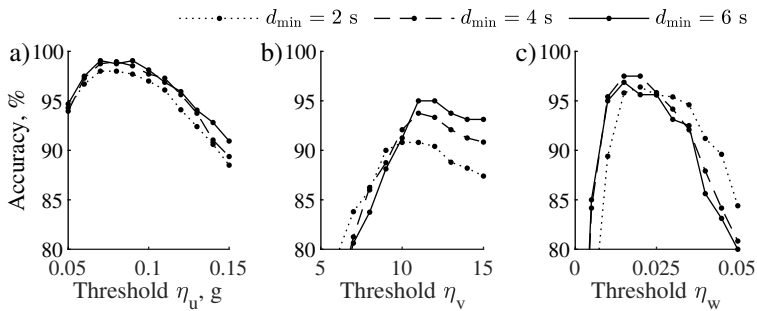

Figure 4.1. Artifact classification accuracy as a function of a classification threshold for a different minimal artifact duration. a) Classification accuracy between two groups of artifacts of which one group contains device displacement and forearm motion, and the other contains hand motion and poor contact. b) Classification accuracy between device displacement and forearm motion. c) Classification accuracy between hand motion and poor contact

4.1.2. Prevalence of different-type artifacts

Analysis of the ambulatory database, described in Section 3.2 on page 42, shows that 26.8% of the total PPG duration is artifact-corrupted, covering from 13.6% to 48.6% depending on the recording (Fig. 4.2). Most of the artifacts were identified as device displacement, forearm motion, and hand motion, corrupting 6.4%, 6.2%, and 6.0%, whereas only 1.8% was assigned to poor contact. In addition, 6.4% of the PPG duration was flagged by the SQI as containing artifacts, but was not attributed to any type due to the artifact duration shorter than 4 s or unavailability of an acceptable-quality reference ECG.

The percentage of the artifact-corrupted PPG within the day is given in Fig. 4.3. On average, at least a quarter of the PPG duration contains artifacts from 06:00 to 22:00 and drops markedly outside this period, which coincides well with the most active period of the day. Based on this finding, PPGs from the ambulatory database
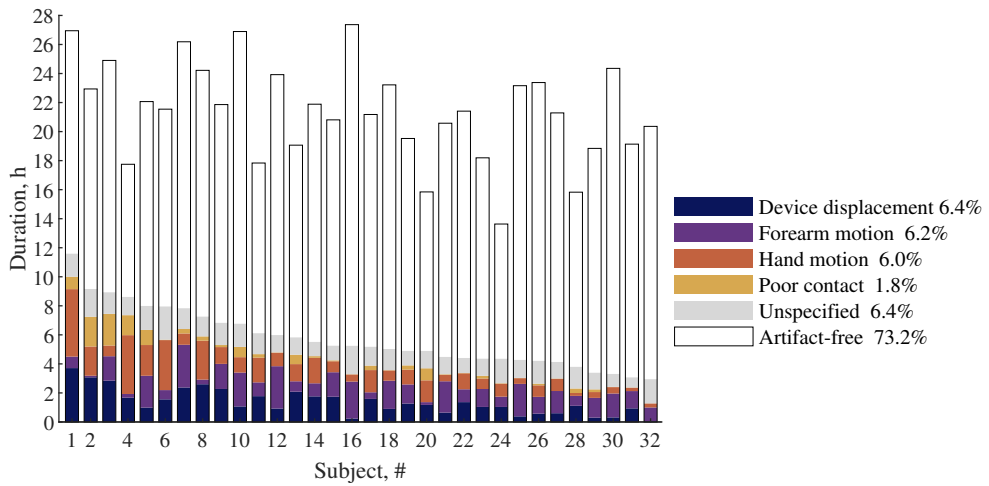
Figure 4.2. Duration of different-type artifacts and artifact-free PPG intervals for all recordings of the ambulatory database. Data are sorted in descending order according to the total artifact duration

are subdivided to the periods of day- (06:00–22:00) and night-time (22:00–06:00). By using such subdivision, 37.0% of the total PPG duration is attributed to artifacts for day-time, and 8.8% for night-time.
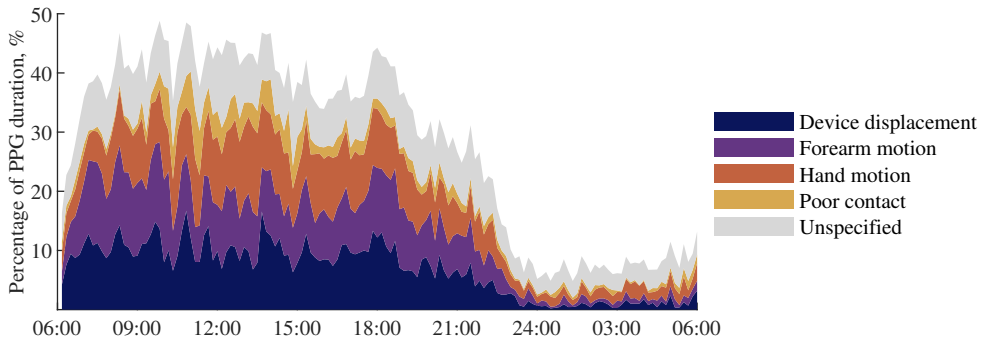
Figure 4.3. Stacked diagram of the percentage of different-type artifacts occurring within the day. The artifact percentage is calculated in 10-min nonoverlapping windows for the entire ambulatory database

Discussion

The analysis of PPGs acquired during cardiac rehabilitation provides insights into the quality of the wrist PPG encountered in free-living activities. In line with the recent findings [100], this work shows that the percentage of the artifact-corrupted PPG markedly increases during day-time, mostly due to device displacement and forearm motion. This result supports a common observation that a substantial part of the day-time PPG is of insufficient quality for use in health monitoring applications [100].

In the ambulatory database, a quarter of the PPG duration was identified as corrupted by artifacts, which is higher than 10.8% reported in [64], but much lower than 44% in [66] and 65.2% in [100]. Possibly, the discrepancy between the studies arose from different conditions to acquire a PPG. Also, varying signal quality requirements, which often depend on the application, may have a substantial impact. Even slight PPG disturbance can be intolerable when PPG morphology is a subject to analysis, but may have a negligible effect on the heart rate estimation. By applying a criterion of successful pulse detection, 42.4% of the total PPG duration was excluded in [67]. However, the percentage of unanalyzable PPG reached 76.0% by also accounting for the accelerometer-identified movement.

The identification of artifacts in the PPG depends on the chosen approach to PPG quality assessment. The most prevalent PPG artifacts are movement-related; therefore, a common practice is to involve an accelerometer for artifact identification [65, 66, 67, 91, 92, 93, 94]. Such approach may be ineffective in certain situations since artifacts may arise from other sources as well, e.g., poor contact and fine hand movements, which do not reflect in the accelerometer signals [87, 91]. On the other hand, accelerometer-identified motion will not necessarily be a sign of the artifacts in the PPG. Relying solely on the accelerometer, a one-sixth of PPG pulses were falsely assigned to artifact-corrupted or artifact-free classes in the ambulatory database. That is, 8.3% of pulses were considered as artifact-free when using the SQI, although flagged as artifacts by analyzing the accelerometer signals. Contrarily, 8.3% of artifact-corrupted pulses, identified by the SQI, were not reflected in the accelerometer signal. In this work, pulse-to-pulse SQI is preferred instead of a fixed-window SQI to achieve finer time resolution. Out of several pulse-to-pulse SQIs [64, 131, 132, 133], only the one in [64] has been tested in long-term wrist PPGs acquired outside the laboratory setting and was therefore implemented in this work.

4.1.3. Characteristics of artifacts in the wrist photoplethysmogram

The estimated transition probabilities from an artifact-free interval to each artifact type for day- and night-time periods are given in Table 4.1. The probabilities of having the device displacement and forearm motion artifacts are lower during night-time due to reduced movement, and vice versa during the day-time.

Table 4.1. Estimated transition probabilities from an artifact-free interval to a particular artifact type

	Device displacement, $\hat{p}_{01}$	Forearm motion, $\hat{p}_{02}$	Hand motion, $\hat{p}_{03}$	Poor contact, $\hat{p}_{04}$
Day-time	0.23	0.37	0.31	0.09
Night-time	0.16	0.24	0.45	0.15

Figure 4.4 shows that the histograms of the duration of different-type artifacts and artifact-free intervals resemble an exponential distribution. Artifact-free intervals are prolonged during the night-time as supported by the decreased rate parameter $\hat{\lambda}_0$. This finding coincides with the fact that all types of artifacts are less frequent and usually shorter during the night-time.
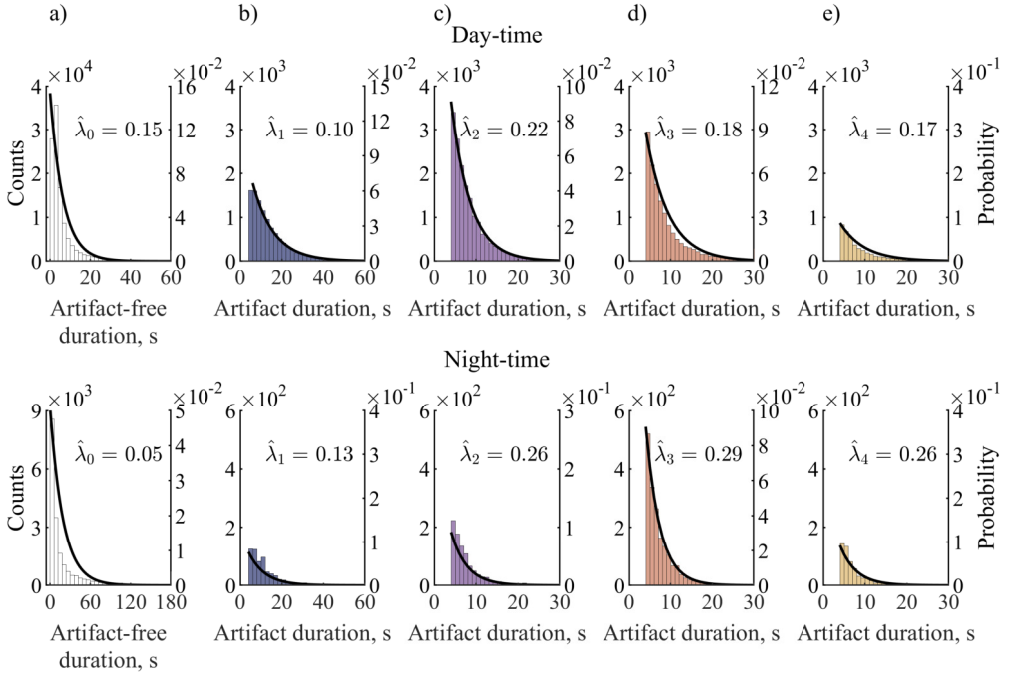

Figure 4.4. Histograms of the day- and night-time duration of a) artifact-free intervals, b) device displacement, c) forearm motion, d) hand motion, and e) poor contact artifacts. The histograms start at 4-s bin because of the chosen minimal artifact duration. Solid lines show the fitted exponential models with the estimated rate parameters $\hat{\lambda}_i$ given above

Figure 4.5 presents the weighted average PSDs and the estimated slopes of different-type artifacts. The PSDs of hand motion and poor contact are apparently flatter because the spectral power is moved towards high frequencies, thus suggesting that artifacts are more noise-like.

The normalized RMS amplitude of different-type artifacts follows a gamma distribution, see Fig. 4.6. Device displacement, on average, causes the largest artifact amplitude which is 22 times larger than that of the pulsatile PPG component. This proportion is considerably smaller for other artifact types.

Section 4.1 has been quoted verbatim from the previously published article: [13].
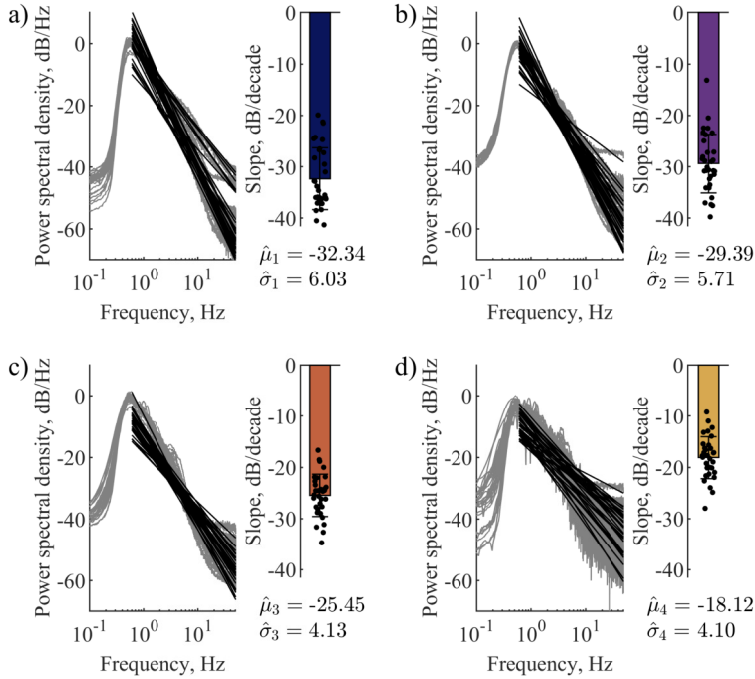
Figure 4.5. Average PSDs and their estimated slopes of a) device displacement, b) forearm motion, c) hand motion, and d) poor contact artifacts for each recording of the ambulatory database. The PSDs up to 0.5 Hz are suppressed due to the removed slow-changing PPG component. Solid black line stands for the fitted PSD slope. Error bars show mean $\hat{\mu}_i \pm$ standard deviation $\hat{\sigma}_i$

4.2. Adequacy of the model of life-threatening arrhythmias

Examples of real and modeled PPG signals with the episodes of extreme bradycardia and ventricular tachycardia are presented in Fig. 4.7. Compared to the real PPG signal, some pulses of extreme bradycardia, simulated by using the original model $\mathcal{M}_o$, is of a considerably larger pulse amplitude. Meanwhile, the amplitude is resembled properly by the adjusted model $\mathcal{M}_a$. The episode of ventricular tachycardia is simulated similarly by both models, though neither modeled signal corresponds precisely to the real PPG.

Figure 4.8 displays RMS error E between the real and simulated PPG signals, obtained on the subset of the database with episodes of life-threatening arrhythmias, described in Section 3.3 on page 43. The advantage of the adjusted model $\mathcal{M}_a$ is particularly obvious for extreme bradycardia, since E computed within the arrhythmia episode is 20.6% lower compared to $\mathcal{M}_o$. On the other hand, when the error is found for the entire signal with the underlying sinus rhythm and the episodes of extreme bradycardia, the difference between the models is less obvious, thus suggesting a similar
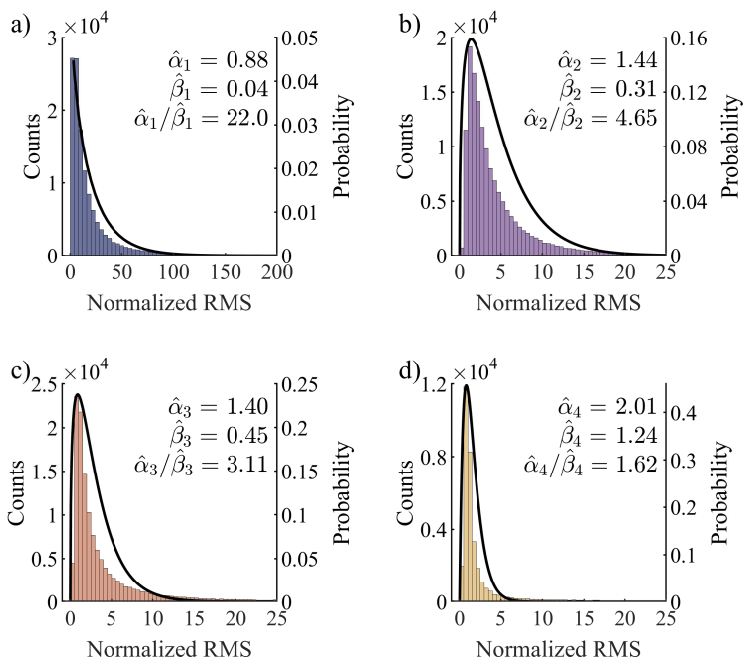
Figure 4.6. Histograms of the normalized RMS amplitude in 1-s segments of a) device displacement, b) forearm motion, c) hand motion, and d) poor contact artifacts. The fitted gamma models are plotted as solid lines with the estimated shape $\hat{\alpha}_i$ and rate $\hat{\beta}_i$ parameters given above. The ratio $\hat{\alpha}_i/\hat{\beta}_i$ yields the mean of the distribution

performance of the models for other rhythms, i.e., the sinus rhythm and premature ectopic beats. This can be supported by the observation that $\mathcal{M}_a$ only slightly improves simulation of ventricular tachycardia, showing a 4.8% lower error for the entire signal and 3.3% for arrhythmia episode. It should be noted that the error computed within the arrhythmia episode is larger for both arrhythmia types due to the manifestation of noise and artifacts.

Discussion

When developing arrhythmia detectors, it is crucial to distinguish between arrhythmia-induced and artifact-induced changes in the PPG signal. This implies that simulated arrhythmia episodes should closely resemble the changes in the pulse amplitude and morphology. The original model assumes that the pulse amplitude is inversely proportional to the duration of the preceding RR interval [101], however, this assumption is debatable [110]. Accordingly, the adjusted model takes into account the relationship between the duration of the RR interval and stroke volume to determine the amplitude of the PPG pulse [110, 111]. The adjusted model outperforms the original when simulating extreme bradycardia thanks to the signal-dependent protective thresh-
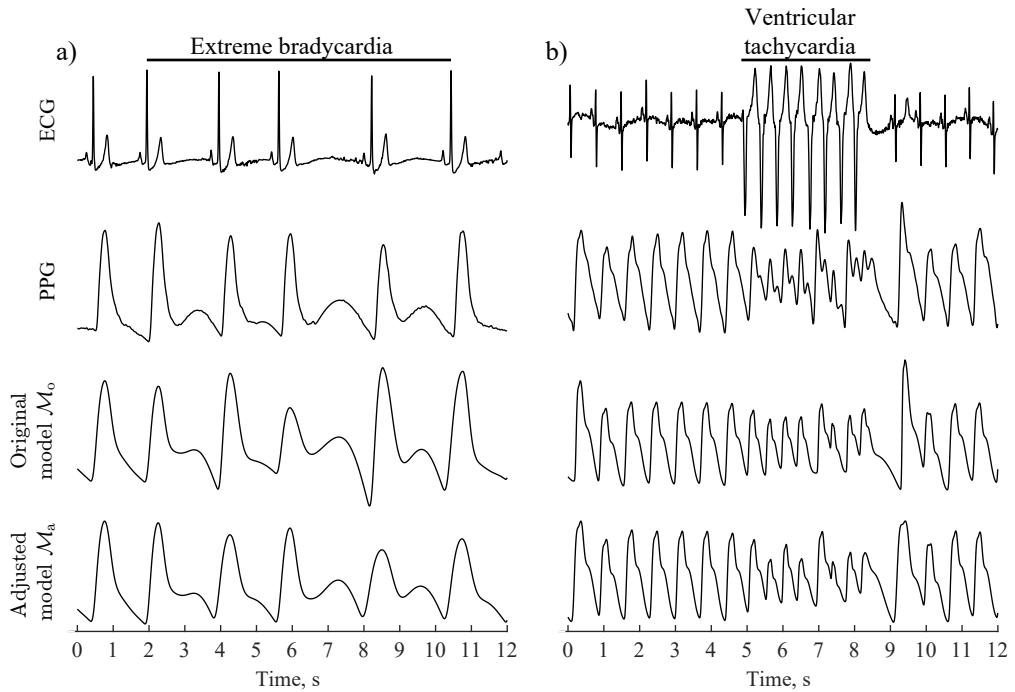
Figure 4.7. ECG, PPG and modeled PPG signals with the episode of a) extreme bradycardia (recording b299l) and b) ventricular tachycardia (recording v206s)
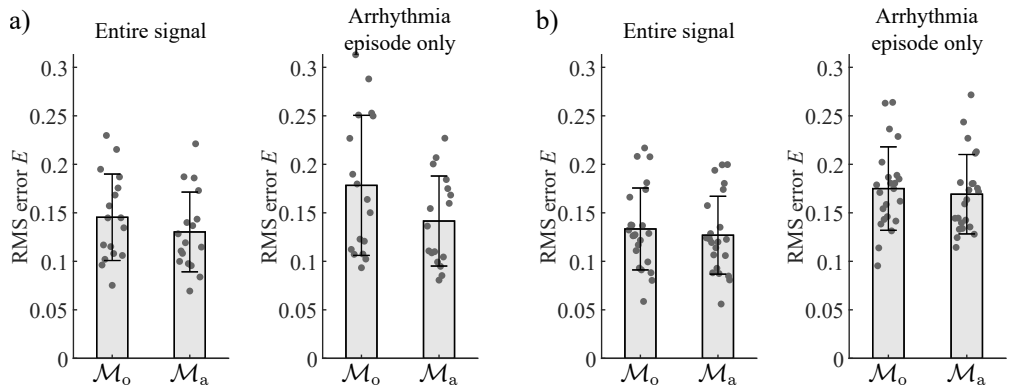
Figure 4.8. RMS error E between real and simulated signals with the episode of a) extreme bradycardia and b) ventricular tachycardia. Error bars show mean $\pm$ standard deviation

old, which sets the maximum duration of the RR interval that still allows variation in the PPG pulse amplitude. The original model was initially developed to simulate PPG signals with atrial fibrillation, which is tachycardia itself [101]. This explains why the error decreased only slightly when ventricular tachycardia was simulated while using the adjusted model.

Section 4.2 has been quoted verbatim from the previously published article: [12].

4.3. Performance of life-threatening arrhythmia detectors

4.3.1. Comparison on real photoplethysmography signals

This section presents the results obtained by using the subsets of the database with episodes of life-threatening arrhythmias, described in Section 3.3 on page 44.

Influence of noise in training PPGs

Figure 4.9 shows detection performance when the CNN was trained with simulated PPGs at different SNRs. For each SNR, 50 training sessions were performed, and the average sensitivity and specificity were obtained. Lowering the SNR of the training signals results in a decrease in sensitivity and an increase in specificity irrespective of whether bradycardia or tachycardia is detected. Since the best performance in terms of both sensitivity and specificity was obtained for noise-free PPGs when training the CNN, the CNN was trained with noise-free simulated PPGs before analyzing test sets I and II, see below.
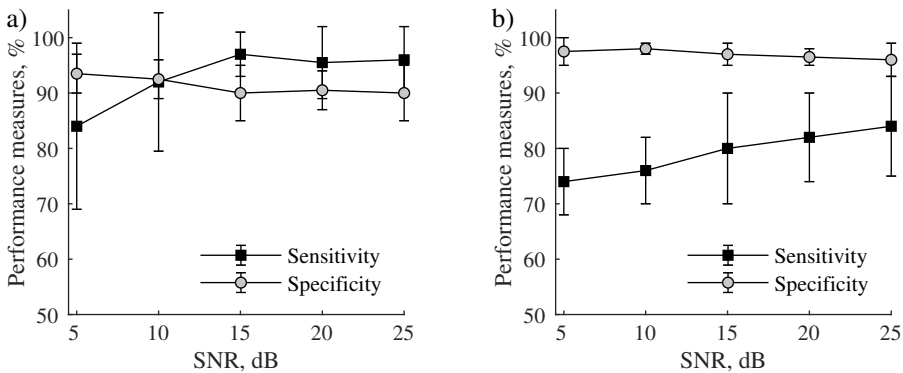
Figure 4.9. a) Extreme bradycardia and b) ventricular tachycardia detection performance for a CNN trained with simulated PPGs at different SNRs. The results are based on test set II

Performance on test set I

Figure 4.10 presents the receiver operating characteristics (ROCs) of CNN-based detection of life-threatening arrhythmias, obtained by varying the two detection thresholds. No ROC is presented for the pulse-based detector as its structure does not embrace a detection threshold.

Table 4.2 presents the performance of the CNN-based detector by using the thresholds that put more emphasis on sensitivity, and the pulse-based detector. Without signal quality assessment, the CNN-based detector offers higher sensitivity for both
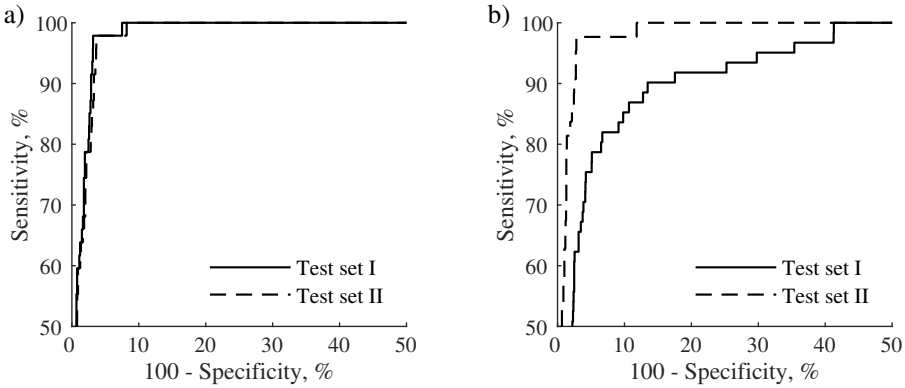
Figure 4.10. ROCs of CNN-based detection of a) extreme bradycardia and b) ventricular tachycardia using test sets I and II

bradycardia and tachycardia, and considerably higher specificity for tachycardia than does the pulse-based detector. The exception is bradycardia specificity which is better for the pulse-based detector.

Table 4.2. Performance and agreement of the CNN- and pulse-based detectors on test set I, without and with signal quality assessment (SQA). Square brackets indicate 95% confidence interval

Test set I		Extreme bradycardia		Ventricular tachycardia	
		No SQA	SQA	No SQA	SQA
CNN-based	*Se*, %	**98.1** [89.3, 100]	**98.1** [88.7, 100]	**79.7** [68.2, 88.5]	**76.6** [65.0, 86.1]
	Sp, %	**96.7** [96.0, 97.2]	**97.9** [97.4, 98.4]	**95.6** [94.9, 96.3]	**96.6** [96.0, 97.2]
Pulse-based	*Se*, %	**96.1** [89.0, 98.8]	**94.7** [87.2, 98.6]	**68.5** [57.1, 78.6]	**67.1** [55.6, 77.2]
	Sp, %	**99.7** [99.5, 99.9]	**99.8** [99.6, 99.9]	**93.0** [92.1, 93.9]	**93.8** [92.9, 94.5]
	κ	**0.42** [0.32, 0.51]	**0.49** [0.39, 0.59]	**0.39** [0.32, 0.46]	**0.39** [0.31, 0.46]

With the signal quality assessment, the specificity increases for both detectors, although the increase is somewhat larger for CNN-based detection. The sensitivity decreases for both detectors and arrhythmias, except for CNN-based extreme brady-cardia detection. This decrease is primarily due to the segments in which ventricular tachycardia is either contaminated with artifacts, or the signal quality is low because of a decreased cardiac output and perfusion leading to lack of periodic pulsations.

Performance on test set II

Table 4.3 presents the performance on test set II, i.e., test set I but excluding 10 problematic tachycardia recordings with heavily reduced or no periodic pulsations. As expected, the exclusion leads to the improved sensitivity and specificity of both

detectors. However, the increase in sensitivity of the CNN-based detection is substantially larger than that of the pulse-based detector. This is likely due to the fact that the pulse-based detector relies on pulse detection rather than on the analysis of the whole 5-s PPG segment as does the CNN-based detector. For both detectors, signal quality assessment has only a minor effect on their performance.

Table 4.3. Performance and agreement of the CNN- and pulse-based detectors on test set II, without and with signal quality assessment (SQA). Square brackets indicate 95% confidence interval

Test set II		Extreme bradycardia		Ventricular tachycardia	
		No SQA	SQA	No SQA	SQA
CNN-based	*Se*, %	**98.1** [88.6, 100]	**98.1** [89.1, 100]	**97.8** [87.7, 100]	**97.8** [87.6, 100]
	Sp, %	**96.2** [95.4, 96.9]	**97.7** [97.1, 98.2]	**97.8** [97.2, 98.3]	**98.4** [97.9, 98.8]
Pulse-based	*Se*, %	**96.1** [89.0, 98.8]	**94.7** [87.3, 98.6]	**74.5** [61.0, 85.3]	**72.6** [58.8, 83.9]
	Sp, %	**99.7** [99.4, 99.9]	**99.7** [99.5, 99.9]	**96.8** [96.1, 97.4]	**97.6** [97.0, 98.2]
	κ	**0.43** [0.33, 0.52]	**0.50** [0.40, 0.60]	**0.39** [0.29, 0.49]	**0.40** [0.29, 0.51]

Figure 4.11 illustrates the outputs of the CNN- and pulse-based detectors together with correct labels. The Cohen's kappa coefficient sheds some light on the disagreement between the detector outputs, mostly dictated by a small number of 5-s segments with arrhythmias in the two test sets, and different patterns of false alarms in either of the detectors.
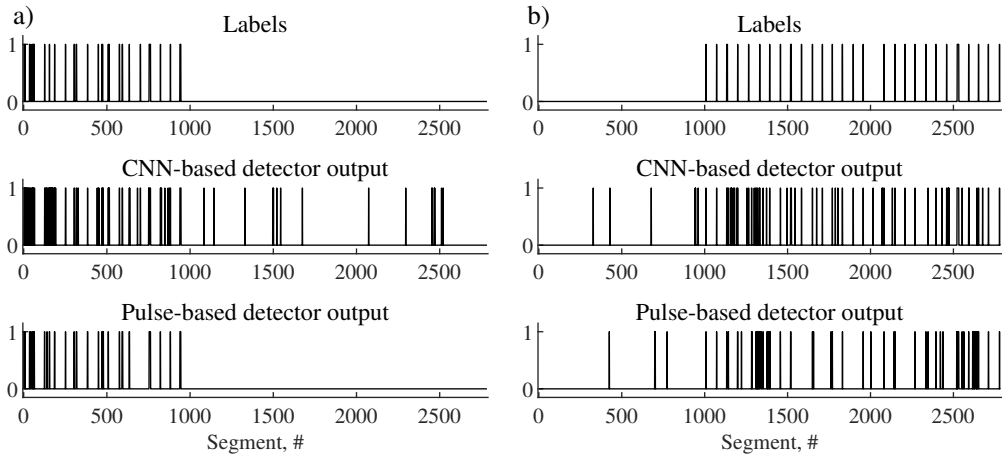
Figure 4.11. Outputs of the CNN- and pulse-based detectors for a) extreme bradycardia and b) ventricular tachycardia detection on test set II, with signal quality assessment

Discussion

Thanks to the input segmentation, the CNN-based tachycardia detector is less

sensitive to situations with reduced-amplitude pulsations than is the pulse-based detector since the scalogram carries additional information on tachycardia which helps to improve the performance. This improvement is supported by the results in Table 4.2 which show that the sensitivity of the CNN-based tachycardia detector on test set I is superior to that of the pulse-based detector, combined with better specificity of the CNN-based detector. The advantage of the CNN-based tachycardia detector becomes even more pronounced on test set II, see Table 4.3. Still, the CNN-based detector is susceptible to pulseless episodes as indicated by the low sensitivity of tachycardia detection on test set I (see Table 4.2), which contained 10 recordings with much reduced or no periodic pulsations during ventricular tachycardia. Since these recordings are excluded from test set II, the sensitivity of the CNN-based tachycardia detector reported in Table 4.3 is considerably higher.

Pairs of pulses with a rate below 40 bpm or above 120 bpm are not considered an arrhythmia. However, the CNN-based detector may falsely detect bradycardia/tachycardia in segments where a single or a slow/fast pulse pair appears, resulting in lower specificity for extreme bradycardia. Such a behavior of the CNN may be the source of disagreement between the two bradycardia detectors resulting in Cohen's kappa values of 0.42–0.50. When detecting tachycardia, CNN- and pulse-based detectors also exhibit different detection patterns as illustrated in Fig. 4.11. Apparently, the sensitivity of the pulse-based detector is highly affected by the tachycardia-caused decrease in the pulse amplitude resulting in missed beats. Even though the specificity for tachycardia detection is comparable, the sources of false alarms of the two detectors are different, and, thus, the agreement in terms of Cohen's kappa is low. Noise mimicking tachycardia misleads the pulse-based detector, whereas frequent premature ectopic beats might trick the CNN-based detector.

When reporting on the detection performance, it is essential to state whether the performance is computed using the annotations of all segments of the recordings or only the annotations of the segments which remain after signal quality assessment; the latter alternative tends to exaggerate the performance by ignoring false negatives corresponding to arrhythmia segments excluded due to unacceptable quality. In this work, the performance measures are computed independently of segment exclusion since the annotations were determined from acceptable-quality ECG signals, not from the PPG signals.

A rather basic CNN architecture was adopted in this work to demonstrate that a deep learning algorithm, trained on simulated data, can be employed to detect life-threatening arrhythmias in PPG signals. The comparison of different machine learning architectures and extensive testing of hyper-parameters are outside the scope of this work. A dual-branch CNN was selected for the detection of ventricular tachycardia and extreme bradycardia in agreement with other studies proposing multi-branch structures of multi-class classifiers, e.g., [134]. It has been argued that such structures are more

robust in mitigating overfitting issues due to a small training dataset. Moreover, each branch of a dual-branch detector can function as an independent detector adapted to ventricular tachycardia or extreme bradycardia detection.

CNN training with different segment lengths was not performed due to the fact that bradycardia and tachycardia episodes are very brief. Segment labeling was defined so that bradycardia should occupy at least 50% of a 5-s segment, while tachycardia should occupy at least 25% of a 5-s segment. Therefore, when using a different length, a segment containing bradycardia or tachycardia may not be labeled as an arrhythmia.

Tachycardia can be of the ventricular or supraventricular origin. In this work, only ventricular tachycardia was investigated as it is more serious. Whether the PPG can be used to distinguish ventricular from supraventricular tachycardia remains to be demonstrated. Since the hemodynamics is more compromised by fast ventricular pacing, the amplitude of PPG pulses should in theory be less affected during supraventricular tachycardia. Still, the difference in PPG characteristics during ventricular and supraventricular tachycardia deserves to be investigated in future studies. The CNN-based detector may be trained to employ such information, while the pulse-based detector is poorly suited for this purpose as it relies on the pulse rate only.

In the pioneering study on the PPG-based detection of bradycardia and tachycardia [70], only 3-min and longer episodes were detected. However, when the aim is to detect life-threatening episodes of extreme bradycardia and ventricular tachycardia, as is the goal of this work, the minimum duration needs to be much shorter to ensure that an episode is composed of just a few beats. As a consequence, it is not meaningful to compare the present results to those presented in [70]. Of course, the intention to detect shorter arrhythmia episodes leads to an increased number of false alarms or missed cases. However, since PPG-based detection is better suited for long-term monitoring outside the clinical setting, it could serve as a screening tool to initiate a clinical investigation of those at risk for life-threatening arrhythmias.

By using the arterial blood pressure signal as the input, the problem of detecting bradycardia and tachycardia has been addressed by synthesis-by-analysis modeling [135]—a technique closely related to the mixture of models proposed in [101, 136, 137]. Such modeling results in a feature vector describing each pulse used for the classifier training (the probabilistic neural network and the random forest were investigated in [135]). This approach was found to be useful to the arterial blood pressure signal, however, it may be equally useful when applied to a PPG signal.

This work shows that simulated PPG signals, based on real RR interval series, are practicable for the training and validation of the CNN-based detector. Although the simulator offers the option to generate signals with realistic noise, noise-free signals were used for the training and validation as this choice was found to produce better performance on the test set consisting of real PPG signals with occasional artifacts. However, if specificity is to be favored, noise should be added to the signals used for

the training and validation. On the other hand, randomly distributed noise episodes (i.e., nonstationary noise) may bias the training of the CNN-based detector, thus resulting in reduced performance.

A limitation of this investigation is the relatively small subset of short recordings from the PhysioNet/CinC 2015 Challenge Database used for the testing. Also, this subset does not include clinical data, and, thus, it is unclear if some confounding factors can influence the performance of the CNN-based detector. However, it is the only publicly available database with synchronous ECG and PPG signals with the labeling of extreme bradycardia and ventricular tachycardia. Since the CNN-based detector was tested on recordings containing the baseline sinus rhythm with episodes of extreme bradycardia and ventricular tachycardia, it is unclear how the network generalizes to discriminate other arrhythmias, e.g., atrial fibrillation. This issue deserves to be investigated in a future research.

Section 4.3.1 has been quoted verbatim from the previously published article: [14].

4.3.2.   Investigation of artifact influence

This section presents the results obtained by using simulated PPGs from the subset of the database with episodes of life-threatening arrhythmias described in Section 3.3 on page 47. Since the CNN-based detector is trained and validated on simulated PPGs, its performance is tested only on the real PPG signals. Thus, simulated PPGs with added artifacts are used to investigate the artifact influence on the detection performance of the pulse-based life-threatening arrhythmia detector only. Table 4.4 presents the arrhythmia detection performance for different types of artifacts. Irrespective of the artifact type, the sensitivity of extreme bradycardia detection drops nearly twice compared to the perfect sensitivity achieved for an artifact-free PPG. This can be explained by artifact-induced additional PPG pulses which increase the pulse rate and mask the episodes of extreme bradycardia, but have less influence on the sensitivity of pulse-based ventricular tachycardia detection. For the same reason, artifacts cause almost no false alarms of extreme bradycardia, resulting in the nearly perfect positive predictive value, but adversely affecting the false alarm rate of ventricular tachycardia. Interestingly, the poor contact causes 2–4 times more false alarms compared to the other artifact types. This can be explained by the poor contact being the most difficult type to distinguish from the pulsatile PPG component.

Figure 4.12 demonstrates the performance of the pulse-based life-threating arrhythmia detector as a function of the percentage of the artifact-corrupted PPG, which is governed by the rate parameter λ_0. By increasing λ_0 from 0.01 to 0.15, the average percentage of the artifact-corrupted PPG increased from 5% to 45%.

By applying the SQI, the amount of the remaining artifacts is reduced with

Table 4.4. Performance of a pulse-based life-threatening arrhythmia detector when a quarter of the PPG duration is contaminated with different types of artifacts

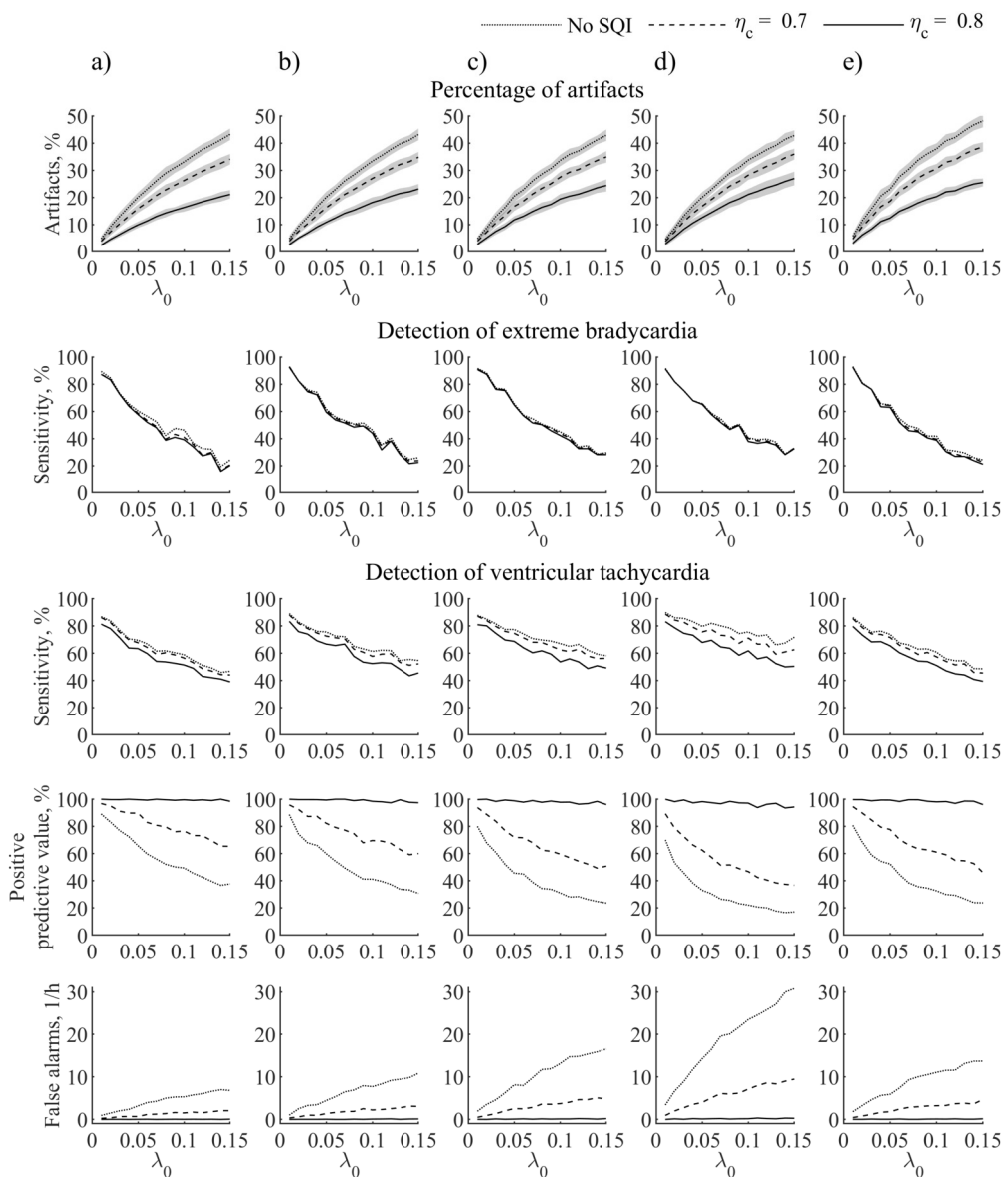|	Artifact-free	Device displacement	Forearm motion	Hand motion	Poor contact	Mixture
Detection of extreme bradycardia						
Sensitivity, %	100	52.4	53.3	54.6	54.6	54.6
Positive predictive value, %	100	100	100	100	100	99.2
False alarms, 1/h	0.00	0.00	0.00	0.00	0.00	0.02
Detection of ventricular tachycardia						
Sensitivity, %	92.3	61.6	72.2	70.7	80.1	67.5
Positive predictive value, %	100	55.9	49.4	38.8	26.4	44.6
False alarms, 1/h	0.00	4.27	6.49	9.80	19.62	7.39

the expense of the duration of analyzable PPG. The use of the SQI has only a slight influence on the reduction in the detection sensitivity of both extreme bradycardia and ventricular tachycardia. However, the number of false alarms of ventricular tachycardia reduces markedly and the positive predictive value approaches 1 (see Fig. 4.12). To nearly eliminate false alarms, a higher SQI threshold, e.g., $\eta_c = 0.8$, should be preferred, obviously, at the expense of undetected arrhythmia episodes.

Discussion

The developed artifact model relies on the characteristics estimated from PPGs acquired during cardiac rehabilitation. Therefore, it is assumed that similar artifacts can be encountered in real-life PPGs. To ensure model flexibility, a transition probability from the artifact-free interval to the artifact, as well as an artifact duration, are free to be tuned to produce a desirable amount of artifacts. Such an approach excels for other PPG simulators which generated stationary artifacts based on the characteristics of a single real artifact [101] or represented them as additive harmonic signals [138].

This work shows that the performance of the pulse-based life-threatening arrhythmia detector is affected differently by different artifact types. Although device displacement substantially distorts the PPG, it is easily identified by the SQI due to the largest amplitude. On the other hand, the poor contact disturbs the PPG so that additional pulses are produced making the identification of artifacts problematic. For this reason, additional pulses often lead to undetected extreme bradycardia, whereas they have little effect on the pulse-based detection of ventricular tachycardia.

This work takes the first step towards investigating the artifact influence on the detection of life-threatening arrhythmias in the PPG. The investigation of an atrial fibrillation detector showed that the specificity and the positive predictive value decrease with an increasing amount of artifacts [67]. The interesting finding of that study is the

No SQI ⋯⋯⋯ $\eta_c = 0.7$ ------ $\eta_c = 0.8$ ———

a) b) c) d) e)

Percentage of artifacts

Artifacts, %

Detection of extreme bradycardia

Sensitivity, %

Detection of ventricular tachycardia

Sensitivity, %

Positive predictive value, %

False alarms, 1/h

Figure 4.12. The performance of pulse-based life-threatening arrhythmia detection as a function of rate parameter λ_0 for different SQI threshold η_c. The functions are obtained for artifacts of a) device displacement, b) forearm motion, c) hand motion, d) poor contact, and e) mixture of all artifact types. When only a single-type artifact is generated, the rate parameters determining the duration of each artifact are set to 0.2. For a mixture of all artifact types, the following estimated day-time values are used: $\hat{\lambda}_1 = 0.10$, $\hat{\lambda}_2 = 0.22$, $\hat{\lambda}_3 = 0.18$ and $\hat{\lambda}_4 = 0.17$. Shaded areas show mean $\pm$ standard deviation. Almost no false alarms are observed when detecting extreme bradycardia, and therefore positive predictive value is always close or equal to 1 (not shown)

increase of the sensitivity proportional to the amount of the excluded artifact-corrupted PPG parts [67]. The present work shows contradictory results, i.e., the decrease in the sensitivity of ventricular tachycardia detection and no change in the sensitivity of extreme bradycardia detection for the increasing amount of the excluded PPGs. The contradiction arises since the sensitivity was calculated by including all arrhythmia episodes in this work, whereas only those episodes remaining after the exclusion of the artifact-corrupted PPG parts were included in [67]. This emphasizes the importance of using modeled PPGs to reveal the true detection performance while taking into account arrhythmia episodes excluded together with unacceptable-quality signals.

A limitation of this work is that the developed model is restricted to simulating artifacts mostly caused by movement and device attachment. However, the intrinsic PPG disturbances originating from physiological processes, such as respiration, or vasoconstriction due to temperature changes or stress [139], have not been considered.

Section 4.3.2 has been quoted verbatim from the previously published article: [13].

4.4. Ectopic burden in hemodialysis patients

4.4.1. Estimation of average daily ectopic burden

After an initial assessment of the PPG quality, 6 recordings with less than 10% of acceptable-quality PPG were excluded, resulting in 41 analyzable recordings from the ambulatory database, described in Section 3.5 on page 48. On average, 51.6% and 82.0% of all PPG and ECG signals, respectively, are of acceptable quality, covering from 15.9% to 86.1% for the PPG, and from 29.3% to 100% for the ECG in individual recordings (Fig. 4.13). The average daily ectopic burden ranges from 3 beats/h to 221 beats/h for the PPG, and from 0 beats/h to 681 beats/h for the reference ECG. A notable exception is the recording from patient #26 with a largely overestimated PPG-based ectopic burden due to intermittent blockade, whose pulse-to-pulse series mimics interval shortenings and elongations typical of ectopic beats.
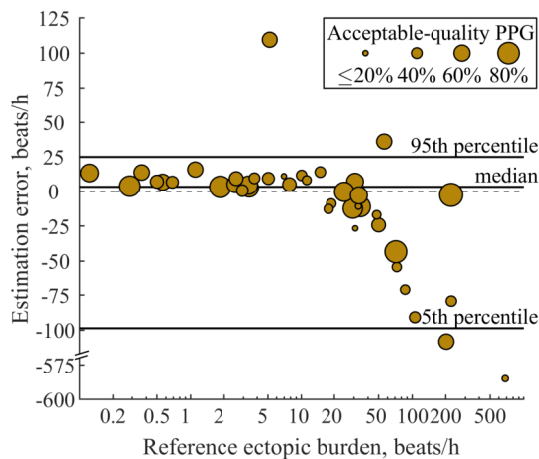
The PPG-based average daily ectopic burden is estimated with a median error of 3 ectopic beats/h (Fig. 4.14). When the reference ectopic burden is low, e.g., <10 beats/h, a PPG-based detector tends to slightly overestimate the ectopic burden, thus showing a positive error due to falsely detected ectopic beats. On the other hand, when ectopic beats are frequent, the PPG-based ectopic burden is considerably underestimated due to the missed ectopic beats. Somehow surprisingly, the error of the PPG-based ectopic burden does not depend on the percentage of the acceptable-quality signal since there is no pattern in error clustering.

Discussion

The wrist PPG quality is a crucial factor that limits the technology from wider
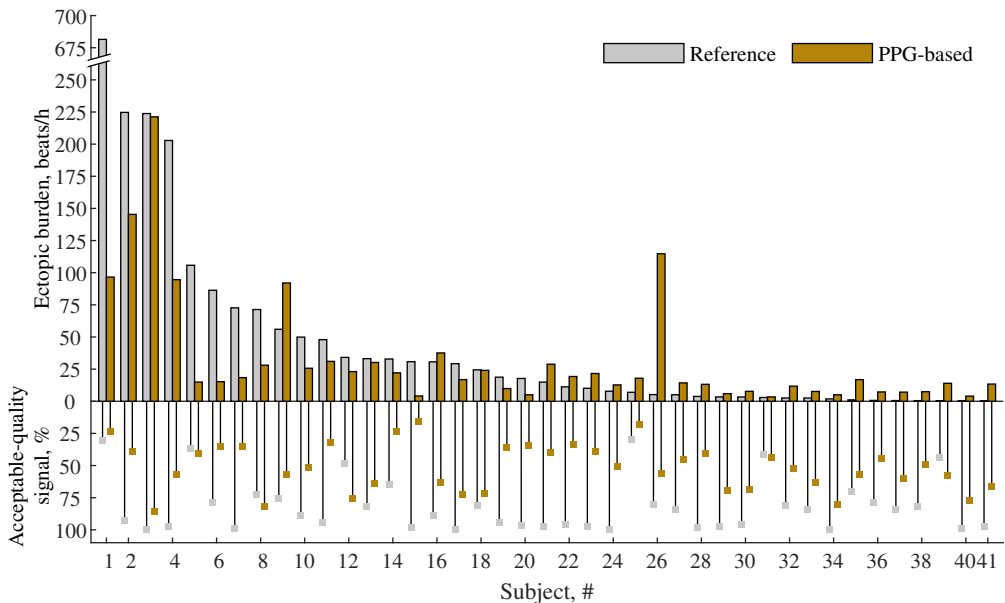
Figure 4.13. The average daily ectopic burden for HD patients. Data are sorted in descending order according to the reference ectopic burden. Recordings with less than 10% of acceptable-quality PPG are not included

Figure 4.14. Error in the estimation of PPG-based average daily ectopic burden with respect to the reference average daily ectopic burden. The size of the marker is linearly proportional to the percentage of acceptable-quality PPG in the recording. Recordings with less than 10% of acceptable-quality PPG are not included

clinical application. Common PPG quality-influencing factors are the skin tone, the obesity level, the age and gender [106]. Meanwhile, the quality of the wrist PPG in ESKD patients can be affected by additional, population-specific factors, such as HD

vintage, the presence of nonfunctional arteriovenous fistula, or vascular calcification. This work shows that more than a half of PPG signals were of the acceptable quality for ectopic beat detection, and the quality considerably depended on the time of the day. That is, 68%, 40%, and 51% of PPGs were of acceptable quality during sleep, daytime (except HD), and HD, respectively.

Unlike other detectors suitable to detect repetitive ectopic beats, e.g., bigeminy, trigeminy, etc., in 10- or 30-s PPG segments [71,74], the detector used in this work [73] operates on the pulse-to-pulse basis, and thus, it is capable of detecting sporadic ectopic beats. This work revealed that the detector tends to overestimate the ectopic burden due to pulse-like artifacts and ectopy-mimicking arrhythmias, e.g., intermittent blockade (see Fig. 4.13, patient #26). Moreover, the signal quality assessment that relies on the correlation between the analyzed and template pulses tends to exclude pulse waves corresponding to the ectopic beats for some patients, which results in the underestimated ectopic burden.

4.4.2. Detection of the high-risk ectopic burden

A total of 979 nonoverlapping 1-h segments were available, of which 757 had acceptable-quality reference ECG. The percentage of acceptable-quality PPG within the segment highly influences the performance of the detection of segments with a high-risk ectopic burden (Fig. 4.15 a). That is, the sensitivity improves from 67.3% to 82.7%, and specificity increases from 84.6% to 89.8% when the requirement of at least 75% of acceptable-quality PPG is applied.
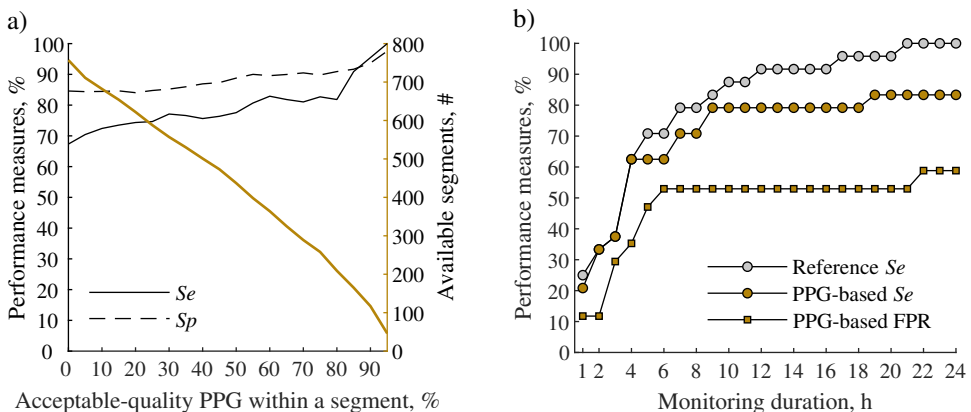

Figure 4.15. a) The performance of the PPG-based detection of 1-h segments with a high-risk ectopic burden as a function of the percentage of acceptable-quality PPG within a segment. b) Influence of monitoring duration on the identification of patients with a high-risk ectopic burden

Figure 4.15 b) demonstrates the influence of monitoring duration on the identifi-

cation of patients with a high-risk ectopic burden. It shows that prolonged monitoring, even in a span of a couple of hours, facilitates the identification of patients with a high-risk ectopic burden. At least 9 h are needed to achieve a sensitivity of 80%, whereas the maximum sensitivity of 83% is reached after 19 h of PPG monitoring. It should be noted that the false positive rate exceeds 50% after 6 h of monitoring.

4.4.3. Tracking of ectopic burden

Figure 4.16 illustrates tracking of the ectopic burden in 24-h recordings with various levels of PPG quality. A considerable increase in the ectopic burden, coinciding with an HD session, can be accurately assessed as shown in Fig. 4.16 a). Figure 4.16 b) shows an increase in the ectopic burden in the morning the next day after HD. Due to the lower PPG quality and missed ectopic beats, the ectopic burden is underestimated; however, the increasing trend is still evident.
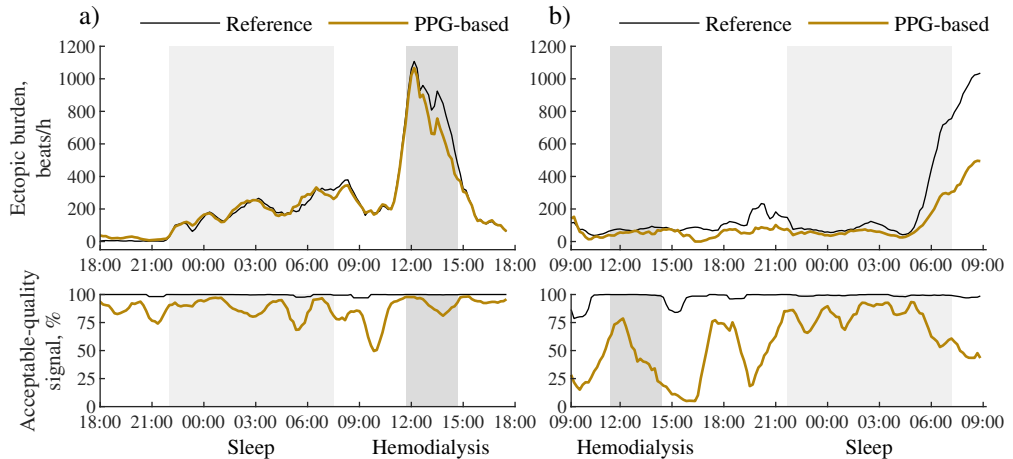
Figure 4.16. Tracking of ectopic burden in a 24-h recording when a) most of PPG is of acceptable quality and b) half of PPG is of acceptable quality. Values are obtained within overlapping 1-h segments with an increment of 10 min

Discussion

An increased ectopic activity during the morning hours, also noticed in this work (see Fig. 4.16 b), may represent a circadian pattern in arrhythmogenesis. This pathophysiological phenomenon is often observed in patients with cardiovascular diseases [140, 141], however, it still remains to be studied in the HD population. Therefore, the monitoring of circadian ectopic patterns could advance the understanding of the efficiency of chronotherapy in reducing arrhythmia manifestation [141].

The proposed PPG-based approach was compared to the reference ECG-based ectopic beat detector. Ectopic beats in ECG were detected by using a bench-marked

open-source software [116, 122], but were not confirmed by expert cardiologists. Therefore, the reference ectopic burden cannot be considered a golden standard, and that is a limitation of this work. Though ectopic beats of the atrial and ventricular origin have distinctive morphology in the ECG, they are difficult to distinguish in the PPG [74]. Therefore, future studies should consider discrimination of ectopic beat types so that the full potential of their prognostic significance in the HD population could be exploited.

Section 4.4 has been quoted verbatim from the manuscript under review: [15].

4.5. Conclusions of the chapter

1. The average artifact classification accuracy of 98% is achieved by setting thresholds of the mean absolute acceleration, adjusted amplitude, and spectral flatness to 0.08 g, 11, and 0.015, respectively.

2. A quarter of the ambulatory PPG duration is corrupted by artifacts. Depending on the recording, this proportion ranges from 14% to 49%. Most of the artifacts are motion-related and contained in the period of day-time, where up to 50% of the PPG signal may be artifact-corrupted.

3. Type-specific analysis of artifacts in the wrist PPG sheds light on the characteristics of artifacts in the ambulatory recordings. The analysis shows that device displacement and forearm motion artifacts are less common during night-time due to reduced movement. Also, the duration of all types of artifacts is decreased during the rest hours. Artifacts due to the poor contact are most noise-like since their spectral power in high frequencies is larger compared to other artifact types, and they exhibit the mean spectral slope of -18.12 dB/decade. In terms of the amplitude, the largest artifacts are caused by the device displacement.

4. The adjusted phenomenological PPG model simulates the episodes of extreme bradycardia more accurately than the original model. The RMS error is decreased by 20.6% due to the improved control of the PPG pulse amplitude.

5. A PPG-based arrhythmia detector, implemented as a dual-branch CNN, trained and validated on simulated PPG signals, is more sensitive for extreme bradycardia (98.1% vs. 94.7%) and ventricular tachycardia (76.6% vs. 67.1%) than the detector relying on pulse analysis. The CNN is also more specific when detecting ventricular tachycardia (96.6% vs. 93.8%). However, when detecting extreme bradycardia, a pulse-based detector outperforms the network in terms of specificity (99.8% vs. 97.4%). Hence, the results suggest that the CNN-based detector can be used for continuous, long-term monitoring, especially in situations where sensitivity is favored over specificity. Also, in contrast to the pulse-based

detector, the CNN-based detector makes it possible to chose various sensitivity and specificity combinations.

6. Different artifact types may influence the performance of the pulse-based arrhythmia detector differently. With a quarter of PPG corrupted by artifacts, the sensitivity drops by 45–48% for extreme bradycardia and by 13–32% for ventricular tachycardia detection. However, no false alarms of extreme bradycardia are caused by artifacts, while the false alarm rate of ventricular tachycardia markedly increases. The poor contact causes 2–4 times more false alarms of ventricular tachycardia compared to the other artifact types under investigation. Having in mind the cost of undetected arrhythmia episodes, a SQI with a threshold of 0.8 may be applied to eliminate false alarms.

7. The unacceptable quality of the wrist PPG prevents the estimation of the ectopic burden half of the time during the monitoring of HD patients. The quality of the signal depends on the time of the day with the acceptable-quality signal covering 68% of sleep-time. The lower quality of the signal affects the ability to accurately track the ectopic burden throughout the day, but the trend of changes can still be obtained.

8. When 1-h segments are used to detect a high-risk ectopic burden of $\geqslant$30 ectopic beats/h, at least 75% of acceptable-quality PPG within the segment is required to reach the sensitivity and specificity of 82.7% and 89.8%, respectively. At least 9 h of monitoring is needed to identify 80% of patients with a high-risk ectopic burden, which justifies the presumption that prolonged monitoring is relevant.

5. CONCLUSIONS

1. Artifacts in the ambulatory PPG signals have been quantitatively assessed by identifying and individually characterizing four types of artifacts, namely, device displacement, forearm motion, hand motion, and poor contact, common to the wrist PPGs. The analysis sheds light on the distribution of different-type artifacts within the day and on the quality of the wrist PPG typical for ambulatory recordings in general. Depending on the recording, 13.6–48.6% of the PPG duration is corrupted by artifacts, mostly due to device displacement, forearm motion, and hand motion, which cover 6.4%, 6.2%, and 6.0% of the total PPG duration in the database, respectively. The acquired artifact characteristics enable the development of the realistic artifact model.

2. A model for simulating episodes of life-threatening arrhythmias and realistic artifacts in PPG signals has been developed. The model simulates episodes of extreme bradycardia with a 20.6% smaller RMS error than its predecessor. Various artifact properties of the proposed model can be controlled to simulate realistic artifacts encountered in the activities of daily living. The suitability of the simulated signals for training and validation of a CNN for the detection of life-threatening arrhythmias is practically demonstrated. The artifact component of the model allows to comprehensively investigate arrhythmia detectors.

3. The performance of two PPG-based life-threatening arrhythmia detectors was investigated. A dual-branch CNN outperforms a pulse-based algorithm by achieving extreme bradycardia and ventricular tachycardia detection sensitivity of 98.1% and 76.6%, respectively, and a specificity of 96.6% for ventricular tachycardia detection. The pulse-based detector still demonstrates a higher specificity of 99.8% for extreme bradycardia detection. The results suggest that the CNN-based detector should be chosen for arrhythmia monitoring in situations where sensitivity is favored over specificity. The reliance on scalograms makes the CNN superior in the detection of ventricular tachycardia with reduced-amplitude pulsations, but also renders it susceptible to false alarms of extreme bradycardia. The performance of the pulse-based life-threatening arrhythmia detector is affected differently by different artifact types. Compared to other artifact types, the poor contact causes 2–4 times more false alarms of ventricular tachycardia.

4. The suitability of continuously acquired wrist PPG to assess the ectopic burden has been investigated. On average, 48.4% of all PPG signals have been found of unacceptable quality for analysis. Hence, the quality of the signals is the main factor limiting the successful clinical application of the technology. Nevertheless,

wrist PPG can still be used to detect a high-risk ectopic burden of $\geqslant 30$ ectopic beats/h with the sensitivity and specificity of 82.7% and 89.8%, respectively, if the acceptable signal quality is ensured for at least 45 min within a 1-h segment. The prolonged monitoring enables the identification of 80% of HD patients with a high-risk ectopic burden.

SANTRAUKA

ĮVADAS

Tyrimo aktualumas

Beveik 700 mln. žmonių, arba 9,1 % pasaulio gyventojų, serga lėtine inkstų liga (LIL). Sergamumas LIL per mažiau nei tris dešimtmečius nuo 1990 m. išaugo 29,3 %, daugiausia dėl populiacijos augimo, senėjimo ir didėjančio LIL rizikos veiksnių, tokių kaip diabetas ir hipertenzija, paplitimo [1]. LIL 2017 m. sukėlė 1,2 mln. mirčių, ir prognozuojama, kad šis skaičius iki 2040 m. išaugs mažiausiai iki 2,2 mln. [1, 2]. LIL yra progresuojanti būklė, kurios paskutinė stadija yra galutinis inkstų nepakankamumas (GIN). Daugiau nei 5 mln. žmonių kenčia nuo GIN, todėl jiems reikalinga pakaitinė inkstų terapija. Klinikoje atliekama hemodializė (HD) iki šiol yra labiausiai paplitęs pakaitinės inkstų terapijos metodas, atliekamas 69,4 % gydomų GIN pacientų. Inicijuojamų HD skaičius nuolat didėja, ypač mažas ir vidutines pajamas gaunančiose šalyse, todėl manoma, kad HD gydomų pacientų skaičius iki 2030 m. padvigubės [3].

LIL ir GIN pacientams būdingas didelis sergamumas gretutinėmis širdies ir kraujagyslių ligomis. Šiomis ligomis serga 63,4 % ankstyvųjų LIL stadijų pacientų, o progresavusiose LIL stadijose ir sergant GIN širdies ir kraujagyslių ligų paplitimas išauga iki 75,3 % [4]. Širdies ir kraujagyslių ligos yra pagrindinė sergančiųjų LIL mirties priežastis, sukelianti net 58 % GIN pacientų mirčių [5]. Didžioji dalis širdies ir kraujagyslių ligų sukeltų mirčių yra staigios mirtys dėl gyvybei pavojingų aritmijų, tokių kaip skilvelių virpėjimas ar ekstremali bradikardija [6]. Asmenims, kuriems reikalinga pirminė arba antrinė staigaus širdies sustojimo prevencija, gali būti svarstoma galimybė implantuoti širdies ritmą normalizuojantį prietaisą. Daugeliui pacientų implantuojamas defibriliatorius, užkertantis kelią skilvelių tachikardijai, galinčiai peraugti į skilvelių virpėjimą. Vis dėlto pacientams, kurių inkstų funkcija sutrikusi, tinkamesnė alternatyva gali būti stimuliatoriai, nes šioje populiacijoje dažnai aptinkami ekstremalios bradikardijos, galinčios peraugti į asistoliją, epizodai [7]. Gyvybei pavojingų aritmijų rizika GIN pacientams, gydomiems taikant HD 3 kartus per savaitę, labai padidėja ilgojo intervalo tarp HD procedūrų metu. HD gydomų pacientų polinkis į aritmijas taip pat pasireiškia padažnėjusiais priešlaikiniais širdies susitraukimais, vadinamais ekstrasistolėmis [8].

Manoma, kad protarpinis kraujo valymas taikant HD prisideda prie aritmijas galinčių sukelti procesų, tokių kaip organizmo skysčių perteklius, toksinų kaupimasis ir staigūs elektrolitų pokyčiai [9]. Deja, potencialią implantuojamų prietaisų naudą GIN sergantiems pacientams mažina šių pacientų polinkis į poprocedūrines komplikacijas [10] ir informacijos apie pasireiškiančias gyvybei pavojingas aritmijas trūkumas. Kadangi kiekvienu atveju būtinas individualus rizikos ir naudos santykio vertinimas, ilgalaikė stebėsena, skirta pirminiams gyvybei pavojingų aritmijų epizodams atpažinti,

galėtų palengvinti sprendimo dėl širdies ritmą normalizuojančio prietaiso implantavimo priėmimą. Žinoma, kiti metodai, galintys sumažinti HD gydomų pacientų polinkį į aritmijas, įskaitant vaistus ir dializės režimo bei dializuojamojo tirpalo pakeitimus, irgi verti apsvarstymo. Visgi šių metodų efektyvumas turėtų būti vertinamas kiekybiškai, pvz., stebint ekstrasistolių dažnio pokyčius.

Elektrokardiografija (EKG) yra pagrindinė aritmijų stebėsenos technologija. Deja, šiuo metu prieinami EKG registravimu pagrįsti įrenginiai yra arba tinkami tik protarpiniams signalams įrašyti, arba nepatogūs nešioti ilgą laiką, arba brangūs. Pastaruoju metu padaryta pažanga dėvimų įrenginių, ypač išmaniųjų laikrodžių, turinčių optinius jutiklius fotopletizmogramai (FPG) registruoti, srityje rodo didžiulį aritmijų stebėsenos potencialą [11]. Ši neinvazinė technologija gali būti ypač naudinga ilgalaikei HD gydomų GIN pacientų stebėsenai. Vis dėlto algoritmų, skirtų kitoms nei prieširdžių virpėjimas aritmijoms atpažinti naudojant ant riešo dėvimus įrenginius, vystymą apsunkina FPG signalo jautrumas artefaktams ir duomenų bazių su anotuotais gyvybei pavojingų aritmijų epizodais trūkumas. Be to, riešo FPG tinkamumas ekstrasistolių dažniui ambulatorinėmis sąlygomis vertinti vis dar neištirtas.

Mokslinė ir technologinė problema bei darbinė hipotezė

Dėl specifinės sveikatos būklės FPG analize pagrįsta ilgalaikė stebėsena, skirta pirminiams gyvybei pavojingų aritmijų epizodams atpažinti ir ekstrasistolių dažniui vertinti, galėtų būti labai naudinga LIL pacientų, ypač sergančių GIN, kuriems atliekama HD, gydymo procesui. Siekiant paspartinti FPG technologijų taikymą šioje srityje, išsamus FPG signalo ištyrimas ir metodai, palengvinantys aritmijų atpažinimo algoritmų vystymą, yra būtini.

Mokslinė ir technologinė problema: Kaip sumažinti kliūtis, ribojančias FPG analize pagrįstų algoritmų, skirtų ilgalaikei aritmijų stebėsenai, vystymą ir taikymą?

Darbinė hipotezė: FPG technologijų taikymo gyvybei pavojingoms aritmijoms atpažinti pažanga gali būti paspartinta atliekant artefaktų analizę, naudojant modeliuotus duomenis ir tiriant FPG analize pagrįstų algoritmų veikimą ambulatorinėmis sąlygomis.

Tyrimo tikslas – sukurti ir ištirti aritmijų vertinimo ambulatoriniuose FPG signaluose metodus.

Tyrimo uždaviniai

1. Ištirti ambulatorinių FPG signalų taikymą apsunkinančius artefaktus.

2. Sukurti ir ištirti FPG signalų modelį atsižvelgiant į gyvybei pavojingų aritmijų ir artefaktų įtaką.

3. Ištirti FPG analize pagrįstų gyvybei pavojingų aritmijų atpažinimo algoritmų patikimumą.

4. Įvertinti FPG signalų tinkamumą didelės rizikos ekstrasistolių dažniui vertinti.

Mokslinis naujumas

Ši daktaro disertacija suteikia įžvalgų apie signalo kokybę, būdingą kasdienės veiklos metu užregistruotai riešo FPG. Skirtingų tipų artefaktų kiekybinės charakteristikos, tokios kaip artefakto trukmė, amplitudė ir spektrinės savybės, pirmą kartą išskirtos iš ambulatorinių FPG signalų. Šios charakteristikos panaudotos kuriant realistiškų artefaktų modelį, kuris pritaikytas gyvybei pavojingų aritmijų detektoriaus patikimumui ištirti.

Šiame darbe FPG signalo modelis pritaikytas gyvybei pavojingų aritmijų epizodams modeliuoti įvertinant šių aritmijų įtaką hemodinamikai. Adaptuotas FPG modelis panaudotas ne tik testuojant pulso ritmo analize pagrįsto aritmijų detektoriaus veikimą, bet ir išmokant bei validuojant konvoliucinį neuroninį tinklą, kuris atpažįsta gyvybei pavojingas aritmijas FPG skalogramose.

Pirmą kartą HD gydomiems pacientams nepertraukiamai užregistruotas riešo FPG signalas pritaikytas vertinant paros ekstrasistolių dažnį nekontroliuojamomis sąlygomis. Taip ne tik pademonstruotas technologijos potencialas, bet ir nustatyti jos trūkumai bei tobulintini aspektai.

Praktinė reikšmė

1. FPG tyrimo rezultatai ir pasiūlytas modelis gali būti naudojami šiais atvejais:

   (a) Pasiūlytas artefaktų modelis gali palengvinti riešo FPG analize pagrįstų aritmijų detektorių, atsparių kasdienei veiklai būdingiems artefaktams, kūrimą ir testavimą.

   (b) Adaptuotas FPG modelis leidžia panaudoti viešai prieinamas EKG signalų duomenų bazes su anotuotais gyvybei pavojingų aritmijų epizodais generuojant FPG signalus, reikalingus vystant aritmijų detektorius. Modeliuoti signalai gali būti naudojami ne tik testuojant algoritmus, bet ir mokant bei validuojant giliojo mokymosi metodus aritmijoms atpažinti.

   (c) Taip pat FPG modelis gali būti naudojamas testuojant ir kalibruojant naujai sukurtus dėvimus įrenginius sveikatos priežiūros reikmėms.

   (d) Modelis naudingas kuriant detektorius, skirtus ilgalaikei HD pacientų ir kitų pacientų grupių, pasižyminčių padidėjusia staigios mirties dėl gyvybei pavojingų aritmijų rizika, stebėsenai. Tokios grupės pavyzdys – miokardo infarkto pacientai pirmaisiais mėnesiais po įvykio.

(e) FPG analize pagrįstas ekstrasistolių dažnio vertinimas potencialiai gali būti taikomas siekiant identifikuoti HD pacientus, kuriems būtų naudingas ankstyvas antiaritminis gydymas.

(f) FPG analize pagrįstas ekstrasistolių dažnio vertinimas gali būti naudojamas tiriant nestandartinių gydymo metodų (pvz., HD modifikavimo ar chronoterapijos) veiksmingumą užkertant kelią aritmijų atsiradimui palankių aplinkybių susidarymui.

2. Šioje daktaro disertacijoje pateikiamiems metodams plėtoti galimybes sudarė Europos Sąjungos struktūrinių fondų finansuojamas projektas „Personalizuotos dėvimos technologijos gyvybei pavojingoms sveikatos būsenoms įvertinti lėtine inkstų liga sergantiems pacientams — KidneyLife" (01.2.2-LMT-K-718-01-0030), 2018–2022 m.

3. Pasiūlytas FPG signalų su gyvybei pavojingų aritmijų epizodais ir judesių sukeltais artefaktais modelis pateiktas atviros prieigos portale „PhysioNet".

Tyrimo rezultatų aprobavimas

Daktaro disertacija remiasi dviem tarptautiniuose moksliniuose žurnaluose, turinčiuose cituojamumo rodiklį „Clarivate Analytics Web of Science" duomenų bazėje, publikuotais straipsniais ir vienu recenzuojamu rankraščiu. Iš viso rezultatai buvo publikuoti septyniuose moksliniuose straipsniuose ir pristatyti keturiose tarptautinėse konferencijose.

2019 m., 2020 m. ir 2022 m. gauta Lietuvos mokslo tarybos stipendija už studijų rezultatus. 2019 m., 2020 m. ir 2021 m. gauta aktyviausio KTU doktoranto stipendija Matavimų inžinerijos studijų kryptyje.

Ginti teikiami teiginiai

1. Didelė dalis ambulatorinių riešo FPG signalų yra užteršta artefaktais. Procentinė artefaktų dalis labai padidėja dienos metu, o tai sutampa su aktyviuoju paros periodu.

2. Adaptuotas FPG modelis tiksliai atkartoja pulso amplitudės ir morfologijos pokyčius gyvybei pavojingų aritmijų metu. Pasiūlyto modelio artefaktų dedamoji generuoja realistiškus judesių sukeltus artefaktus, būdingus kasdienės veiklos metu užregistruotai riešo FPG.

3. Skirtingi artefaktų tipai skirtingai veikia pulso ritmo analize pagrįsto gyvybei pavojingų aritmijų detektoriaus patikimumą. Atpažįstant ekstremalios bradikardijos ir skilvelių tachikardijos epizodus, su modeliuotais signalais išmokytas ir

validuotas konvoliucinis neuroninis tinklas yra jautresnis nei pulso ritmo analize pagrįstas detektorius. Vis dėlto pastarasis detektorius yra specifiškesnis atpažįstant ekstremalios bradikardijos epizodus.

4. Riešo FPG gali būti taikoma ekstrasistolių dažniui vertinti ir didelės rizikos ekstrasistolių dažniui atpažinti HD pacientų populiacijoje.

Bendradarbiavimas

Šiame darbe tiriamas konvoliucinis neuroninis tinklas, skirtas gyvybei pavojingoms aritmijomis atpažinti, yra sukurtas Andriaus Sološenko.

1. ARITMIJŲ ATPAŽINIMO METODŲ INKSTŲ LIGA SERGANTIEMS PACIENTAMS APŽVALGA

LIL diagnozuojama, kai inkstų pažeidimo arba pablogėjusios inkstų funkcijos požymiai, turintys įtakos sveikatai, pasireiškia ilgiau nei tris mėnesius. Šią lėtinę ligą dažniausiai sukelia patologiniai procesai inkstuose, susiję su pirminėmis inkstų ligomis arba sisteminėmis ligomis, pažeidžiančiomis inkstus [16]. Prasidėjusi LIL progresuoja, o vykstantys patologiniai procesai ne tik sukelia komplikacijas, bet ir skatina tolesnį inkstų funkcijos blogėjimą [16]. Progresuojant LIL, didėja GIN išsivystymo ir kitų neigiamų padarinių, tokių kaip ūminis inkstų pažeidimas, širdies ir kraujagyslių ligos, hospitalizavimas ir mirtis, rizika.

Didelė dalis LIL pacientų mirčių įvyksta dėl širdies ir kraujagyslių ligų. Ši dalis auga progresuojant LIL ir GIN pacientams siekia net 58 % [5, 22]. Patologinis sutrikimas, kai sutrikusi inkstų funkcija sukelia širdies funkcinius pokyčius, vadinamas 4 tipo kardiorenaliniu arba lėtiniu renokardialiniu sindromu [26]. Neigiamas pablogėjusios inkstų funkcijos poveikis širdžiai ir kraujagyslėms ypač išryškėja vėlyvosiose LIL stadijose, kuriose mirčių skaičius nuo širdies ir kraujagyslių ligų yra didžiausias [5]. Daugiau nei pusė šių LIL pacientų mirčių priskiriama staigiai mirčiai dėl gyvybei pavojingų aritmijų [31]. GIN pacientams ši dalis išauga net iki 82 % [6]. Staigios mirties rizika ypač padidėja pirmaisiais mėnesiais pradėjus pakaitinę inkstų terapiją HD procedūromis [32]. Tai gali paaiškinti žemus pacientų, pradėjusių HD, išgyvenamumo rodiklius pirmaisiais terapijos metais [6].

Nors staigią mirtį dažniausiai sukelia skilvelių tachikardija, perauganti į skilvelių virpėjimą [35], pastarųjų metų tyrimai rodo, kad staigią LIL ir GIN pacientų mirtį greičiausiai sukelia ekstremali bradikardija, perauganti į asistoliją [7, 36, 37, 38, 39, 40, 41, 42]. Paradoksalu, tačiau gyvybę gelbėjanti HD procedūra gali veikti ir kaip gyvybei pavojingas aritmijas provokuojantis veiksnys [19, 34]. Šių aritmijų rizikos ilgojo intervalo tarp HD procedūrų metu padidėjimas siejamas su padidėjusiu skysčių kiekiu organizme, toksinų kaupimusi ir elektrolitų disbalansu. Pati HD procedūra taip pat sukelia staigius skysčių ir elektrolitų koncentracijos pokyčius, kurie neigiamai veikia širdį ir gali išprovokuoti aritmijas [9].

Staigios mirties dėl gyvybei pavojingų aritmijų rizika LIL pacientams potencialiai gali būti mažinama implantuojant širdies ritmą normalizuojantį prietaisą, skiriant atitinkamus vaistus, o HD pacientams – ir modifikuojant pačios procedūros atlikimą [34]. Deja, LIL pacientai pasižymi didele poprocedūrinių komplikacijų rizika [10], todėl, vertinant potencialią prietaiso implantavimo naudą, būtina atlikti ilgalaikę stebėseną pirminiams gyvybei pavojingų aritmijų epizodams atpažinti [38]. Kitų nei implantuojami prietaisai metodų efektyvumas mažinant HD pacientų polinkį į aritmijas taip pat turi būti objektyviai įvertintas. Tai gali būti atlikta stebint ekstrasistolių dažnio pokyčius, kadangi dažnos ekstrasistolės siejamos su kitų aritmijų pasireiškimu

ir net staigios mirties rizika [48, 49]. Didelei daliai HD pacientų ekstrasistolių dažnis yra padidėjęs dėl ligos ir jos gydymo specifikos [8, 50].

Įprastai naudojamos aritmijų atpažinimo technologijos yra pagrįstos EKG signalo analize. Dalis neinvazinių įrenginių leidžia EKG signalą registruoti protarpiais, todėl yra tinkami aritmijoms su jaučiamais simptomais atpažinti [57], bet ne ekstrasistolių dažniui vertinti. Kiti įrenginiai gali būti naudojami nepertraukiamai stebėsenai nuo kelių dienų iki mėnesio, tačiau jie dažnai yra nepatogūs ir varžantys judesius, o klijuojami elektrodai gali sukelti nepageidaujamas odos reakcijas [11, 53]. Be to, net ir mėnuo yra palyginti trumpas laikotarpis siekiant atpažinti pirminius gyvybei pavojingų aritmijų epizodus ar stengiantis suprasti aritmijas provokuojančius veiksnius remiantis ekstrasistolių dažnio pokyčių stebėsena. Implantuojamas registratorius leistų užtikrinti ilgalaikę, net kelis metus trunkančią aritmijų stebėseną [58], tačiau jam reikalinga invazinė procedūra ir didelės piniginės išlaidos. Be to, implantuojamas registratorius nėra tinkamas ekstrasistolių dažniui vertinti dėl jo paskirties pavieniams aritmijų epizodams registruoti ir saugoti.

Pastarąjį dešimtmetį suintensyvėjęs dėvimų įrenginių, galinčių registruoti optinį FPG signalą, vystymas rodo šios technologijos potencialą aritmijų stebėsenai. Nors FPG gali būti registruojama ir išmaniojo telefono kamera, ir integruojant jutiklį į ausines, žiedus, galvos bei rankos juostas, išmanieji laikrodžiai, taip pat atliekantys ir aksesuaro bei komunikacijos priemonės funkcijas, pirmauja kaip patogiausia potenciali EKG alternatyva aritmijoms stebėti [11, 62]. Išmanusis laikrodis arba kitas ant riešo dėvimas įrenginys tyrimuose dažniausiai naudojamas prieširdžių virpėjimui atpažinti [63, 64, 65, 66, 67, 68]. Tai plačiai paplitusi, ilgiau nei kelias sekundes trunkanti aritmija, kurią galima atpažinti iš nereguliaraus ritmo. Deja, kitų rečiau pasitaikančių ar sudėtingiau atpažįstamų aritmijų detektorių, pagrįstų FPG analize, vystymas nėra taip patobulėjęs. Iki šiol atlikti tik pavieniai tyrimai, kuriuose bandyta riešo FPG panaudoti gyvybei pavojingoms aritmijoms ar ekstrasistolėms atpažinti [70, 71].

Pagrindinė priežastis, ribojanti FPG analize pagrįstų aritmijų detektorių taikymą ilgalaikei stebėsenai, yra signalo jautrumas artefaktams. Siekiant praktinio aritmijų atpažinimo algoritmų panaudojimo, būtina ištirti jų veikimo patikimumą pasireiškiant kasdienių veiklų sukeliamiems artefaktams, ypač kai FPG signalui registruoti naudojami ant riešo dėvimi įrenginiai [103]. Tam reikia suprasti artefaktų charakteristikas ir jų daromą poveikį aritmijų detektoriams. Algoritmų vystymą taip pat riboja viešai prieinamų duomenų bazių su anotuotais aritmijų epizodais trūkumas. Tai ypač aktualu kuriant gyvybei pavojingų aritmijų detektorius, nes signalus su šiomis aritmijomis užregistruoti sudėtinga dėl kur kas mažesnio nei, pvz., prieširdžių virpėjimas, paplitimo. Dėl šios priežasties modelis, leidžiantis panaudoti anotuotas EKG duomenų bazes su gyvybei pavojingų aritmijų epizodais FPG signalams modeliuoti, palengvintų šių aritmijų detektorių vystymą. FPG modelio papildymas realistiškų artefaktų komponente leistų užtikrinti detektorių atsparumą artefaktams.

2. FOTOPLETIZMOGRAMOS TAIKYMO GYVYBEI PAVOJINGOMS ARITMIJOMS ATPAŽINTI TYRIMO METODAI

2.1 Riešo fotopletizmogramos artefaktų analizė

Artefaktų analizė, kurios diagrama pateikiama 2.1 pav., atliekama keturiais etapais. Pirmiausia artefaktais užteršti intervalai identifikuojami panaudojant FPG signalo kokybės indeksą su $\eta_c = 0{,}7$ slenksčio verte [64]. Artefaktai iš FPG signalo šiuose intervaluose išskiriami adaptyviuoju filtru pašalinant sumodeliuotą pulsinę FPG signalo be artefaktų komponentę, kurios gavimas detaliau aprašomas 2.2.1 skyriuje.
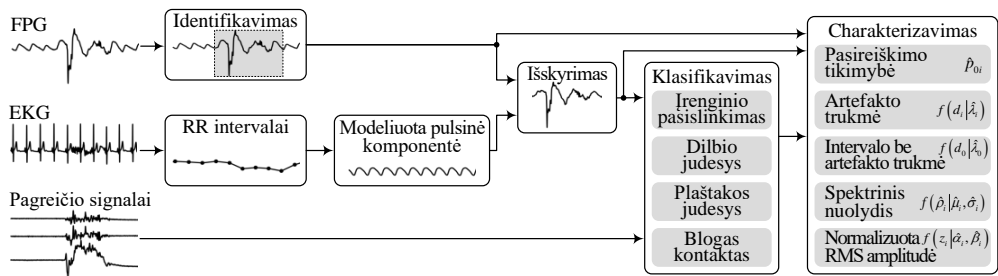
2.1 pav. Artefaktų analizės blokinė diagrama, kurią sudaro artefaktų identifikavimo, išskyrimo, klasifikavimo ir charakterizavimo blokai

Išskirti artefaktai klasifikuojami į keturis riešo FPG signalui būdingus artefaktų tipus: įrenginio pasislinkimą, dilbio judesį, plaštakos judesį ir blogą kontaktą (2.2 pav.). Klasifikavimas atliekamas remiantis sinchroniškai užregistruotu pagreičio signalu, iš kurio apskaičiuojama vidutinė absoliutinė akceleracija artefakto metu, ir paties artefakto savybėmis: santykine bendra amplitude ir spektro plokštumu.
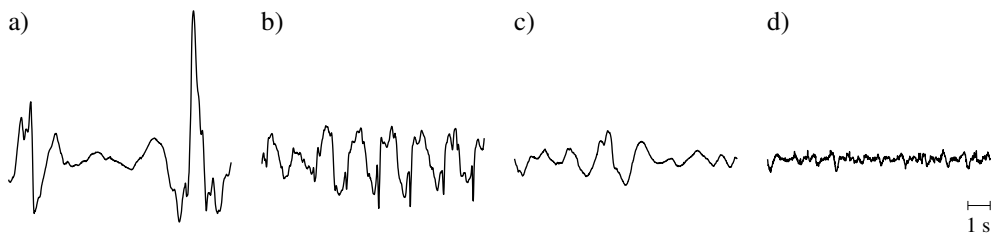
2.2 pav. Riešo FPG signalui būdingų artefaktų pavyzdžiai pašalinus modeliuotą pulsinę komponentę: a) įrenginio pasislinkimas, b) dilbio judesys, c) plaštakos judesys ir d) blogas kontaktas

Kiekvienas artefakto tipas i, kur 1 reiškia įrenginio pasislinkimą, 2 – dilbio judesį, 3 – plaštakos judesį ir 4 – blogą kontaktą, charakterizuojamas pasireiškimo tikimybe $\hat{p}_{0i}$ bei artefakto trukmės d_i, spektrinio nuolydžio ρ_i ir normalizuotos vidutinės kvadratinės (RMS) amplitudės z_i skirstinių parametrais. Artefaktų trukmių histogramai apibūdinti

pritaikomas eksponentinis skirstinys, aprašomas dažnio parametru $\hat{\lambda}_i$. Spektriniai nuolydžiai pasiskirstę pagal normalųjį skirstinį, aprašomą vidurkiu $\hat{\mu}_i$ ir standartiniu nuokrypiu $\hat{\sigma}_i$. Normalizuotų RMS amplitudžių histogramai apibūdinti pritaikomas gama skirstinys, aprašomas formos $\hat{\alpha}_i$ ir dažnio $\hat{\beta}_i$ parametrais.

2.2 Fotopletizmogramos modeliavimas

2.2.1 Gyvybei pavojingų aritmijų epizodų modeliavimas

Šiame darbe fenomenologinis modelis, sukurtas normalaus sinusinio ritmo FPG signalams su ekstrasistolėmis ir prieširdžių virpėjimo epizodais modeliuoti [101], adaptuotas gyvybei pavojingų aritmijų (ekstremalios bradikardijos ir skilvelių tachikardijos) epizodams modeliuoti. Tiek originalus $\mathcal{M}_\mathrm{o}$, tiek adaptuotas $\mathcal{M}_\mathrm{a}$ modeliai atskiram FPG pulsui modeliuoti naudoja lognormaliosios ir dviejų normaliųjų funkcijų kombinaciją. Pavieniai pulsai modifikuojami keičiant sistolinės ir diastolinės fazių trukmes bei amplitudę, o tada sujungiami į vientisą FPG signalą atsižvelgiant į trukmes tarp gretimų širdies susitraukimų (RR intervalų), išskirtų iš EKG signalo (2.3 pav.).
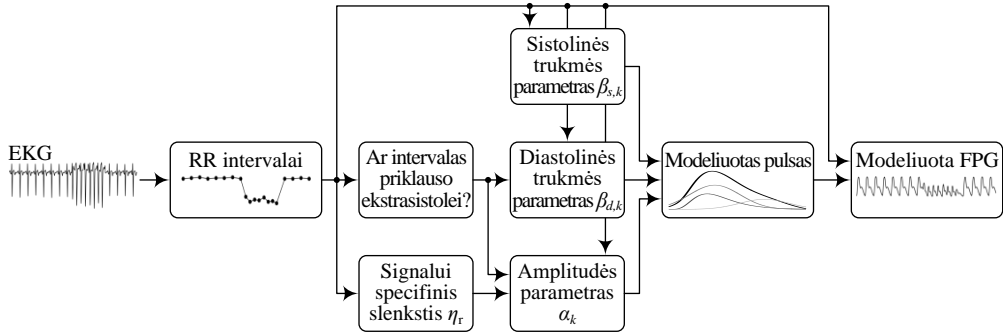
2.3 pav. Individualaus FPG pulso ir sujungto FPG signalo su gyvybei pavojingomis aritmijomis modeliavimo blokinė diagrama

Siekiant adaptuoti modelį, įvestos išsamesnės ekstrasistolių atpažinimo taisyklės pagal [109]. RR intervalas r_k, esantis prieš k-ąjį FPG pulsą, priskiriamas ekstrasistolei, jei tenkinama bent viena iš šių sąlygų:

$$1{,}15r_k < r_{k-1} \ \text{ ir } \ 1{,}15r_k < r_{k+1} \tag{2.1}$$

arba

$$\left| r_{k-1} - r_k \right| < 0{,}3 \ \text{ ir } r_{k-1} < 0{,}8 \ \text{ ir } r_k < 0{,}8 \ \text{ ir } 1{,}2 \cdot \frac{r_{k-1} + r_k}{2} < r_{k+1} \tag{2.2}$$

arba

$$\left| r_k - r_{k+1} \right| < 0{,}3 \ \text{ ir } r_k < 0{,}8 \ \text{ ir } r_{k+1} < 0{,}8 \ \text{ ir } r_{k-1} > 1{,}2 \cdot \frac{r_k + r_{k+1}}{2}. \tag{2.3}$$

Adaptuotas modelis, kitaip nei originalus, susieja FPG pulso amplitudę su kairiojo skilvelio sistoliniu kraujo tūriu [110]. Pirmiausia įvedamas signalui specifinis slenkstis η_r, atitinkantis RR intervalo trukmę, kurią viršijus bradikardijos metu sistolinis tūris kairiajame skilvelyje nebedidėja:

$$\eta_\mathrm{r} = \max\left(\frac{\dfrac{1}{K}\sum\limits_{k=1}^{K} r_k}{1 - \dfrac{1}{6K}\sum\limits_{k=1}^{K} r_k}, 0{,}75\right),\tag{2.4}$$

čia K yra bendras RR intervalų skaičius signale. Kai $r_k < \eta_\mathrm{r}$, sistolinio tūrio, o kartu ir FPG pulso amplitudės pokytis, aprašomas [111]:

$$\Delta\alpha_k = -\int\limits_{1/\eta_\mathrm{r}}^{1/r_k} \left(0{,}136r^2 - 10{,}044r + 21{,}18\right) dr.\tag{2.5}$$

Ekstrasistolė apriboja kairiojo skilvelio prisipildymą krauju [113], todėl iš jos kylančio FPG pulso amplitudės pokytis aprašomas eksponentiniu dėsniu [114]. Širdies susitraukimas po ekstrasistolės dažniausiai yra pavėlintas, kompensacinis [113], todėl FPG pulso amplitudė gali padidėti net tuo atveju, kai $r_k \geqslant \eta_\mathrm{r}$. Atsižvelgiant į šias detales, normalizuoto FPG pulso amplitudė aprašoma:

$$\alpha_k = \begin{cases} \left(\dfrac{r_k}{\eta_\mathrm{r}}\right)^{1.32}, & \text{jei } r_k \text{ yra ekstrasistolinis,}\\[2mm] 1 + \dfrac{\Delta\alpha_k}{C \cdot \eta_\mathrm{r}}, & \text{jei } r_k < \eta_\mathrm{r} \text{ arba } r_{k-1} \text{ yra ekstrasistolinis,}\\[2mm] 1, & \text{kitu atveju,} \end{cases}\tag{2.6}$$

čia C yra integravimo konstanta, lygi 25 [111].

FPG pulso sistolinės ir diastolinės fazių trukmės modifikuojamos laikiniais parametrais $\beta_{s,k}$ ir $\beta_{d,k}$:

$$\beta_{s,k} = \frac{1}{r_k},\tag{2.7}$$

$$\beta_{d,k} = \begin{cases} \dfrac{1}{r_{k+1}}, & \text{jei } r_k \text{ yra ekstrasistolinis,}\\[2mm] \dfrac{1}{r_k}, & \text{kitu atveju.} \end{cases}\tag{2.8}$$

Naudojant $\beta_{s,k}$, $\beta_{d,k}$ ir α_k parametrus, FPG pulsas modifikuojamas ir jungiamas į vientisą FPG signalą taip pat, kaip ir originalaus modelio atveju [101].

2.2.2 Riešo artefaktų modeliavimas

Modeliuojant artefaktus, perėjimas tarp artefakto ir signalo intervalo be artefaktų įgyvendinamas Markovo procesu, kuriame 0 būsena atitinka intervalą be artefaktų, o būsenos nuo 1 iki 4 – skirtingų tipų artefaktus. Iš intervalo be artefaktų perėjimas leidžiamas į visų keturių tipų artefaktus, tačiau iš artefakto įmanomas tik perėjimas į intervalą be artefaktų. Tokio Markovo proceso generavimo matrica:

$$Q = \begin{bmatrix} -\lambda_0 & \lambda_0 p_{01} & \lambda_0 p_{02} & \lambda_0 p_{03} & \lambda_0 p_{04} \\ \lambda_1 & -\lambda_1 & 0 & 0 & 0 \\ \lambda_2 & 0 & -\lambda_2 & 0 & 0 \\ \lambda_3 & 0 & 0 & -\lambda_3 & 0 \\ \lambda_4 & 0 & 0 & 0 & -\lambda_4 \end{bmatrix}. \tag{2.9}$$

Tipo i artefaktas modeliuojamas baltą triukšmą nufiltruojant taip, kad jo spektrinis nuolydis atitiktų gautąjį iš normaliojo skirstinio su parametrais $\hat{\mu}_i$ ir $\hat{\sigma}_i$. Tuomet artefakto amplitudė dauginama iš normalizuotos RMS amplitudės, gautos iš gama skirstinio su parametrais $\hat{\alpha}_i$ ir $\hat{\beta}_i$. Galiausiai suformuota artefaktų ir intervalų be artefaktų seka sudedama su pulsine komponente. Taip gaunamas modeliuotas FPG signalas su gyvybei pavojingų aritmijų epizodais ir realistiškais artefaktais (2.4 pav.).
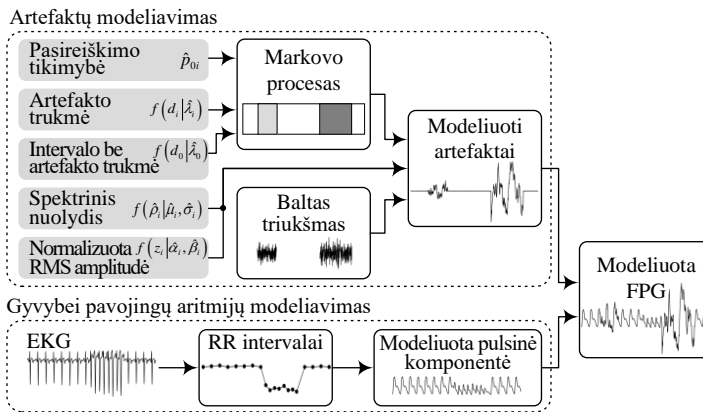
2.4 pav. FPG signalo su gyvybei pavojingomis aritmijomis ir artefaktais modeliavimo blokinė diagrama

2.3 Gyvybei pavojingų aritmijų atpažinimas

Šiame darbe tiriami du gyvybei pavojingų aritmijų atpažinimo algoritmai. Pirmasis detektorius ekstremaliai bradikardijai ir skilvelių tachikardijai atpažinti naudoja giluajį mokymąsi, o antrasis yra pagrįstas pulso ritmo analize.

Konvoliucinis neuroninis tinklas

Giliuoju mokymusi pagrįstą aritmijų atpažinimo metodą sudaro pradinis signalo apdorojimas, segmentavimas, signalo kokybės vertinimas, skalogramų skaičiavimas ir sprendimo priėmimas naudojant dviejų dalių konvoliucinį neuroninį tinklą (KNT). Pirmiausia FPG filtruojama juostiniu filtru (0,5–40 Hz) ir suskirstoma į 5 s trukmės nepersidengiančius segmentus. Kiekvieno segmento signalo kokybė įvertinama apskaičiavus jo spektrą. Jei didžiausias spektro pikas yra už 0,6–3 Hz intervalo ribų, segmentas atmetamas kaip netinkamas analizei. Tinkamos kokybės segmentai transformuojami į skalogramas, kurios KNT analizuojamos kaip dvimačiai vaizdai. Ekstremali bradikardija ir skilvelių tachikardija atpažįstamos dviem atskirais KNT, kurie tarpusavyje skiriasi tik branduolių dydžiais: bradikardijai atpažinti naudojamas 13×13, o tachikardijai – 5×5 dydžio branduolys. Kiekvienas KNT klasifikuoja segmentus į atitinkamos gyvybei pavojingos aritmijos arba kito ritmo klases.

KNT išmokyti ir validuoti naudojami modeliuoti FPG signalai. Mokymo procesui valdyti naudojamas Adam optimizatorius. Tinklų mokymas stabdomas tada, kai klasifikavimo tikslumas, naudojant validavimo duomenis, nustoja didėti. Išėjimo sluoksnio slenksčiai abiem KNT parenkami teikiant pirmenybę jautrumui, o ne specifiškumui.

Pulso ritmo analize pagrįstas detektorius

Gyvybei pavojingoms aritmijoms atpažinti taip pat naudojamas pulso ritmo analize pagrįstas detektorius, panašus į aprašytą [70]. Kitaip nei KNT atveju, FPG filtruojama siauresniu (0,5–6 Hz) juostiniu filtru. Pulso ritmas nustatomas iš trukmių tarp gretimų pulsų, prieš tai pulso viršūnes atpažinus slenkstiniu detektoriumi, panašiu į aprašytą [107]. Kiekvieno pulso kokybė įvertinama panaudojant jau minėtą signalo kokybės indeksą [64]. Šiuo atveju pulsas vertinamas kaip tinkamos kokybės, jei viršijama $\eta_c = 0{,}6$ kokybės indekso slenksčio vertė. Detektorius atpažįsta ekstremalios bradikardijos epizodą, jei pulso ritmas yra mažesnis nei 40 dūžių/min bent 3 tinkamos kokybės pulsus iš eilės. Skilvelių tachikardijos epizodas yra atpažįstamas, jei pulso ritmas yra didesnis nei 120 dūžių/min bent 3 tinkamos kokybės pulsus iš eilės. Siekiant palyginti pulso ritmo analize pagrįsto detektoriaus patikimumą su KNT, rezultatas, gautas kiekvienam FPG pulsui, padalinamas į 5 s segmentus.

Pulso ritmo analize pagrįstas detektorius taip pat naudojamas tiriant artefaktų įtaką gyvybei pavojingų aritmijų atpažinimui. Šiuo atveju minimali atpažįstamo gyvybei pavojingos aritmijos epizodo trukmė yra ne 3, o 5 pulsai.

2.4 Ekstrasistolių dažnio vertinimas

Prieš atpažįstant ekstrasistoles, FPG signalas nufiltruojamas juostiniu filtru, jame atpažįstamos pulsų viršūnės [107], naudojant signalo kokybės indeksą, įvertinama kiekvieno pulso kokybė [64]. Kadangi ekstrasistolės atpažįstamos pavieniuose pulsuose, siekiant sumažinti klaidingų aliarmų skaičių, taikomas aukštesnis signalo

kokybės indekso slenkstis $\eta_c = 0{,}8$. Skilvelinės ir prieširdinės ekstrasistolės (2.5 pav.) atpažįstamos tinkamos kokybės FPG signalo intervaluose panaudojant tiesioginio sklidimo dirbtinį neuroninį tinklą, analizuojantį trukmes tarp gretimų pulsų [73]. Vidutinis paros ekstrasistolių dažnis apskaičiuojamas padalinus visame įraše atpažintų ekstrasistolių skaičių iš tinkamos kokybės signalo trukmės valandomis. Ekstrasistolių dažnis 1 h segmente apskaičiuojamas padalinus segmente atpažintų ekstrasistolių skaičių iš tinkamos kokybės signalo dalies tame segmente.
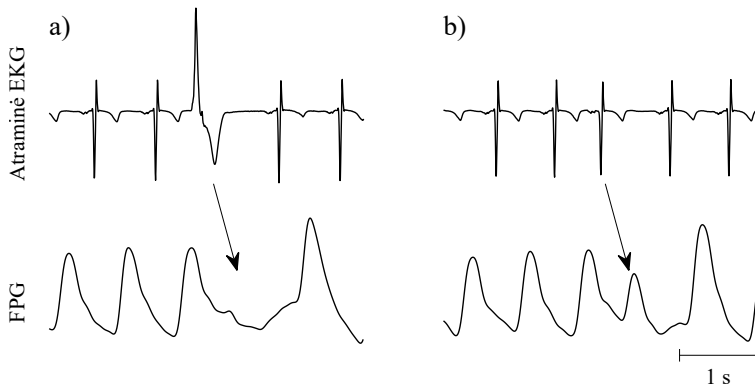
2.5 pav. a) Skilvelinė ir b) prieširdinė ekstrasistolės atraminėje EKG ir FPG

Atraminis ekstrasistolių dažnis vertinamas sinchroniškai užregistruotame EKG signale. Signalo kokybei įvertinti ir širdies susitraukimus atitinkantiems QRS kompleksams atpažinti panaudota atviro kodo programinė įranga „PhysioNet Cardiovascular Signal Toolbox" [116, 117, 120, 121]. Atviro kodo programinė įranga „R-DECO" pritaikyta ekstrasistolėms atpažinti tinkamos kokybės EKG signalo intervaluose pagal tipinius RR intervalų sutrumpėjimus ir po jų einančius pailgėjimus [122].

3. DUOMENŲ BAZĖS

Šiame darbe naudojamos keturios skirtingos duomenų bazės ir vienas modeliuotų signalų duomenų rinkinys. Viena iš duomenų bazių yra viešai prieinama portale „PhysioNet", o kitos trys duomenų bazės buvo užregistruotos naudojant ant riešo dėvimą įrenginį, galintį nepertraukiamai registruoti sinchroniškus žalios šviesos FPG, dviejų atvadų EKG ir trijų ašių pagreičio signalus bent parą.

Standartizuotų artefaktų duomenų bazė

Duomenų bazę sudaro Kauno technologijos universiteto Biomedicininės inžinerijos institute 10 sveikų savanorių užregistruoti signalai. Standartizuoti įrenginio pasislinkimo, dilbio judesio, plaštakos judesio ir blogo kontakto artefaktai riešo FPG signale gauti dalyviams atliekant protokole aprašytus veiksmus. Standartizuotų artefaktų duomenų bazė panaudota nustatant slenksčius, pagal kuriuos artefaktai klasifikuojami į keturis tipus.

**Ambulatorinė duomenų bazė artefaktams charakterizuoti**

Duomenų bazę sudaro Lietuvos sveikatos mokslų universiteto ligoninės Kauno klinikų Kulautuvos reabilitacijos ligoninėje 32 kardiologinės reabilitacijos pacientams po miokardo infarkto užregistruoti signalai (bioetikos leidimo Nr. BE-2-20). Bendra ambulatorinėmis sąlygomis užregistruotų signalų trukmė 656,1 h (vidutiniškai 21,4 h vienam pacientui). Ambulatorinė duomenų bazė panaudota riešo FPG būdingus artefaktus charakterizuojantiems parametrams išskirti.

Duomenų bazė su gyvybei pavojingų aritmijų epizodais

„PhysioNet/CinC Challenge 2015" duomenų bazė yra viena iš nedaugelio viešai prieinamų FPG signalų duomenų bazių su gyvybei pavojingų aritmijų epizodais [102, 127]. Tyrime naudojami tik normalaus sinusinio ritmo duomenų bazės įrašai su ekstremalios bradikardijos (< 40 dūžių/min) arba skilvelių tachikardijos (> 120 dūžių/min) epizodais, turintys bent vieną tinkamos kokybės EKG signalą RR intervalams išskirti. Gyvybei pavojingos aritmijos epizodo anotacija kiekviename įraše patikslinta remiantis širdies ritmu ir EKG signalo morfologija (3.1 pav.).

„PhysioNet/CinC Challenge 2015" duomenų bazė šiame darbe naudojama trims tikslams. FPG signalo su gyvybei pavojingomis aritmijomis modelio adekvatumas įvertintas su 40 įrašų (17 bradikardijos ir 23 tachikardijos), apskaičiuojant vidutinę kvadratinę paklaidą E tarp realaus ir modeliuoto FPG signalo paskutinę įrašo minutę. KNT ir pulso ritmo analize pagrįsto detektoriaus patikimumo įverčiai, atpažįstant gyvybei pavojingas aritmijas realiuose FPG signaluose, palyginti naudojant 54 įrašus (15 bradikardijos ir 39 tachikardijos, bendra trukmė 283 min). Palyginimas taip pat pakartotas pašalinus 10 įrašų su ypač maža arba dingusia FPG amplitudės pulsacija
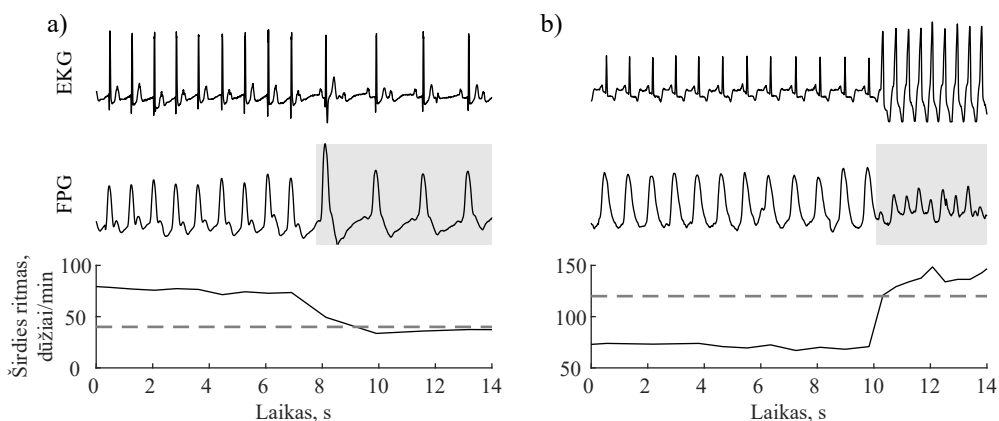
3.1 pav. Sinchroniškų „PhysioNet/CinC Challenge 2015" duomenų bazės EKG and FPG signalų pavyzdžiai su a) ekstremalios bradikardijos (< 40 dūžių/min) ir b) skilvelių tachikardijos (> 120 dūžių/min) epizodais. EKG pagrįsta anotacija pažymėta pilku tonu

skilvelių tachikardijos metu, t. y. naudojant 44 įrašus (bendra trukmė 232 min). Tiriant artefaktų įtaką gyvybei pavojingų aritmijų atpažinimui, panaudoti 55 „PhysioNet/CinC Challenge 2015" duomenų bazės įrašų (16 bradikardijos ir 39 tachikardijos) EKG signalai. Iš jų išskirti RR intervalai leido sugeneruoti 55 h trukmės FPG signalų su gyvybei pavojingomis aritmijomis ir artefaktais duomenų rinkinį.

Modeliuotų signalų su gyvybei pavojingų aritmijų epizodais duomenų rinkinys

Dėl viešai prieinamų FPG signalų duomenų bazių su anotuotais gyvybei pavojingų aritmijų epizodais trūkumo KNT išmokytas ir validuotas su modeliuotais FPG signalais. RR intervalų sekos signalams sugeneruoti išskirtos iš anotuotų viešai prieinamų EKG duomenų bazių. Sinusinio ritmo RR intervalai iš „MIT–BIH Normal Sinus Rhythm Database" ir 147 RR intervalai su aritmija iš „PhysioNet/CinC Challenge 2017" duomenų bazių panaudoti FPG signalams su ekstremalios bradikardijos epizodais modeliuoti. RR intervalai iš 94 „Spontaneous Ventricular Tachyarrhythmia Database" duomenų bazės įrašų panaudoti FPG signalams su skilvelių tachikardijos epizodais modeliuoti. Bendra modeliuotų FPG signalų duomenų rinkinyje trukmė 30 h.

Hemodializuojamiems pacientams užregistruota ambulatorinė duomenų bazė

Duomenų bazę sudaro Lietuvos sveikatos mokslų universiteto ligoninės Kauno klinikų Nefrologijos skyriuje 50 HD pacientų užregistruoti signalai (bioetikos leidimo Nr. BE-2-43). Atlikus pirminę peržiūrą, du įrašai atmesti dėl nuolatinio prieširdžių virpėjimo, vienas – dėl prarasto atraminio EKG signalo. Bendra ambulatorinėmis sąlygomis užregistruotų signalų trukmė 1142,7 h (vidutiniškai 24,3 h vienam pacientui). Duomenų bazė panaudota ekstrasistolių dažnio vertinimo riešo FPG signale galimybių tyrime.

4. REZULTATAI

### 4.1 Artefaktų charakteristikos ambulatorinėje riešo fotopletizmogramoje

Reabilitacijos pacientams užregistruotų ambulatorinių signalų analizė parodė, kad 26,8 % visų FPG signalų užteršti artefaktais, kurie pavieniuose įrašuose sudaro nuo 13,6 % iki 48,6 % įrašo trukmės (4.1 pav.). Dauguma artefaktų priskirti įrenginio pasislinkimo (6,4 %), dilbio judesio (6,2 %) ir plaštakos judesio (6,0 %) tipams. Tik 1,8 % signalų priskirti blogo kontakto artefaktų tipui. Dalis (6,4 %) artefaktų nepriskirti jokiam tipui dėl per mažos trukmės arba kokybiško atraminio EKG signalo trūkumo.
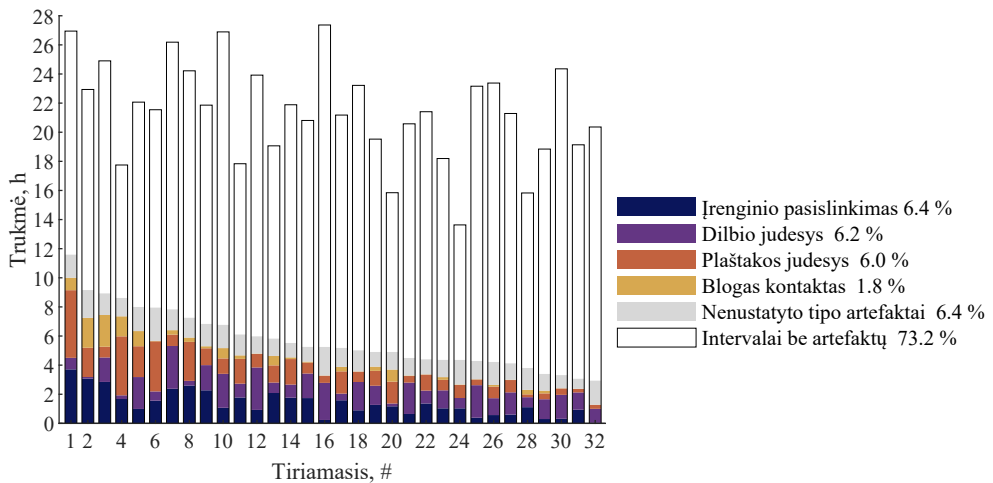
4.1 pav. Skirtingų tipų artefaktų ir FPG intervalų be artefaktų trukmė visuose reabilitacijos pacientams užregistruotos ambulatorinės duomenų bazės įrašuose. Duomenys išrikiuoti mažėjimo tvarka pagal bendrą artefaktų trukmę signale

Procentinė artefaktais užterštų FPG signalų dalis paros metu iliustruojama 4.2 pav. Vidutiniškai bent ketvirtadalis FPG signalo būna užterštas artefaktais nuo 6.00 iki 22.00, kai dominuoja kasdienės veiklos, tačiau artefaktų labai sumažėja už šio laiko periodo ribų. Atsižvelgiant į tai, FPG signalai padalinti į dienos (6.00–22.00) ir nakties (22.00–6.00) periodus, kuriuose artefaktai sudarė atitinkamai 37,0 % ir 8,8 % visos signalo trukmės.

Įvertintos skirtingų tipų artefaktų pasireiškimo tikimybės ir kitų charakteristikų skirstinių parametrai pateikti 4.1 lentelėje. Intervalų be artefaktų ilgėjimą nakties metu rodo mažesnis dažnio parametras $\hat{\lambda}_0$. Šis rezultatas patvirtina prielaidą, kad visų tipų artefaktai yra retesni ir trumpesni nakties metu. Blogo kontakto artefaktų spektrinio nuolydžio vidutinė absoliutinė vertė mažiausia (spektras plokščiausias) dėl didesnės nei kitų artefaktų spektrinės galios aukštuose dažniuose. Tai rodo, kad šio tipo artefaktai yra labiau nei kiti panašūs į triukšmą. Įrenginio pasislinkimas sukelia didžiausios amplitudės artefaktus, kurie vidutiniškai 22 kartus viršija FPG pulsinės komponentės
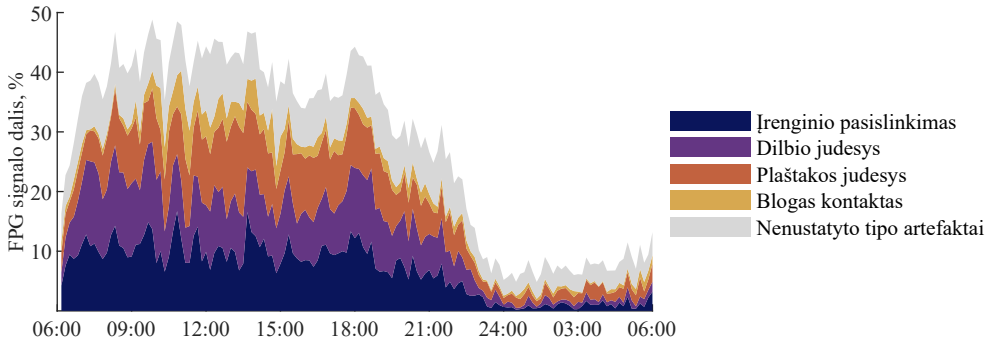
4.2 pav. Skirtingų tipų artefaktų trukmių procentinė diagrama paros metu. Procentinė artefaktų dalis apskaičiuota 10 min nepersidengiančiuose languose visai ambulatorinei duomenų bazei

amplitudę.

4.1 lentelė. Įvertintos skirtingų tipų artefaktų pasireiškimo tikimybės ir artefaktų trukmės, spektrinio nuolydžio bei normalizuotos RMS amplitudės skirstinių parametrai

|	Intervalas be artefaktų, $i = 0$	Įrenginio pasislinkimas, $i = 1$	Dilbio judesys, $i = 2$	Plaštakos judesys, $i = 3$	Blogas kontaktas, $i = 4$
			Pasireiškimo tikimybė $\hat{p}_{0i}$		
Diena	–	0,23	0,37	0,31	0,09
Naktis	–	0,16	0,24	0,45	0,15
		Artefaktų trukmės d_i eksponentinio skirstinio dažnio parametras $\hat{\lambda}_i$			
Diena	0,15	0,10	0,22	0,18	0,17
Naktis	0,05	0,13	0,26	0,29	0,26
		Spektrinio nuolydžio ρ_i normaliojo skirstinio vidurkis $\hat{\mu}_i$ ir standartinis nuokrypis $\hat{\sigma}_i$			
	–	-32,34 ir 6,03	-29,39 ir 5,71	-25,45 ir 4,13	-18,12 ir 4,10
		Normalizuotos RMS amplitudės z_i gama skirstinio formos $\hat{\alpha}_i$ ir dažnio $\hat{\beta}_i$ parametrai			
	–	0,88 ir 0,04	1,44 ir 0,31	1,40 ir 0,45	2,01 ir 1,24

4.2 Gyvybei pavojingų aritmijų modelio adekvatumas

Gyvybei pavojingoms aritmijos modeliuoti adaptuotas modelis $\mathcal{M}_a$ pranašesnis už originalų modelį $\mathcal{M}_o$ simuliuojant ekstremalios bradikardijos epizodus dėl tiksliau atkuriamos FPG signalo pulso amplitudės. Abu modeliai panašiai modeliuoja skilvelių tachikardijos epizodus. Realių ir modeliuotų FPG signalų su gyvybei pavojingų aritmijų epizodais pavyzdžiai pateikiami 4.3 pav.

Adaptuotu modeliu $\mathcal{M}_a$ pasiekta 20,6 % mažesnė vidutinė kvadratinė paklaida E modeliuojant ekstremalios bradikardijos epizodus (4.4 pav., a), tačiau viso signalo (sinusinis ritmas su ekstremalios bradikardijos epizodu) atveju skirtumas tarp modelių
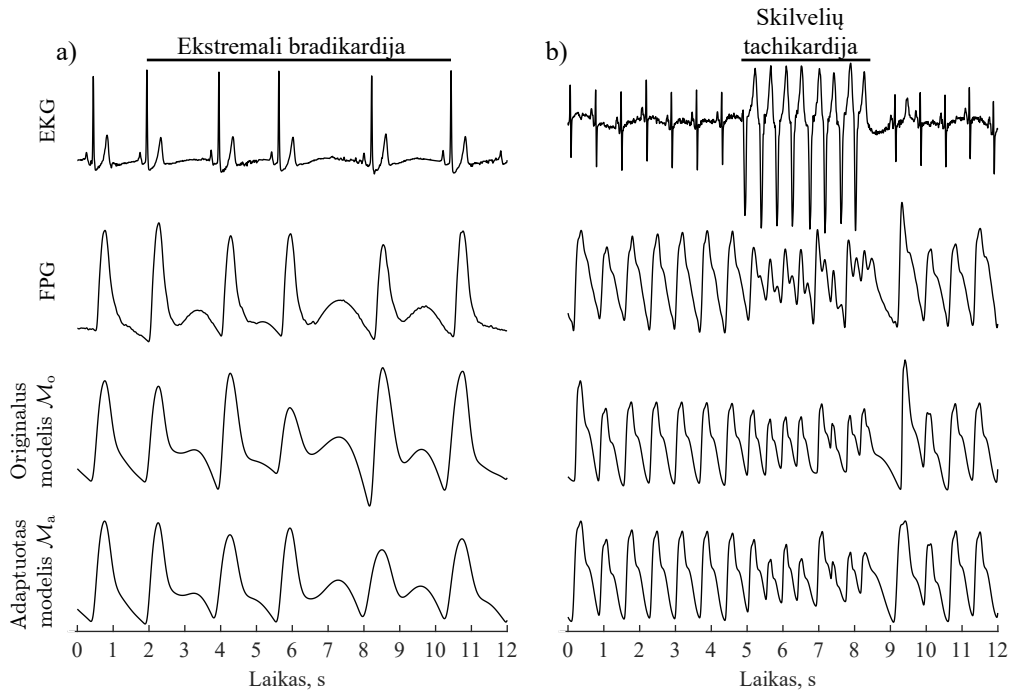
4.3 pav. Realūs EKG ir FPG signalai bei modeliuoti FPG signalai su a) ekstremalios bradikardijos (įrašas b299l) ir b) skilvelių tachikardijos (įrašas v206s) epizodais
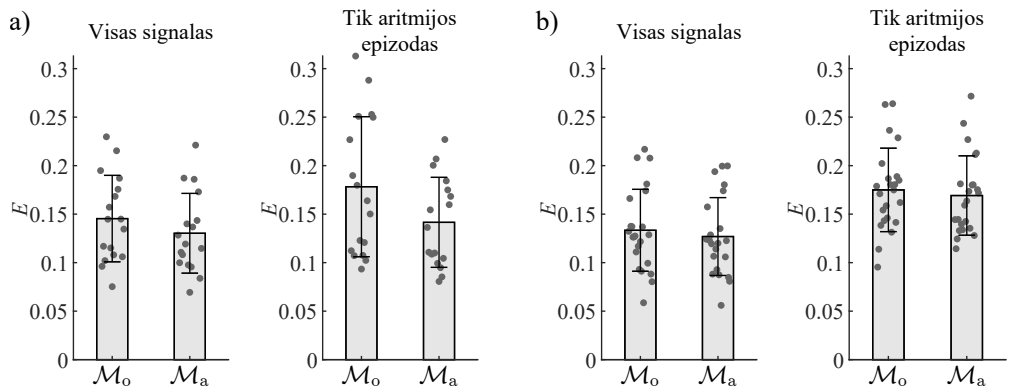
4.4 pav. Vidutinė kvadratinė paklaida E tarp realaus ir modeliuoto FPG signalo esant a) ekstremaliai bradikardijai ir b) skilvelių tachikardijai. Rezultatai pateikiami vidurkiu ir standartiniu nuokrypiu

nėra toks akivaizdus. Tai rodo panašų modelių veikimą esant kitiems ritmams. Šį pastebėjimą pagrindžia ir tai, kad adaptuotas modelis $\mathcal{M}_a$ tik nedaug pagerina epizodų su skilvelių tachikardija modeliavimą – pasiekta 3,3 % mažesnė paklaida modeliuojant aritmijos epizodus ir 4,8 % mažesnė paklaida modeliuojant visą signalą su skilvelių

tachikardijos epizodais (4.4 pav., b). Abiejų modelių paklaida, apskaičiuota aritmijų metu, dėl triukšmo ir artefaktų yra didesnė.

4.3 Gyvybei pavojingų aritmijų detektorių patikimumo tyrimas

4.3.1 Palyginimas naudojant realius signalus

KNT ir pulso ritmo analize pagrįsto detektoriaus patikimumas atpažįstant gyvybei pavojingas aritmijas 54 „PhysioNet/CinC Challenge 2015" duomenų bazės įrašuose pateiktas 4.2 lentelėje. Nevertinant signalo kokybės, KNT yra atitinkamai 2,0 ir 11,2 procentiniais punktais jautresnis atpažįstant ekstremalią bradikardiją ir skilvelių tachikardiją. Giliuoju mokymusi pagrįstas detektorius taip pat yra 2,6 procentiniais punktais specifiškesnis skilvelių tachikardijai, tačiau šiuo aspektu nusileidžia 3,0 procentiniais punktais atpažįstant ekstremalią bradikardiją. Vertinant signalo kokybę, abiejų detektorių specifiškumas padidėja nuo 0,1 iki 1,3 procentinių punktų, o KNT skilvelių tachikardijos atpažinimo jautrumas sumažėja 3,1 procentiniais punktais dėl epizodo metu atsirandančių artefaktų arba smarkiai sumažėjusios pulsacijų amplitudės.

4.2 lentelė. KNT ir pulso ritmo analize (PRA) pagrįsto detektoriaus gyvybei pavojingų aritmijų atpažinimo jautrumas (Se) ir specifiškumas (Sp) bei tarpusavio sutapimas, išreikštas Koheno kapa κ verte. Rezultatai apskaičiuoti naudojant 54 „PhysioNet/CinC Challenge 2015" duomenų bazės įrašus be ir su signalo kokybės vertinimu (SKV). Laužtiniuose skliaustuose pateiktas 95 % pasikliautinasis intervalas

54 įrašai		Ekstremali bradikardija		Skilvelių tachikardija	
		Be SKV	SKV	Be SKV	SKV
KNT	Se, %	**98,1** [89,3; 100]	**98,1** [88,7; 100]	**79,7** [68,2; 88,5]	**76,6** [65,0; 86,1]
	Sp, %	**96,7** [96,0; 97,2]	**97,9** [97,4; 98,4]	**95,6** [94,9; 96,3]	**96,6** [96,0; 97,2]
PRA pagrįstas	Se, %	**96,1** [89,0; 98,8]	**94,7** [87,2; 98,6]	**68,5** [57,1; 78,6]	**67,1** [55,6; 77,2]
	Sp, %	**99,7** [99,5; 99,9]	**99,8** [99,6; 99,9]	**93,0** [92,1; 93,9]	**93,8** [92,9; 94,5]
	κ	**0,42** [0,32; 0,51]	**0,49** [0,39; 0,59]	**0,39** [0,32; 0,46]	**0,39** [0,31; 0,46]

Ekvivalenčiai gauti rezultatai iš analizės pašalinus 10 įrašų su ypač maža arba dingusia FPG amplitudės pulsacija skilvelių tachikardijos metu pateikti 4.3 lentelėje. Dėl šių įrašų pašalinimo padidėja abiejų detektorių skilvelių tachikardijos atpažinimo jautrumas (nuo 5,5 iki 21,2 procentinių punktų) ir specifiškumas (nuo 1,8 iki 3,8 procentinių punktų). Vis dėlto KNT jautrumo pokytis didesnis. Taip yra todėl, kad KNT, kitaip nei pulso ritmo analize pagrįstas detektorius, analizuoja visą 5 s FPG segmento skalogramoje esančią informaciją, o ne tik pulso ritmą.

Gyvybei pavojingų aritmijų detektorių tarpusavio sutapimas, išreikštas Koheno kapa κ verte, yra žemas ir siekia 0,39–0,50. Tai daugiausia lemia nesubalansuota testavimo duomenų bazė ir skirtingos detektorių klaidingų aliarmų priežastys. Atpažįstant

4.3 lentelė. KNT ir pulso ritmo analize (PRA) pagrįsto detektoriaus gyvybei pavojingų aritmijų atpažinimo jautrumas (Se) ir specifiškumas (Sp) bei tarpusavio sutapimas, išreikštas Koheno kapa κ verte. Rezultatai apskaičiuoti naudojant 44 „PhysioNet/CinC Challenge 2015" duomenų bazės įrašus (atmetus 10 įrašų su ypač maža arba dingusia FPG amplitudės pulsacija skilvelių tachikardijos metu) be ir su signalo kokybės vertinimu (SKV). Laužtiniuose skliaustuose pateiktas 95 % pasikliautinasis intervalas

44 įrašai, likę atmetus įrašus su nykstama pulsacija		Ekstremali bradikardija		Skilvelių tachikardija	
		Be SKV	SKV	Be SKV	SKV
KNT	Se, %	**98,1** [88,6; 100]	**98,1** [89,1; 100]	**97,8** [87,7; 100]	**97,8** [87,6; 100]
	Sp, %	**96,2** [95,4; 96,9]	**97,7** [97,1; 98,2]	**97,8** [97,2; 98,3]	**98,4** [97,9; 98,8]
PRA pagrįstas	Se, %	**96,1** [89,0; 98,8]	**94,7** [87,3; 98,6]	**74,5** [61,0; 85,3]	**72,6** [58,8; 83,9]
	Sp, %	**99,7** [99,4; 99,9]	**99,7** [99,5; 99,9]	**96,8** [96,1; 97,4]	**97,6** [97,0; 98,2]
	κ	**0,43** [0,33; 0,52]	**0,50** [0,40; 0,60]	**0,39** [0,29; 0,49]	**0,40** [0,29; 0,51]

ekstremalią bradikardiją, KNT, kitaip nei pulso ritmo analize pagrįstas detektorius, gali klaidingai atpažinti aritmiją esant vos vienam ar dviem lėtiems širdies susitraukimams, pvz., kompensuojantiems ekstrasistolę. Skilvelių tachikardijos atpažinimo atveju artefaktai, panašūs į FPG pulsus, gali suklaidinti pulso ritmo analize pagrįstą detektorių, o dažnos ekstrasistolės – KNT.

4.3.2 Artefaktų įtakos tyrimas

Pulso ritmo analize pagrįsto gyvybei pavojingų aritmijų atpažinimo patikimumo priklausomybė nuo artefaktų procentinės dalies signale pateikta 4.5 pav. Didinant dažnio parametro λ_0 vertę nuo 0,01 iki 0,15, vidutinė artefaktais užteršto FPG signalo dalis padidėja nuo 5 % iki 45 %. Ekstremalios bradikardijos atpažinimo jautrumas smarkiai mažėja daugėjant artefaktų, nepriklausomai nuo jų tipo. Tai gali lemti į pulsus panašūs artefaktai, kurie klaidingai padidina pulso ritmą ir taip užmaskuoja bradikardijos epizodą, tačiau daro mažesnę įtaką skilvelių tachikardijos atpažinimo jautrumui. Dėl tos pačios priežasties artefaktai beveik nesukelia klaidingų ekstremalios bradikardijos aliarmų, tačiau labai padidina klaidingų skilvelių tachikardijos aliarmų skaičių. Palyginti su kitais artefaktų tipais, blogas kontaktas sukelia 2–4 kartus daugiau klaidingų aliarmų. To priežastis gali būti itin komplikuotas šio artefaktų tipo atskyrimas nuo pulsinės FPG komponentės.

Naudojant signalo kokybės indeksą, galima sumažinti artefaktų skaičių, kartu sutrumpinant analizuojamo FPG signalo trukmę. Signalo kokybės indekso naudojimas šiek tiek pablogina aritmijų atpažinimo jautrumą, tačiau stipriai sumažina klaidingų skilvelių tachikardijos aliarmų skaičių ir leidžia pasiekti teigiamą prognostinę vertę, artimą 1. Siekiant eliminuoti daugumą klaidingų aliarmų, turėtų būti pasirenkama aukštesnė signalo kokybės indekso slenksčio vertė (pvz., $\eta_c = 0{,}8$), tačiau klaidingų aliarmų sumažinimas lems didėjantį neatpažintų aritmijos epizodų skaičių.
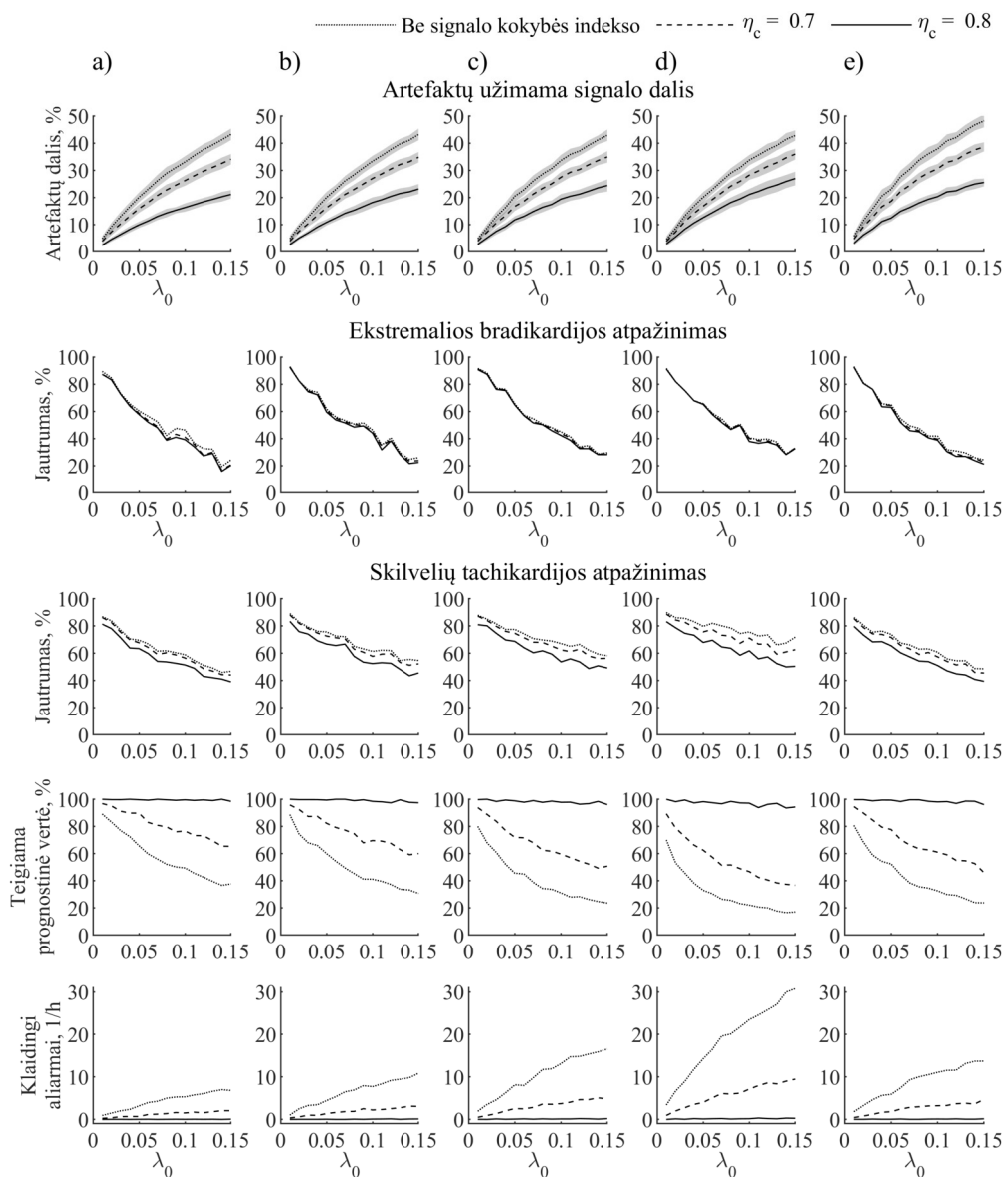
4.5 pav. Pulso ritmo analize pagrįsto gyvybei pavojingų aritmijų atpažinimo patikimumo priklausomybė nuo intervalų be artefaktų dažnio parametro λ_0, taikant skirtingus signalo kokybės indekso slenksčius η_c, a) įrenginio pasislinkimo, b) dilbio judesio, c) plaštakos judesio, d) blogo kontakto ir e) visų tipų artefaktams. Pilkas plotas žymi vidurkį $\pm$ standartinį nuokrypį. Dėl itin mažo klaidingų aliarmų skaičiaus atpažįstant ekstremalią bradikardiją teigiama prognostinė vertė visada artima 1 (nerodoma)

4.4   Ekstrasistolių dažnis hemodializuojamų pacientų įrašuose

HD pacientams užregistruotų ambulatorinių signalų analizė parodė, kad 51,6 % visų FPG ir 82,0 % visų EKG signalų yra tinkamos kokybės ekstrasistolėms atpažinti

(4.6 pav.). Pavieniuose įrašuose tinkamos kokybės FPG sudaro nuo 15,9 % iki 86,1 %, o tinkamos kokybės EKG – nuo 29,3 % iki 100 % įrašo trukmės. Vidutinis paros ekstrasistolių dažnis, pagrįstas FPG analize, pavieniuose įrašuose kinta nuo 3 iki 221 dūžių/h, o pagrįstas atraminės EKG analize – nuo 0 iki 681 dūžių/h. FPG analize pagrįstas vidutinis paros ekstrasistolių dažnis įvertintas su 3,2 dūžių/h medianine paklaida.
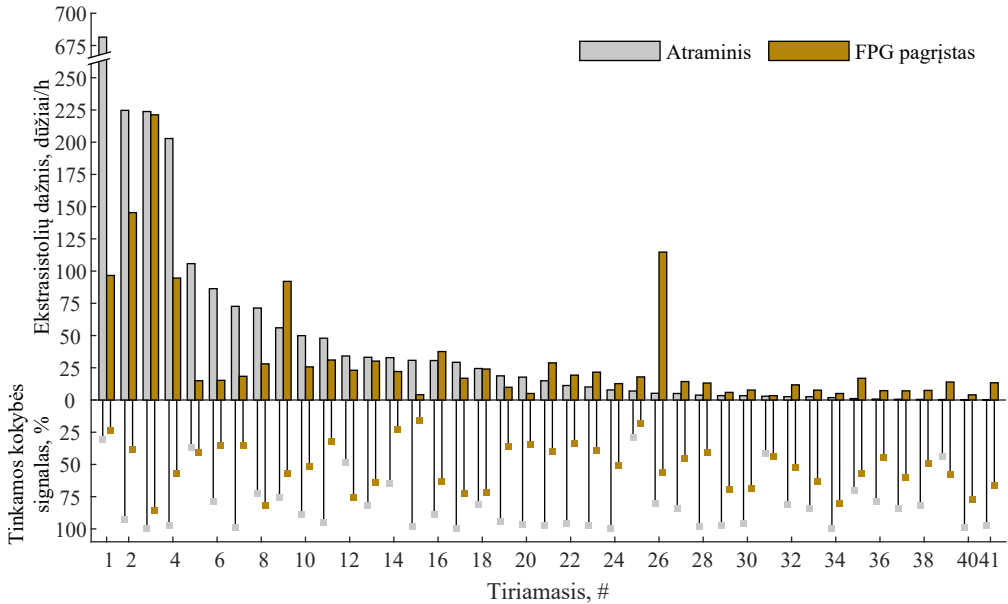

4.6 pav. Vidutinis paros ekstrasistolių dažnis ir tinkamos kokybės signalo dalis visuose HD pacientams užregistruotos ambulatorinės duomenų bazės įrašuose. Duomenys išrikiuoti mažėjimo tvarka pagal atraminį EKG analize pagrįstą vidutinį paros ekstrasistolių dažnį. Dėl nepakankamos kokybės nerodomi šeši įrašai

Analizuojamą duomenų bazę iš viso sudaro 979 nepersidengiantys 1 h trukmės segmentai, tačiau tik 757, turintys tinkamos kokybės atraminį EKG signalą, naudojami tyrimui atlikti. Tinkamos kokybės FPG signalo dalis segmente daro didelę įtaką didelės rizikos ($\geqslant$ 30 dūžių/h) ekstrasistolių dažnio 1 h trukmės segmentuose atpažinimo patikimumui (4.7 pav., a). Dėl šios priežasties jautrumas padidėja nuo 67,3 % iki 82,7 %, o specifiškumas – nuo 84,6 % iki 89,8 %, kai tenkinama bent 75 % tinkamos kokybės FPG signalo dalies segmente sąlyga.

Tiriamųjų, kuriems būdingas didelės rizikos ekstrasistolių dažnis, identifikavimo patikimumo priklausomybė nuo stebėsenos trukmės pateikta 4.7 pav., b. Nustatyta, kad, norint identifikuoti 80 % pacientų, kuriems būdingas didelės rizikos ekstrasistolių dažnis, reikalinga bent 9 h trukmės stebėsena. Maksimalus 83 % jautrumas pasiekiamas po 19 h FPG analize pagrįstos stebėsenos. Deja, būtina atkreipti dėmesį į tai, kad klaidingai teigiamų atvejų rodiklis viršija 50 % po 6 h stebėsenos.
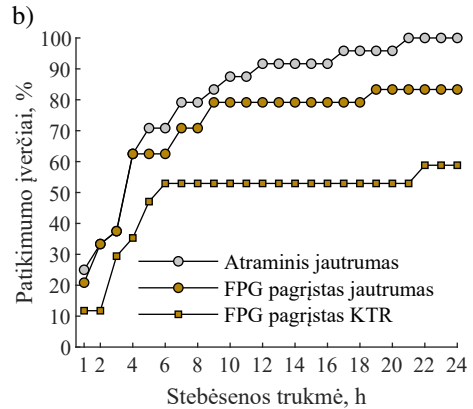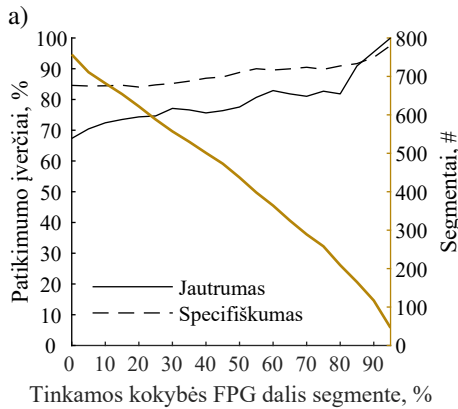
4.7 pav. a) Didelės rizikos ($\geqslant$ 30 dūžių/h) ekstrasistolių dažnio 1 h trukmės segmentuose atpažinimo patikimumo priklausomybė nuo tinkamos kokybės FPG signalo dalies segmente; b) tiriamųjų, kuriems būdingas didelės rizikos ekstrasistolių dažnis, identifikavimo patikimumo priklausomybė nuo stebėsenos trukmės. KTR, klaidingai teigiamų atvejų rodiklis

Ekstrasistolių dažnio stebėsenos visos paros metu pavyzdžiai esant skirtingai tinkamos kokybės FPG signalo daliai įraše pateikti 4.8 pav. Pirmajame pavyzdyje ryškus ekstrasistolių dažnio padidėjimas HD procedūros metu gana tiksliai įvertintas dėl didelės tinkamos kokybės FPG signalo dalies (4.8 pav., a). Antrajame pavyzdyje ekstrasistolių dažnio padidėjimas matomas ryte, kitą dieną po HD procedūros (4.8 pav., b). Dėl prastesnės signalo kokybės ir neatpažintų ekstrasistolių FPG analize pagrįsto ekstrasistolių dažnio padidėjimas yra nuvertintas, tačiau kitimo tendenciją vis tiek galima įžvelgti.
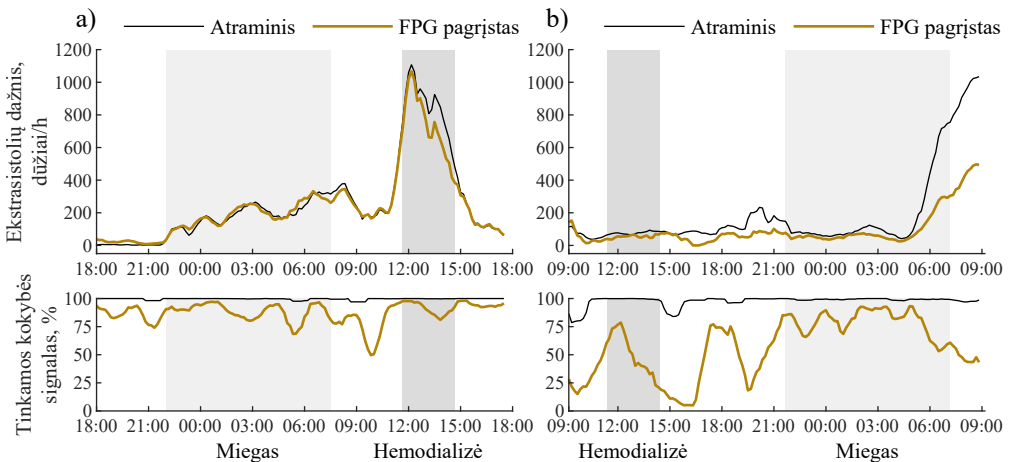
4.8 pav. Ekstrasistolių dažnio stebėsena 24 h įraše, kai a) didžioji FPG dalis yra tinkamos kokybės, b) pusė FPG yra netinkamos kokybės ekstrasistolėms atpažinti. Vertės apskaičiuotos valandos segmentuose, persidengiančiuose 50 min

IŠVADOS

1. Identifikuojant ir atskirai charakterizuojant keturis riešo FPG signalui būdingus artefaktų tipus, sukeltus įrenginio pasislinkimo, dilbio judesio, plaštakos judesio ir blogo kontakto, kiekybiškai ištirti ambulatoriniai FPG artefaktai. Analizė suteikia žinių apie skirtingų tipų artefaktų pasiskirstymą paros metu ir riešo FPG kokybę, būdingą ambulatoriniams įrašams. Pavieniuose įrašuose nuo 13,6 % iki 48,6 % FPG signalo trukmės sudaro artefaktai, dažniausiai sukelti įrenginio pasislinkimo, dilbio judesio ir plaštakos judesio. Šių artefaktų tipai atitinkamai užteršia 6,4 %, 6,2 % ir 6,0 % visų duomenų bazės FPG signalų. Išskirti artefaktus charakterizuojantys parametrai leidžia sukurti realistišką artefaktų modelį.

2. Sukurtas FPG signalų su gyvybei pavojingų aritmijų epizodais ir realistiškais artefaktais modelis. Adaptuotas modelis ekstremalios bradikardijos epizodus modeliuoja su 20,6 % mažesne vidutine kvadratine paklaida nei jo pirmtakas. Keičiant įvairias pasiūlyto modelio artefaktų savybes, gali būti modeliuojami realistiški, kasdienei veiklai būdingi artefaktai. Modeliuotų signalų tinkamumas išmokyti ir validuoti KNT, skirtą gyvybei pavojingoms aritmijoms atpažinti, pademonstruotas praktiškai. Modelio artefaktų dedamoji leidžia visapusiškai ištirti aritmijų detektorius.

3. Ištirtas dviejų FPG analize pagrįstų gyvybei pavojingų aritmijų detektorių patikimumas. KNT pranoksta pulso ritmo analize pagrįstą algoritmą pasiekdamas 98,1 % ekstremalios bradikardijos ir 76,6 % skilvelių tachikardijos atpažinimo jautrumą bei 96,6 % skilvelių tachikardijos atpažinimo specifiškumą. Pulso ritmo analize pagrįstas detektorius yra specifiškesnis (99,8 %) atpažįstant ekstremalią bradikardiją. Rezultatai rodo, kad KNT pagrįstas detektorius turėtų būti pasirinktas aritmijoms stebėti situacijose, kai jautrumas svarbesnis nei specifiškumas. Kadangi KNT veikia analizuodamas FPG skalogramas, jis geriau atpažįsta skilvelių tachikardiją esant mažesnės amplitudės pulsacijoms, tačiau yra jautrus klaidingiems ekstremalios bradikardijos aliarmams. Skirtingi artefaktų tipai skirtingai veikia pulso ritmo analize pagrįsto gyvybei pavojingų aritmijų detektoriaus patikimumą. Palyginti su kitais artefaktų tipais, blogas kontaktas sukelia 2–4 kartais daugiau klaidingų skilvelių tachikardijos aliarmų.

4. Ištirtas nuo riešo registruojamos FPG tinkamumas ekstrasistolių dažniui vertinti. Vidutiniškai 48,4 % visų FPG signalų yra analizei netinkamos kokybės. Tai rodo, kad signalo kokybė yra pagrindinis veiksnys, ribojantis sėkmingą klinikinį technologijos pritaikymą šioje srityje. Vis dėlto, jei 1 h trukmės segmente užtikrinama bent 45 min tinkamos kokybės signalo, riešo FPG gali būti naudojama

didelės rizikos ($\geq$ 30 dūžių/h) ekstrasistolių dažniui atpažinti pasiekiant 82,7 % jautrumą ir 89,8 % specifiškumą. Ilgalaikė stebėsena leidžia identifikuoti 80 % HD pacientų, kuriems būdingas didelės rizikos ekstrasistolių dažnis.

REFERENCES

1. BIKBOV, B., PURCELL, C. A., LEVEY, A. S., SMITH, M., ABDOLI, A. *et al.* Global, regional, and national burden of chronic kidney disease, 1990–2017: a systematic analysis for the Global Burden of Disease Study 2017. *The Lancet.* 2020, 395(10225), 709–733.

2. FOREMAN, K. J., MARQUEZ, N., DOLGERT, A., FUKUTAKI, K., FULL-MAN, N. *et al.* Forecasting life expectancy, years of life lost, and all-cause and cause-specific mortality for 250 causes of death: reference and alternative scenarios for 2016–40 for 195 countries and territories. *The Lancet.* 2018, 392(10159), 2052–2090.

3. PECOITS-FILHO, R., OKPECHI, I. G., DONNER, J.-A., HARRIS, D. C., ALJUBORI, H. M. *et al.* Capturing and monitoring global differences in untreated and treated end-stage kidney disease, kidney replacement therapy modality, and outcomes. *Kidney International Supplements.* 2020, 10(1), e3–e9.

4. MATSUSHITA, K., BALLEW, S. H., WANG, A. Y.-M., KALYESUBULA, R., SCHAEFFNER, E., and AGARWAL, R. Epidemiology and risk of cardiovascular disease in populations with chronic kidney disease. *Nature Reviews Nephrology.* 2022, 18(11), 696–707.

5. GANSEVOORT, R. T., CORREA-ROTTER, R., HEMMELGARN, B. R., JA-FAR, T. H., HEERSPINK, H. J. L. *et al.* Chronic kidney disease and cardio-vascular risk: epidemiology, mechanisms, and prevention. *The Lancet.* 2013, 382(9889), 339–352.

6. UNITED STATES RENAL DATA SYSTEM. 2021 Annual Data Report: Epidemi-ology of kidney disease in the United States. Volume 2: End stage renal disease. *American Journal of Kidney Diseases.* 2022, 79(4, Suppl. 1), S178–S575.

7. ROBERTS, P. R., STROMBERG, K., JOHNSON, L. C., WILES, B. M., MAVRAKANAS, T. A., and CHARYTAN, D. M. A systematic review of the incidence of arrhythmias in hemodialysis patients undergoing long-term monitor-ing with implantable loop recorders. *Kidney International Reports.* 2021, 6(1), 56–65.

8. ABE, S., YOSHIZAWA, M., NAKANISHI, N., YAZAWA, T., YOKOTA, K., HONDA, M., and SLOMAN, G. Electrocardiographic abnormalities in patients receiving hemodialysis. *American Heart Journal.* 1996, 131(6), 1137–1144.

9. SAMANTA, R., CHAN, C., and CHAUHAN, V. S. Arrhythmias and sudden cardiac death in end stage renal disease: Epidemiology, risk factors, and management. *Canadian Journal of Cardiology*. 2019, 35(9), 1228–1240.

10. POLYZOS, K. A., KONSTANTELIAS, A. A., and FALAGAS, M. E. Risk factors for cardiac implantable electronic device infection: a systematic review and meta-analysis. *EP Europace*. 2015, 17(5), 767–777.

11. SVENNBERG, E., TJONG, F., GOETTE, A., AKOUM, N., DI BIASE, L. *et al.* How to use digital devices to detect and manage arrhythmias: an EHRA practical guide. *EP Europace*. 2022, 24(6), 979–1005.

12. PALIAKAITĖ, B., PETRĖNAS, A., SOLOŠENKO, A., and MAROZAS, V. Photoplethysmogram modeling of extreme bradycardia and ventricular tachycardia. In *Proceedings of 15th Mediterranean Conference on Medical and Biological Engineering and Computing (MEDICON 2019)*. 2020, 76, 1165–1174.

13. PALIAKAITĖ, B., PETRĖNAS, A., SOLOŠENKO, A., and MAROZAS, V. Modeling of artifacts in the wrist photoplethysmogram: Application to the detection of life-threatening arrhythmias. *Biomedical Signal Processing and Control*. 2021, 66, 102421.

14. SOLOŠENKO, A., PALIAKAITĖ, B., MAROZAS, V., and SÖRNMO, L. Training convolutional neural networks on simulated photoplethysmography data: Application to bradycardia and tachycardia detection. *Frontiers in Physiology*. 2022, 13, 928098.

15. PALIAKAITĖ, B., SOLOŠENKO, A., DAUKANTAS, S., KUŠLEIKAITĖ-PERE, N., VAIČIŪNIENĖ, R., MAROZAS, V., and PETRĖNAS, A. Wrist photoplethysmography-based assessment of ectopic burden in hemodialysis patients. 2022. Under review.

16. KDIGO 2012 clinical practice guideline for the evaluation and management of chronic kidney disease. *Kidney International Supplements*. 2013, 3(1), 1–150.

17. ROMAGNANI, P., REMUZZI, G., GLASSOCK, R., LEVIN, A., JAGER, K. J. *et al.* Chronic kidney disease. *Nature Reviews Disease Primers*. 2017, 3(1), 17088.

18. WEBSTER, A. C., NAGLER, E. V., MORTON, R. L., and MASSON, P. Chronic kidney disease. *The Lancet*. 2017, 389(10075), 1238–1252.

19. KALANTAR-ZADEH, K., JAFAR, T. H., NITSCH, D., NEUEN, B. L., and PERKOVIC, V. Chronic kidney disease. *The Lancet*. 2021, 398(10302), 786–802.

20. BOENINK, R., ASTLEY, M. E., HUIJBEN, J. A., STEL, V. S., KERSCHBAUM, J. *et al.* The ERA Registry Annual Report 2019: summary and age comparisons. *Clinical Kidney Journal*. 2022, 15(3), 452–472.

21. DALRYMPLE, L. S., KATZ, R., KESTENBAUM, B., SHLIPAK, M. G., SARNAK, M. J. *et al.* Chronic kidney disease and the risk of end-stage renal disease versus death. *Journal of General Internal Medicine*. 2011, 26(4), 379–385.

22. THOMPSON, S., JAMES, M., WIEBE, N., HEMMELGARN, B., MANNS, B., KLARENBACH, S., and TONELLI, M. Cause of death in patients with reduced kidney function. *Journal of the American Society of Nephrology*. 2015, 26(10), 2504–2511.

23. GO, A. S., CHERTOW, G. M., FAN, D., MCCULLOCH, C. E., and HSU, C.-Y. Chronic kidney disease and the risks of death, cardiovascular events, and hospitalization. *New England Journal of Medicine*. 2004, 351(13), 1296–1305.

24. FOX, C. S., MATSUSHITA, K., WOODWARD, M., BILO, H. J., CHALMERS, J. *et al.* Associations of kidney disease measures with mortality and end-stage renal disease in individuals with and without diabetes: a meta-analysis. *The Lancet*. 2012, 380(9854), 1662–1673.

25. MAHMOODI, B. K., MATSUSHITA, K., WOODWARD, M., BLANKESTIJN, P. J., CIRILLO, M. *et al.* Associations of kidney disease measures with mortality and end-stage renal disease in individuals with and without hypertension: a meta-analysis. *The Lancet*. 2012, 380(9854), 1649–1661.

26. RONCO, C., BELLASI, A., and DI LULLO, L. Cardiorenal syndrome: An overview. *Advances in Chronic Kidney Disease*. 2018, 25(5), 382–390.

27. JANKOWSKI, J., FLOEGE, J., FLISER, D., BÖHM, M., and MARX, N. Cardiovascular disease in chronic kidney disease. *Circulation*. 2021, 143(11), 1157–1172.

28. DI LULLO, L., HOUSE, A., GORINI, A., SANTOBONI, A., RUSSO, D., and RONCO, C. Chronic kidney disease and cardiovascular complications. *Heart Failure Reviews*. 2015, 20(3), 259–272.

29. RONCO, C., HAAPIO, M., HOUSE, A. A., ANAVEKAR, N., and BELLOMO, R. Cardiorenal syndrome. *Journal of the American College of Cardiology*. 2008, 52(19), 1527–1539.

30. 2022 ESC Guidelines for the management of patients with ventricular arrhythmias and the prevention of sudden cardiac death: Developed by the task force for

the management of patients with ventricular arrhythmias and the prevention of sudden cardiac death of the European Society of Cardiology (ESC) Endorsed by the Association for European Paediatric and Congenital Cardiology (AEPC). *European Heart Journal*. 2022, 1–130.

31. PUN, P. H., SMARZ, T. R., HONEYCUTT, E. F., SHAW, L. K., AL-KHATIB, S. M., and MIDDLETON, J. P. Chronic kidney disease is associated with increased risk of sudden cardiac death among patients with coronary artery disease. *Kidney International*. 2009, 76(6), 652–658.

32. LAI, A. C., BIENSTOCK, S. W., SHARMA, R., SKORECKI, K., BEERKENS, F. *et al.* A personalized approach to chronic kidney disease and cardiovascular disease. *Journal of the American College of Cardiology*. 2021, 77(11), 1470–1479.

33. SHAMSEDDIN, M. K. and PARFREY, P. S. Sudden cardiac death in chronic kidney disease: epidemiology and prevention. *Nature Reviews Nephrology*. 2011, 7(3), 145–154.

34. DI LULLO, L., RIVERA, R., BARBERA, V., BELLASI, A., COZZOLINO, M. *et al.* Sudden cardiac death and chronic kidney disease: From pathophysiology to treatment strategies. *International Journal of Cardiology*. 2016, 217, 16–27.

35. YANG, K.-C., KYLE, J. W., MAKIELSKI, J. C., and DUDLEY, S. C. Mechanisms of sudden cardiac death. *Circulation Research*. 2015, 116(12), 1937–1955.

36. KALRA, P. A., GREEN, D., and POULIKAKOS, D. Arrhythmia in hemodialysis patients and its relation to sudden death. *Kidney International*. 2018, 93(4), 781–783.

37. FOLEY, R. N., GILBERTSON, D. T., MURRAY, T., and COLLINS, A. J. Long interdialytic interval and mortality among patients receiving hemodialysis. *New England Journal of Medicine*. 2011, 365(12), 1099–1107.

38. BORIANI, G., SAVELIEVA, I., DAN, G.-A., DEHARO, J. C., FERRO, C. *et al.* Chronic kidney disease in patients with cardiac rhythm disturbances or implantable electrical devices: clinical significance and implications for decision making-a position paper of the European Heart Rhythm Association endorsed by the Heart Rhythm Society and the Asia Pacific Heart Rhythm Society. *EP Europace*. 2015, 17(8), 1169–1196.

39. WONG, M. C., KALMAN, J. M., PEDAGOGOS, E., TOUSSAINT, N., VOHRA, J. K. *et al.* Temporal distribution of arrhythmic events in chronic kidney disease:

Highest incidence in the long interdialytic period. *Heart Rhythm*. 2015, 12(10), 2047–2055.

40. WONG, M. C., KALMAN, J. M., PEDAGOGOS, E., TOUSSAINT, N., VOHRA, J. K. *et al.* Bradycardia and asystole is the predominant mechanism of sudden cardiac death in patients with chronic kidney disease. *Journal of the American College of Cardiology*. 2015, 65(12), 1263–1265.

41. ROY-CHAUDHURY, P., TUMLIN, J. A., KOPLAN, B. A., COSTEA, A. I., KHER, V. *et al.* Primary outcomes of the Monitoring in Dialysis Study indicate that clinically significant arrhythmias are common in hemodialysis patients and related to dialytic cycle. *Kidney International*. 2018, 93(4), 941–951.

42. GENOVESI, S., BORIANI, G., COVIC, A., VERNOOIJ, R. W. M., COMBE, C. *et al.* Sudden cardiac death in dialysis patients: different causes and management strategies. *Nephrology Dialysis Transplantation*. 2021, 36, 396–405.

43. MC CAUSLAND, F. R., TUMLIN, J. A., ROY-CHAUDHURY, P., KOPLAN, B. A., COSTEA, A. I. *et al.* Intradialytic hypotension and cardiac arrhythmias in patients undergoing maintenance hemodialysis. *Clinical Journal of the American Society of Nephrology*. 2020, 15(6), 805–812.

44. PUN, P. H., LEHRICH, R. W., SMITH, S. R., and MIDDLETON, J. P. Predictors of survival after cardiac arrest in outpatient hemodialysis clinics. *Clinical Journal of the American Society of Nephrology*. 2007, 2(3), 491–500.

45. GOLDENBERG, I., MOSS, A. J., MCNITT, S., ZAREBA, W., ANDREWS, M. L. *et al.* Relations among renal function, risk of sudden cardiac death, and benefit of the implanted cardiac defibrillator in patients with ischemic left ventricular dysfunction. *American Journal of Cardiology*. 2006, 98(4), 485–490.

46. JUKEMA, J. W., TIMAL, R. J., ROTMANS, J. I., HENSEN, L. C. R., BUITEN, M. S. *et al.* Prophylactic use of implantable cardioverter-defibrillators in the prevention of sudden cardiac death in dialysis patients. *Circulation*. 2019, 139(23), 2628–2638.

47. KUSUMOTO, F. M., BAILEY, K. R., CHAOUKI, A. S., DESHMUKH, A. J., GAUTAM, S. *et al.* Systematic review for the 2017 AHA/ACC/HRS guideline for management of patients with ventricular arrhythmias and the prevention of sudden cardiac death. *Circulation*. 2018, 138(13), e392–e414.

48. ATAKLTE, F., ERQOU, S., LAUKKANEN, J., and KAPTOGE, S. Meta-analysis of ventricular premature complexes and their relation to cardiac mortality in general populations. *American Journal of Cardiology*. 2013, 112(8), 1263–1270.

49. HIMMELREICH, J. C. L., LUCASSEN, W. A. M., HEUGEN, M., BOSSUYT, P. M. M., TAN, H. L. *et al.* Frequent premature atrial contractions are associated with atrial fibrillation, brain ischaemia, and mortality: a systematic review and meta-analysis. *Europace*. 2018, 21(5), 698–707.

50. RANTANEN, J. M., RIAHI, S., SCHMIDT, E. B., JOHANSEN, M. B., SØ-GAARD, P., and CHRISTENSEN, J. H. Arrhythmias in patients on maintenance dialysis: A cross-sectional study. *American Journal of Kidney Diseases*. 2020, 75(2), 214–224.

51. TURAKHIA, M. P., BLANKESTIJN, P. J., CARRERO, J.-J., CLASE, C. M., DEO, R. *et al.* Chronic kidney disease and arrhythmias: conclusions from a Kidney Disease: Improving Global Outcomes (KDIGO) Controversies Conference. *European Heart Journal*. 2018, 39(24), 2314–2325.

52. RODRIGUES, A. S., PETRĖNAS, A., PALIAKAITĖ, B., KUŠLEIKAITĖ-PERE, N., JARUŠEVIŠIUS, G. *et al.* Noninvasive monitoring of potassium fluctuations during the long interdialytic interval. *IEEE Access*. 2020, 8, 188 488–188 502.

53. TURAKHIA, M. P., HOANG, D. D., ZIMETBAUM, P., MILLER, J. D., FROELICHER, V. F. *et al.* Diagnostic utility of a novel leadless arrhythmia monitoring device. *American Journal of Cardiology*. 2013, 112(4), 520–524.

54. HECKBERT, S. R., AUSTIN, T. R., JENSEN, P. N., FLOYD, J. S., PSATY, B. M., SOLIMAN, E. Z., and KRONMAL, R. A. Yield and consistency of arrhythmia detection with patch electrocardiographic monitoring: The Multi-Ethnic Study of Atherosclerosis. *Journal of Electrocardiology*. 2018, 51(6), 997–1002.

55. BAYOUMY, K., GABER, M., ELSHAFEEY, A., MHAIMEED, O., DINEEN, E. H. *et al.* Smart wearable devices in cardiovascular care: where we are and how to move forward. *Nature Reviews Cardiology*. 2021, 18(8), 581–599.

56. BACEVIČIUS, J., ABRAMIKAS, Ž., DVINELIS, E., AUDZIJONIENĖ, D., PETRYLAITĖ, M. *et al.* High specificity wearable device with photoplethysmography and six-lead electrocardiography for atrial fibrillation detection challenged by frequent premature contractions: DoubleCheck-AF. *Frontiers in Cardiovascular Medicine*. 2022, 9, 869730.

57. VARMA, N., CYGANKIEWICZ, I., TURAKHIA, M., HEIDBUCHEL, H., HU, Y. *et al.* 2021 ISHNE/ HRS/ EHRA/ APHRS collaborative statement on mHealth in arrhythmia management: Digital medical tools for heart rhythm professionals. *Annals of Noninvasive Electrocardiology*. 2021, 26(2), e12795.

58. KWOK, C. S., DARLINGTON, D., MAYER, J., PANCHAL, G., WALKER, V. *et al.* A review of the wide range of indications and uses of implantable loop recorders: A review of the literature. *Hearts*. 2022, 3(2), 45–53.

59. BOUDREAUX, B. D., HEBERT, E. P., HOLLANDER, D. B., WILLIAMS, B. M., CORMIER, C. L. *et al.* Validity of wearable activity monitors during cycling and resistance exercise. *Medicine and Science in Sports and Exercise*. 2018, 50(3), 624–633.

60. ETIWY, M., AKHRASS, Z., GILLINOV, L., ALASHI, A., WANG, R. *et al.* Accuracy of wearable heart rate monitors in cardiac rehabilitation. *Cardiovascular Diagnosis and Therapy*. 2019, 9(3), 262–271.

61. NIELSEN, J. C., LIN, Y.-J., DE OLIVEIRA FIGUEIREDO, M. J., SEPEHRI SHAMLOO, A., ALFIE, A. *et al.* European Heart Rhythm Association (EHRA)/Heart Rhythm Society (HRS)/Asia Pacific Heart Rhythm Society (APHRS)/Latin American Heart Rhythm Society (LAHRS) expert consensus on risk assessment in cardiac arrhythmias: use the right tool for the right outcome, in the right population. *EP Europace*. 2020, 22(8), 1147–1148.

62. CHEUNG, C. C., KRAHN, A. D., and ANDRADE, J. G. The emerging role of wearable technologies in detection of arrhythmia. *Canadian Journal of Cardiology*. 2018, 34(8), 1083–1087.

63. TISON, G. H., SANCHEZ, J. M., BALLINGER, B., SINGH, A., OLGIN, J. E. *et al.* Passive detection of atrial fibrillation using a commercially available smartwatch. *JAMA Cardiology*. 2018, 3(5), 409–416.

64. SOLOŠENKO, A., PETRĖNAS, A., PALIAKAITĖ, B., SÖRNMO, L., and MAROZAS, V. Detection of atrial fibrillation using a wrist-worn device. *Physiological Measurement*. 2019, 40(2), 025003.

65. PEREZ, M. V., MAHAFFEY, K. W., HEDLIN, H., RUMSFELD, J. S., GARCIA, A. *et al.* Large-scale assessment of a smartwatch to identify atrial fibrillation. *New England Journal of Medicine*. 2019, 381(20), 1909–1917.

66. BONOMI, A. G., SCHIPPER, F., EERIKÄINEN, L. M., MARGARITO, J., VAN DINTHER, R. *et al.* Atrial fibrillation detection using a novel cardiac ambulatory monitor based on photo-plethysmography at the wrist. *Journal of the American Heart Association*. 2018, 7(15), e009351.

67. EERIKÄINEN, L. M., BONOMI, A. G., SCHIPPER, F., DEKKER, L. R. C., VULLINGS, R., DE MORREE, H. M., and AARTS, R. M. Comparison between

electrocardiogram- and photoplethysmogram-derived features for atrial fibrillation detection in free-living conditions. *Physiological Measurement*. 2018, 39(8), 084001.

68. EERIKÄINEN, L. M., BONOMI, A. G., DEKKER, L. R., VULLINGS, R., and AARTS, R. M. Atrial fibrillation monitoring with wrist-worn photoplethysmography-based wearables: State-of-the-art review. *Cardiovascular Digital Health Journal*. 2020, 1(1), 45–51.

69. 2020 ESC Guidelines for the diagnosis and management of atrial fibrillation developed in collaboration with the European Association for Cardio-Thoracic Surgery (EACTS): The Task Force for the diagnosis and management of atrial fibrillation of the European Society of Cardiology (ESC) Developed with the special contribution of the European Heart Rhythm Association (EHRA) of the ESC. *European Heart Journal*. 2020, 42(5), 373–498.

70. BONOMI, A. G., EERIKÄINEN, L. M., SCHIPPER, F., AARTS, R. M., DE MORREE, H. M., and DEKKER, L. Detecting episodes of brady- and tachy-cardia using photo-plethysmography at the wrist in free-living conditions. In *Proceedings of 2017 Computing in Cardiology Conference (CinC)*. 2017, 44, 1–4.

71. HAN, D., BASHAR, S. K., MOHAGHEGHIAN, F., DING, E., WHITCOMB, C., MCMANUS, D. D., and CHON, K. H. Premature atrial and ventricular contraction detection using photoplethysmographic data from a smartwatch. *Sensors*. 2020, 20(19), 5683.

72. GIL, E., LAGUNA, P., MARTÍNEZ, J. P., BARQUERO-PÉREZ, Ó., GARCÍA-ALBEROLA, A., and SÖRNMO, L. Heart rate turbulence analysis based on photoplethysmography. *IEEE Transactions on Biomedical Engineering*. 2013, 60(11), 3149–3155.

73. SOLOŠENKO, A., PETRĖNAS, A., and MAROZAS, V. Photoplethysmography-based method for automatic detection of premature ventricular contractions. *IEEE Transactions on Biomedical Circuits and Systems*. 2015, 9(5), 662–669.

74. LIU, Z., ZHOU, B., JIANG, Z., CHEN, X., LI, Y., TANG, M., and MIAO, F. Multiclass arrhythmia detection and classification from photoplethysmography signals using a deep convolutional neural network. *Journal of the American Heart Association*. 2022, 11(7), e023555.

75. CHONG, J. W., ESA, N., MCMANUS, D. D., and CHON, K. H. Arrhythmia discrimination using a smart phone. *IEEE Journal of Biomedical and Health Informatics*. 2015, 19(3), 815–824.

76. HOSANEE, M., CHAN, G., WELYKHOLOWA, K., COOPER, R., KYRIA-COU, P. A. *et al.* Cuffless single-site photoplethysmography for blood pressure monitoring. *Journal of Clinical Medicine*. 2020, 9(3), 723.

77. PALIAKAITĖ, B., CHARLTON, P., RAPALIS, A., PLUŠČIAUSKAITĖ, V., PIARTLI, P., KANIUSAS, E., and MAROZAS, V. Blood pressure estimation based on photoplethysmography: Finger versus wrist. In *Proceedings of 2021 Computing in Cardiology Conference (CinC)*. 2021, 48, 1–4.

78. CHARLTON, P. H., PALIAKAITĖ, B., PILT, K., BACHLER, M., ZANELLI, S. *et al.* Assessing hemodynamics from the photoplethysmogram to gain insights into vascular age: a review from vascagenet. *American Journal of Physiology-Heart and Circulatory Physiology*. 2022, 322(4), H493–H522.

79. ZHANG, Z., PI, Z., and LIU, B. TROIKA: A general framework for heart rate monitoring using wrist-type photoplethysmographic signals during intensive physical exercise. *IEEE Transactions on Biomedical Engineering*. 2015, 62(2), 522–531.

80. KHAN, E., AL HOSSAIN, F., UDDIN, S. Z., ALAM, S. K., and HASAN, M. K. A robust heart rate monitoring scheme using photoplethysmographic signals corrupted by intense motion artifacts. *IEEE Transactions on Biomedical Engineering*. 2016, 63(3), 550–562.

81. FALLET, S. and VESIN, J.-M. Robust heart rate estimation using wrist-type photoplethysmographic signals during physical exercise: an approach based on adaptive filtering. *Physiological Measurement*. 2017, 38(2), 155–170.

82. FUJITA, Y., HIROMOTO, M., and SATO, T. PARHELIA: Particle filter-based heart rate estimation from photoplethysmographic signals during physical exercise. *IEEE Transactions on Biomedical Engineering*. 2018, 65(1), 189–198.

83. CHUNG, H., LEE, H., and LEE, J. Finite state machine framework for instantaneous heart rate validation using wearable photoplethysmography during intensive exercise. *IEEE Journal of Biomedical and Health Informatics*. 2019, 23(4), 1595–1606.

84. CASSON, A. J., VAZQUEZ GALVEZ, A., and JARCHI, D. Gyroscope vs. accelerometer measurements of motion from wrist PPG during physical exercise. *ICT Express*. 2016, 2(4), 175–179.

85. LEE, H., CHUNG, H., and LEE, J. Motion artifact cancellation in wearable photoplethysmography using gyroscope. *IEEE Sensors Journal*. 2019, 19(3), 1166–1175.

86. ZHOU, C., FENG, J., HU, J., and YE, X. Study of artifact-resistive technology based on a novel dual photoplethysmography method for wearable pulse rate monitors. *Journal of Medical Systems*. 2015, 40(3), 56.

87. ZHANG, Y., SONG, S., VULLINGS, R., BISWAS, D., SIMÕES-CAPELA, N. *et al.* Motion artifact reduction for wrist-worn photoplethysmograph sensors based on different wavelengths. *Sensors*. 2019, 19(3), 673.

88. LEE, H., CHUNG, H., KIM, J., and LEE, J. Motion artifact identification and removal from wearable reflectance photoplethysmography using piezoelectric transducer. *IEEE Sensors Journal*. 2019, 19(10), 3861–3870.

89. WANDER, J. D. and MORRIS, D. A combined segmenting and non-segmenting approach to signal quality estimation for ambulatory photoplethysmography. *Physiological Measurement*. 2014, 35(12), 2543–2561.

90. ROY, B. and GUPTA, R. MoDTRAP: Improved heart rate tracking and pre-processing of motion-corrupted photoplethysmographic data for personalized healthcare. *Biomedical Signal Processing and Control*. 2020, 56, 101676.

91. BASHAR, S. K., HAN, D., HAJEB-MOHAMMADALIPOUR, S., DING, E., WHITCOMB, C., MCMANUS, D. D., and CHON, K. H. Atrial fibrillation detection from wrist photoplethysmography signals using smartwatches. *Scientific Reports*. 2019, 9, 15054.

92. DÖRR, M., NOHTURFFT, V., BRASIER, N., BOSSHARD, E., DJURDJE-VIC, A. *et al.* The WATCH AF Trial: SmartWATCHes for detection of Atrial Fibrillation. *JACC-Clinical Electrophysiology*. 2019, 5(2), 199–208.

93. CORINO, V. D. A., LAUREANTI, R., FERRANTI, L., SCARPINI, G., LOM-BARDI, F., and MAINARDI, L. T. Detection of atrial fibrillation episodes using a wristband device. *Physiological Measurement*. 2017, 38(5), 787–799.

94. FALLET, S., LEMAY, M., RENEVEY, P., LEUPI, C., PRUVOT, E., and VESIN, J.-M. Can one detect atrial fibrillation using a wrist-type photoplethysmographic device? *Medical & Biological Engineering & Computing*. 2019, 57(2), 477–487.

95. CHEN, L. Y., CHUNG, M. K., ALLEN, L. A., EZEKOWITZ, M., FURIE, K. L. *et al.* Atrial fibrillation burden: Moving beyond atrial fibrillation as a binary entity: A scientific statement from the American Heart Association. *Circulation*. 2018, 137(20), e623–e644.

96. PETTERSON, M. T., BEGNOCHE, V. L., and GRAYBEAL, J. M. The effect of motion on pulse oximetry and its clinical significance. *Anesthesia and Analgesia*. 2007, 105(6), S78–S84.

97. GARCÍA-LÓPEZ, I. and RODRIGUEZ-VILLEGAS, E. Characterization of artifact signals in neck photoplethysmography. *IEEE Transactions on Biomedical Engineering*. 2020, 67(10), 2849–2861.

98. MAEDA, Y., SEKINE, M., and TAMURA, T. Relationship between measurement site and motion artifacts in wearable reflected photoplethysmography. *Journal of Medical Systems*. 2011, 35(5), 969–976.

99. MAEDA, Y., SEKINE, M., and TAMURA, T. The advantages of wearable green reflected photoplethysmography. *Journal of Medical Systems*. 2011, 35(5), 829–834.

100. PRADHAN, N., RAJAN, S., and ADLER, A. Evaluation of the signal quality of wrist-based photoplethysmography. *Physiological Measurement*. 2019, 40(6), 065008.

101. SOLOŠENKO, A., PETRĖNAS, A., MAROZAS, V., and SÖRNMO, L. Modeling of the photoplethysmogram during atrial fibrillation. *Computers in Biology and Medicine*. 2017, 81, 130–138.

102. GOLDBERGER, A. L., AMARAL, L. A. N., GLASS, L., HAUSDORFF, J. M., IVANOV, P. C. *et al.* PhysioBank, PhysioToolkit, and PhysioNet: components of a new research resource for complex physiologic signals. *Circulation*. 2000, 101(23), e215–e220.

103. EERIKÄINEN, L. M., BONOMI, A. G., SCHIPPER, F., DEKKER, L., VULLINGS, R., DE MORREE, H. M., and AARTS, R. M. How accurately can we detect atrial fibrillation using photoplethysmography data measured in daily life? In *Proceedings of 2019 Computing in Cardiology Conference (CinC)*. 2019, 46, 1–4.

104. WARTZEK, T., BRÜSER, C., SCHLEBUSCH, T., BRENDLE, C., SANTOS, S. *et al.* Modeling of motion artifacts in contactless heart rate measurements. In *Proceedings of 2013 Computing in Cardiology Conference (CinC)*. 2013, 40, 931–934.

105. BERIEF, F., LEONHARDT, S., and HOOG ANTINK, C. Modelling and synthesizing motion artifacts in unobtrusive multimodal sensing using copulas. In *Proceedings of 40th Annual International Conference of the IEEE Engineering in Medicine and Biology Society (EMBC 2018)*. 2018, 6006–6009.

106. FINE, J., BRANAN, K. L., RODRIGUEZ, A. J., BOONYA-ANANTA, T., AJMAL *et al.* Sources of inaccuracy in photoplethysmography for continuous cardiovascular monitoring. *Biosensors*. 2021, 11(4), 126.

107. ABOY, M., MCNAMES, J., TRAN THONG, TSUNAMI, D., ELLENBY, M. S., and GOLDSTEIN, B. An automatic beat detection algorithm for pressure signals. *IEEE Transactions on Biomedical Engineering*. 2005, 52(10), 1662–1670.

108. DAWBER, T. R., THOMAS, H. E., and MCNAMARA, P. M. Characteristics of the dicrotic notch of the arterial pulse wave in coronary heart disease. *Angiology*. 1973, 24(4), 244–255.

109. TSIPOURAS, M., FOTIADIS, D., and SIDERIS, D. An arrhythmia classification system based on the RR-interval signal. *Artificial Intelligence in Medicine*. 2005, 33(3), 237–250.

110. CHUNG, C. S., KARAMANOGLU, M., and KOVÁCS, S. J. Duration of diastole and its phases as a function of heart rate during supine bicycle exercise. *American Journal of Physiology-Heart and Circulatory Physiology*. 2004, 287(5), H2003–H2008.

111. MELBIN, J., DETWEILER, D. K., RIFFLE, R. A., and NOORDERGRAAF, A. Coherence of cardiac output with rate changes. *American Journal of Physiology-Heart and Circulatory Physiology*. 1982, 243(4), H499–H504.

112. COHN, K. and KRYDA, W. The influence of ectopic beats and tachyarrhythmias on stroke volume and cardiac output. *Journal of Electrocardiology*. 1981, 14(3), 207–218.

113. ZHENG, D., ALLEN, J., and MURRAY, A. Determination of aortic valve opening time and left ventricular peak filling rate from the peripheral pulse amplitude in patients with ectopic beats. *Physiological Measurement*. 2008, 29(12), 1411–1419.

114. SARNARI, R., KAMAL, R. Y., FRIEDBERG, M. K., and SILVERMAN, N. H. Doppler assessment of the ratio of the systolic to diastolic duration in normal children: Relation to heart rate, age and body surface area. *Journal of the American Society of Echocardiography*. 2009, 22(8), 928–932.

115. KINGMA, D. P. and BA, J. Adam: A method for stochastic optimization. *arXiv preprint*. 2014, arXiv:1412.6980.

116. VEST, A. N., POIAN, G. D., LI, Q., LIU, C., NEMATI, S., SHAH, A. J., and CLIFFORD, G. D. An open source benchmarked toolbox for cardiovascular waveform and interval analysis. *Physiological Measurement*. 2018, 39(10), 105004.

117. BEHAR, J., JOHNSON, A., CLIFFORD, G. D., and OSTER, J. A comparison of single channel fetal ECG extraction methods. *Annals of Biomedical Engineering*. 2014, 42(6), 1340–1353.

118. JOHNSON, A. E., BEHAR, J., ANDREOTTI, F., CLIFFORD, G. D., and OSTER, J. R-peak estimation using multimodal lead switching. In *Proceedings of 2014 Computing in Cardiology Conference (CinC)*. 2014, 41, 281–284.

119. LI, Q., MARK, R. G., and CLIFFORD, G. D. Robust heart rate estimation from multiple asynchronous noisy sources using signal quality indices and a Kalman filter. *Physiological Measurement*. 2008, 29(1), 15–32.

120. BEHAR, J., OSTER, J., LI, Q., and CLIFFORD, G. D. ECG signal quality during arrhythmia and its application to false alarm reduction. *IEEE Transactions on Biomedical Engineering*. 2013, 60(6), 1660–1666.

121. MARTINEZ, J., ALMEIDA, R., OLMOS, S., ROCHA, A. P., and LAGUNA, P. A wavelet-based ECG delineator: evaluation on standard databases. *IEEE Transactions on Biomedical Engineering*. 2004, 51(4), 570–581.

122. MOEYERSONS, J., AMONI, M., VAN HUFFEL, S., WILLEMS, R., and VARON, C. R-DECO: an open-source Matlab based graphical user interface for the detection and correction of R-peaks. *PeerJ Computer Science*. 2019, 5, e226.

123. MOEYERSONS, J., AMONI, M., VAN HUFFEL, S., WILLEMS, R., and VARON, C. R-DECO: an open-source Matlab based graphical user interface for the detection and correction of R-peaks (version 1.0.0). *PhysioNet*. 2020.

124. HUANG, T.-C., LEE, P.-T., HUANG, M.-S., SU, P.-F., and LIU, P.-Y. Higher premature atrial complex burden from the Holter examination predicts poor cardiovascular outcome. *Scientific Reports*. 2021, 11, 12198.

125. SOKAS, D., PETRĖNAS, A., DAUKANTAS, S., RAPALIS, A., PALIAKAITĖ, B., and MAROZAS, V. Estimation of heart rate recovery after stair climbing using a wrist-worn device. *Sensors*. 2019, 19(9), 2113.

126. SOKOLOVA, M. and LAPALME, G. A systematic analysis of performance measures for classification tasks. *Information Processing & Management*. 2009, 45(4), 427–437.

127. CLIFFORD, G. D., SILVA, I., MOODY, B., LI, Q., KELLA, D. *et al.* The PhysioNet/Computing in Cardiology Challenge 2015: Reducing false arrhythmia alarms in the ICU. In *Proceedings of 2015 Computing in Cardiology Conference (CinC)*. 2015, 42, 273–276.

128. MCHUGH, M. L. Interrater reliability: the kappa statistic. *Biochemia Medica*. 2012, 22(3), 276–282.

129. CLIFFORD, G. D., LIU, C., MOODY, B., LI-WEI, H. L., SILVA, I. *et al.* AF classification from a short single lead ECG recording: The PhysioNet/Computing in Cardiology Challenge 2017. In *Proceedings of 2017 Computing in Cardiology Conference (CinC)*. 2017, 44, 1–4.

130. BINICI, Z., INTZILAKIS, T., NIELSEN, O. W., KOBER, L., and SAJADIEH, A. Excessive supraventricular ectopic activity and increased risk of atrial fibrillation and stroke. *Circulation*. 2010, 121(17), 1904–1911.

131. SUKOR, J. A., REDMOND, S. J., and LOVELL, N. H. Signal quality measures for pulse oximetry through waveform morphology analysis. *Physiological Measurement*. 2011, 32(3), 369–384.

132. KARLEN, W., KOBAYASHI, K., ANSERMINO, J. M., and DUMONT, G. A. Photoplethysmogram signal quality estimation using repeated gaussian filters and cross-correlation. *Physiological Measurement*. 2012, 33(10), 1617–1629.

133. LIM, P. K., NG, S.-C., LOVELL, N. H., YU, Y. P., TAN, M. P. *et al.* Adaptive template matching of photoplethysmogram pulses to detect motion artefact. *Physiological Measurement*. 2018, 39(10), 105005.

134. ZHAO, X., ZHANG, H., ZHU, G., YOU, F., KUANG, S., and SUN, L. A multi-branch 3D convolutional neural network for EEG-based motor imagery classification. *IEEE Transactions on Neural Systems and Rehabilitation Engineering*. 2019, 27(10), 2164–2177.

135. CHOU, Y., GU, J., LIU, J., GU, Y., and LIN, J. Bradycardia and tachycardia detection using a synthesis-by-analysis modeling approach of pulsatile signal. *IEEE Access*. 2019, 7, 131 256–131 269.

136. LIU, C., ZHENG, D., MURRAY, A., and LIU, C. Modeling carotid and radial artery pulse pressure waveforms by curve fitting with Gaussian functions. *Biomedical Signal Processing and Control*. 2013, 8, 449–454.

137. HE, D., WANG, L., FAN, X., YAO, Y., GENG, N., SUN, Y., and QIAN, W. A new mathematical model of wrist pulse waveforms characterizes patients with cardiovascular disease – A pilot study. *Medical Engineering & Physics*. 2017, 48, 142–149.

138. TANG, Q., CHEN, Z., WARD, R., and ELGENDI, M. Synthetic photoplethysmogram generation using two Gaussian functions. *Scientific Reports*. 2020, 10, 13883.

139. ALLEN, J. Photoplethysmography and its application in clinical physiological measurement. *Physiological Measurement*. 2007, 28(3), R1–R39.

140. BLACK, N., D'SOUZA, A., WANG, Y., PIGGINS, H., DOBRZYNSKI, H., MORRIS, G., and BOYETT, M. R. Circadian rhythm of cardiac electrophysiology, arrhythmogenesis, and the underlying mechanisms. *Heart Rhythm*. 2019, 16(2), 298–307.

141. PORTALUPPI, F. and HERMIDA, R. C. Circadian rhythms in cardiac arrhythmias and opportunities for their chronotherapy. *Advanced Drug Delivery Reviews*. 2007, 59(9), 940–951.

LIST OF PUBLICATIONS ON THE SUBJECT OF THE DOCTORAL THESIS

Publications in the journals referred in the *Clarivate Analytics Web of Science* database with impact factor

1. **Paliakaitė, Birutė**; Petrėnas, Andrius; Sološenko, Andrius; Marozas, Vaidotas. Modeling of Artifacts in the Wrist Photoplethysmogram: Application to the Detection of Life-Threatening Arrhythmias. *Biomedical Signal Processing and Control*. 2021, vol. 66, art. no. 102421, p. 1–10. [IF 5.076, Q2, 2021]

2. Sološenko, Andrius; **Paliakaitė, Birutė**; Marozas, Vaidotas; Sörnmo, Leif. Training Convolutional Neural Networks on Simulated Photoplethysmography Data: Application to Bradycardia and Tachycardia Detection. *Frontiers in Physiology*. 2022, vol. 13, art. no. 928098, p. 1662–1670. [IF: 4.755, Q1, 2021]

3. Charlton, Peter H.; **Paliakaitė, Birutė**; Pilt, Kristjan; Bachler, Martin; Zanelli, Serena; Kulin, Daniel; Allen, John; Hallab, Magid; Bianchini, Elisabetta; Mayer, Christopher C.; Terentes-Printzios, Dimitrios; Dittrich, Verena; Hametner, Bernhard; Veerasingam, Dave; Žikić, Dejan; Marozas, Vaidotas. Assessing Hemodynamics from the Photoplethysmogram to Gain Insights into Vascular Age: A Review from VascAgeNet. *American Journal of Physiology - Heart and Circulatory Physiology*. 2022, vol. 322, iss. 4, p. H493–H522. [IF 5.125, Q1, 2021]

Publications referred in the *Clarivate Analytics Web of Science* database without impact factor

1. **Paliakaitė, Birutė**; Petrėnas, Andrius; Sološenko, Andrius; Marozas, Vaidotas. Photoplethysmogram Modeling of Extreme Bradycardia and Ventricular Tachycardia. In *Proceedings of 15th Mediterranean Conference on Medical and Biological Engineering and Computing (MEDICON 2019)*. 2020, vol. 76, p. 1165–1174.

2. **Paliakaitė, Birutė**; Charlton, Peter H.; Rapalis, Andrius; Pluščiauskaitė, Vilma; Piartli, Povilas; Kaniusas, Eugenijus; Marozas, Vaidotas. Blood Pressure Estimation Based on Photoplethysmography: Finger Versus Wrist. In *Proceedings of 2021 Computing in Cardiology Conference (CinC)*. 2021, vol. 48, p. 1–4.

3. Santos Rodrigues, Ana; **Paliakaitė, Birutė**; Daukantas, Saulius; Sološenko, Andrius; Petrėnas, Andrius; Marozas, Vaidotas. Personalized Evaluation of Life-Threatening Conditions in Chronic Kidney Disease Patients: The Concept of Wearable Technology and Case Analysis. In *Proceedings of 15th International Joint Conference on Biomedical Engineering Systems and Technologies (BIOSTEC 2022)*. 2022, p. 244–250.

Peer-reviewed publications referred in other international databases

1. Jančiulevičiūtė, Karolina; **Paliakaitė, Birutė**; Marozas, Vaidotas. Influence of Signal Acquisition Location on Blood Pressure Parameters in Photoplethysmogram. In *Proceedings of 13th International Conference on Biomechanics, Medical Diagnostics, Locomotion and Rehabilitation (BIOMDLORE 2021)*. 2021, p. 1–4.

Conference presentation abstracts

1. **Paliakaitė, Birutė**. Hemodializuojamų pacientų ekstrasistolių dažnio vertinimas panaudojant riešo fotopletizmografiją. In *Bioateitis: gamtos ir gyvybės mokslų perspektyvos: 15-oji Lietuvos jaunųjų mokslininkų konferencija: pranešimų tezės*. 2022, p. 24–25.

List of attended conferences

1. **Paliakaitė, Birutė**; Petrėnas, Andrius; Sološenko, Andrius; Marozas, Vaidotas. Photoplethysmogram Modeling of Extreme Bradycardia and Ventricular Tachycardia. *15th Mediterranean Conference on Medical and Biological Engineering and Computing* (MEDICON): September 26–28, 2019, Coimbra, Portugal.

2. **Paliakaitė, Birutė**; Charlton, Peter H.; Rapalis, Andrius; Pluščiauskaitė, Vilma; Piartli, Povilas; Kaniusas, Eugenijus; Marozas, Vaidotas. Blood Pressure Estimation Based on Photoplethysmography: Finger Versus Wrist. *Conference on Computing in Cardiology* (CinC): September 12–15, 2021, Brno, Czech Republic.

3. **Paliakaitė, Birutė**. Hemodializuojamų pacientų ekstrasistolių dažnio vertinimas panaudojant riešo fotopletizmografiją. *Bioateitis: gamtos ir gyvybės mokslų perspektyvos 2022: 15-oji Lietuvos jaunųjų mokslininkų konferencija*: November 24, 2022, Vilnius, Lithuania.

Patents registered by the State Patent Bureau of the Republic of Lithuania

1. Personalizuotos gyvybei pavojingų būsenų stebėsenos sistema ir būdas lėtine inkstų liga sergantiems pacientams / išradėjai: V. Marozas, A. Petrėnas, **B. Paliakaitė**, A. Lukoševičius, D. Jegelevičius, A. Sološenko, S. Daukantas, A. Rapalis, N. Kušleikaitė-Pere, I. A. Bumblytė; savininkai: Kauno technologijos universitetas, Lietuvos sveikatos mokslų universitetas. LT 6780 B. 2020-11-10. [Lietuvos Respublikos patentų duomenų bazė; Espacenet]

Patent applications

1. A system and method for personalized monitoring of life-threatening health conditions in patients with chronic kidney disease: European patent application / inventors: V. Marozas, A. Petrėnas, **B. Paliakaitė**, A. Lukoševičius, D. Jegelevičius, A. Sološenko, S. Daukantas, A. Rapalis, N. Kušleikaitė-Pere, I.A. Bumblytė; applicant: Kaunas University of Technology. EP 3654347 A1. 2020-05-20. [Espacenet]

Publicly available software

1. Sološenko, Andrius; Petrėnas, Andrius; **Paliakaitė, Birutė**; Marozas, Vaidotas; Sörnmo, Leif. Model for Simulating ECG and PPG Signals with Arrhythmia Episodes (version 1.3.1). *PhysioNet*. 2022.

ACKNOWLEDGMENTS